NOTE TO USERS

Seismic Microzonation of the Island of Montreal

By

Ricardo Adolfo Madriz

Department of Civil Engineering and Applied Mechanics
McGill University
Montreal, Canada
August 2004

A Thesis submitted to the
Faculty of Graduate Studies and Research
in partial fulfillment of the requirements for the degree of
Master of Engineering

Your file Votre référence
ISBN: 0-494-12630-2
Our file Notre référence
ISBN: 0-494-12630-2

Abstract

Montreal is the third largest city in Canada according to the size of its population, and ranks second in terms of seismic vulnerability. In the past decades many studies of the soil deposits of the Montreal Island have taken place without considering the influence of unconsolidated soils. The objective of this thesis is to determine the predominant frequency and amplification of the ground acceleration of the unconsolidated soils, on the Island of Montreal.

The methodology consists of applying the widely known Nakamura's technique to obtain the predominant frequency of resonance. The technique consists in calculating the ratio between the horizontal and vertical components of the response spectra. 1One-dimensional analyses of soil columns are used to validate the frequency of the first method and to estimate the amplification factors. The analysis is carried out using Shake 91. A thorough study of the soils and their characteristics was necessary to conduct the analysis. The final product includes maps for the predominant frequency and amplification factors for four seismic scenarios.

Résumé

Montréal est la deuxième ville en importance au Canada par rapport au risque sismique. La présente étude a été effectuée dans le cadre d'une analyse de risques sismiques pour la ville de Montréal. Cette thèse représente la première étude approfondie sur la micro-zonation sismique de Montréal.

L'objective principal de la microzonation est de caractériser la fréquence fondamentale des sols à travers l'île de Montréal ainsi que d'estimer le facteur d'amplification des ondes sismiques.

La microzonation a été effectuée à partir de plus de 700 mesures de bruit de fonds répartie sur le territoire de la ville ainsi que d'analyses numériques effectuées avec Shake91 à partir d'une base données de plus de 30000 forages sur les caractéristiques des sols.

Acknowledgements

The author would like to express his appreciation to the people that have been involved in the project. First, I would like to thank Prof. Luc Chouinard for giving me the opportunity to work on this project, his supervision and guidance throughout the execution. I also would like to thank Dr. Philippe Rosset for starting this project, selecting and proving the methodology and guide me through my first days with the research.

The author would like to sincerely thank Ph. D. Candidate Alejandro de la Puente for spending all those nights measuring ground ambient noise and for all his encouragement, help and invaluable advice during all the stages. Special thanks to the Geological Survey of Canada for providing the equipment and assistance when ever it was necessary and the City of Montreal for providing the borehole database.

I specially thank my loving partner Ms. Talia Garcia for helping me with the writing, her constructive criticism and advice in planning and organizing this research.

The author would like to express all his appreciation to his sister, Ofelia Madriz, for all her assistance in critical moments of this thesis, without her advice and technical expertise this thesis could not have been completed.

I would like to thank my parents for their constant trust and support during all my life, for teaching me the values of honesty and hard work, and for giving me the opportunity to study abroad and continue with my graduate studies. I dedicate this thesis to my parents, with whom I am eternally grateful.

Table of Contents

List of Figures

List of Tables

Chapter 1 - Introduction

1.1 Overview

Montreal is the third largest city in Canada and ranks second in seismic risk nationwide, after Vancouver. Most of its existing infrastructures are old, were built before any modern seismic design standard was available and have begun to deteriorate. Seismic risk analysis has been identified as a high priority by the Engineering Preparedness Centre of the Montreal Urban Community (MUC) and it is supported by the National Earthquake Hazard Program-East (Rosset, 2003).

Soft soil deposits can be a key factor in the seismic response of structures. Usually, damage associated with an earthquake decreases as a function of distance from the epicenter; however, this is not always the case when structures are located over unconsolidated deposits (Rosset, 2003). Soft soil deposits can affect the response of a structure in many ways: (Filialtrault, 2002):

1. Seismic loads may be amplified due to an increase in the predominant period of shaking and amplification of seismic waves.
2. The soil may loose its load-bearing capacity and liquefy, and
3. The soil may compact and result in differential settlements of the foundations.

The objective of this thesis is primarily to estimate seismic site response across the Island of Montreal. Current practice usually assigns an increase of 2 units on the MM (Modified Mercalli) scale for structures located over soft soil deposits as compared to structures founded on rock. Widely known examples of soil amplification are the San Francisco (1906) and Mexico City (1985) earthquakes. However, many other earthquakes exhibited similar amplification: Iran (1990), Philippines (1990), Northridge (1994), Kobe (1995), Armenia, Spitak Armenia (1998), Columbia (1999) and Turkey (1999) (Lacave et al., 1999).

Soft sediments are common along river valleys, which are also common locations for human settlements. This is the case for Montreal which is an island located in the St. Laurent River Valley. The soft soil deposits on the island are the result of a sequence of events starting with alternating periods of glaciation, followed by the emergence of the Champlain Sea, and finally by reworking and further deposits by the St. Laurent River and its secondary channels (Rosset, 2003).

Some regions of the Province of Quebec are located in zones of very high seismicity (Figure 1.0). Regions where the seismic activity is significant are: Western Quebec, the Charlevoix region and the Lower St. Laurent. Table 1 lists the most recent significant earthquakes that occurred in the three seismic regions. (Filiatrault, 2002).

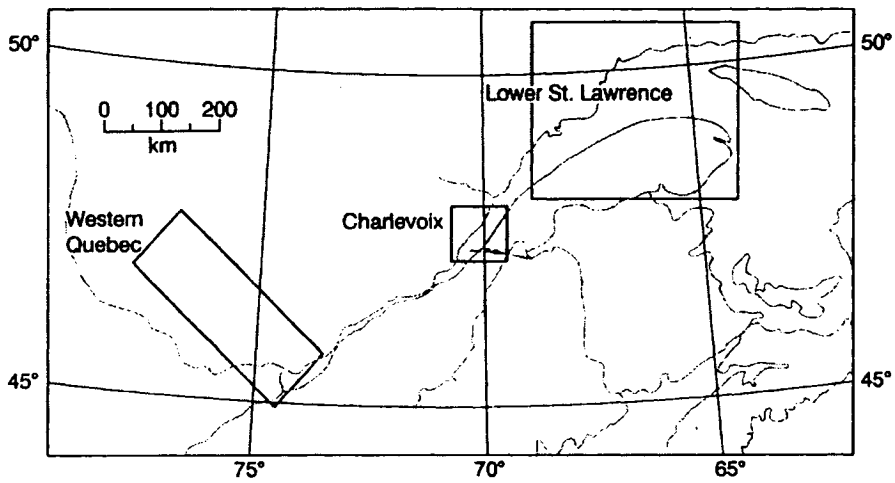

Figure 1.1: Seismicity of eastern Canada before 1987: western Quebec, Charlevoix, And the lower St. Laurent (Filiatrault, 2002)

Montreal is located in the Western Quebec seismic zone. The seismic activity in Western Quebec seismic zone seems to be distributed among two distinct strips that can be considered as two separate zones (Adams et al, 1989):

1. The first strip follows mostly the Ottawa River from Lake Témiscamingue to Ottawa, then expands south-west to Cornwall and eastward to Montreal. The

earthquakes along the strip are associated with an active fault zone along the Ottawa River.

2. The second strip is oriented north-northwest and covers an area from Montreal to the Baskatong Reservoir. The earthquakes occur more often and are of less intensity than in the first strip, but their origin is not clear.

Table 1-1: Major earthquakes in Eastern Canada from 1663 to 1994 (Filiatrault, 2002)

Region	Location	Year	Magnitude
Western Quebec	Montreal	1732	~ 6,0
		1816	~ 5,5
		1897 (2)	~ 5,5
	Ottawa	1861	~ 5,5
	Temiscamingue	1935	$M_L = 6,2$
	Cornwall-Massena	1944	$M_L = 5,7$
Charlevoix	Malbaie region	1663	~ 7,0
		1665	~ 5,5
		1791	~ 6,0
		1831 (2)	~ 5,0
		1860	~ 6,0
		1870	~ 6,5
		1924	~ 5,5
		1925	$M_L = 7,0$
	Saguenay	1988	$M_s = 6,0$
Lower St. Lawrence	-	-	-

The two strips are quite distinct in the North, but relatively similar around the Montreal area. The National Building Code of Canada (NBCC 1995) indicates that in Montreal a peak ground acceleration of 0.16g can be expected for a return period of 475 years (Filiatrault, 2002).

A pilot study, from July 2001 to July 2002, described the basic methodology developed for the microzonation of the island (Rosset et al., 2003).

The two main objectives of the project are as follows.

1. To estimate the soft soil response during an earthquake by applying a method that is fast, economical and useful in urban areas.
2. To create seismic microzonation maps for:
    a. The predominant frequency of resonance of the soil deposits, and
    b. The amplification of the peak ground acceleration.

Buildings may sustain some damage during earthquakes when the natural frequency of the ground motion coincides with the natural frequency of the structure. Resonance increases the swaying motion of the structure and given sufficient duration, will result in damage or destruction of the structure.

The microzonation methodology consists of field studies coupled with numerical models in zones where geotechnical data is available. Software analysis tools were developed to implement the methodology.

Field investigations are based on applying the spectral ratio H/V technique (also called ground ambient noise (GAN) technique) developed by Nakamura (1989). It uses horizontal and vertical components of microtremors produced by wind-structure interaction, traffic, and man-made vibrations. The procedure is based on the premise that the vertical component of the microtremors is not affected by soil condition while the horizontal are greatly affected.

The numerical approach consists of a one-dimensional analysis with SHAKE91 with input rock motions representative for the region. The analysis includes several input motions in order to cover a wide range of excitation periods. Appropriate geotechnical properties are crucial to estimate accurately the period of resonance and amplification factor. The *peak ground acceleration* (PGA) defined by SHAKE is used to determine the maximum horizontal forces to be expected during a large seismic event. The largest soil amplification effect occurs at the lowest natural frequency or frequency of resonance, also called the *characteristic site*. When soil thickness and average shear

wave velocity is known for each soil layer, the spatial variation in the characteristic site period can be modeled and mapped.

The island was divided into 70 square cells to record the microtremors and apply the field approach. The density of samples was higher in zones where thick and soft quaternary soils are present than in shallow areas with stiff soils. The numerical approach was applied when borehole data was available within 100m from sites with GAN measurements.

1.2 Outline of the Thesis

The thesis contains nine chapters and one appendix. Chapter 2 provides a short review of seismology principles relevant to microzonation. Chapters 3 and 4 describe the methodologies for field investigations and 1-D numerical modeling respectively. Chapter 5 describes the geology of the Island of Montreal. The results of the microzonation are presented in Chapter 6 followed by the recommendations to improve microzonation results in Chapter 7. The last chapter presents the final maps and conclusions. The appendix includes illustrative results for two locations in Montreal where the predominant frequencies are similar but the amplification factors are different. It would not be feasible to include in the appendix the detailed results for all the sites considered in the thesis.

Chapter 2 - Causes of Earthquakes and Definition of Seismic Waves

2.1 Introduction

To better understand Nakamura's method it is useful to review the causes of the earthquakes and the associated seismic waves. Most earthquakes occur in the earth's crust, between 60 and 100 km below the surface. There are two main theories that explain the origin of earthquakes (Filiatrault, 2002):

a. the theory of plat tectonics and
b. Reid's elastic rebound theory.

2.2 Theory of Plate Tectonics

The earth's crust is composed of several large plates that support continents and oceans and float on a viscous medium. The plates move from 1 to 15 cm every year. According to this theory, developed in the 1960's, the earthquakes arise at the boundaries of adjacent plates and occur when the resistance of the rock is exceeded. These conditions create a fracture and releases energy. The energy stored between two plates (fault) can be estimated, but the occurrence of its release is impossible to predict with current technology.

Three types of plate motions can be observed:

1. Transformation motions: the plates slide past each other;
2. Divergence motion: the plates diverge from each other, forming ocean ridges; and
3. Subduction motions: the plates converge on each other, causing the subduction of one plate under another.

2.3 Reid's Elastic Rebound Theory

Reid proposed his elastic rebound theory following the San Francisco Earthquake of 1906 (Figure 2.1). According to the theory, a fault is incapable of movement until enough strain has accumulated in the rock on either side due to gradual shifting of the earth's crust. The rock becomes distorted but holds its position. When the resistance of the rock is overcome the earth snaps back to the unstrained position, releasing energy and producing waves that travel through the earth in every direction.

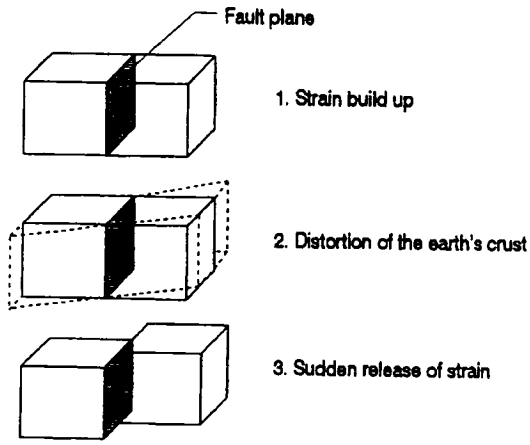

Figure 2.1 Reid's Elastic Rebound Theory (Filiatrault, 2002)

2.4 Intraplate Earthquakes

Not all earthquakes occur at plate boundaries. Intraplate earthquakes occur far from those boundaries. Records from intraplate earthquakes of large magnitude have been recorded (New Madrid with M_w=8.0, 1811 and South Carolina with M_w=7.6, 1886). Widespread damages were caused by these events over large distances since the seismic energy is transmitted more efficiently in the rigid continental crust than on the fractured crust near plate boundaries. Earthquakes near Montreal are intraplate earthquakes.

Areas that have been severely loaded, such as during an ice age or due to meteorite impact, will slowly return to their equilibrium position over time. Intraplate earthquakes occur when such readjustments occur. Charlevoix region is known to have such type of earthquakes.

Another possible cause of intraplate earthquakes is the accumulation of compressive stresses parallel to the St. Laurent. Those stresses are created by the separation of the Atlantic Ridge towards the West and the subduction of the Juan de Fuca Plate towards the East (Figure 2.2).

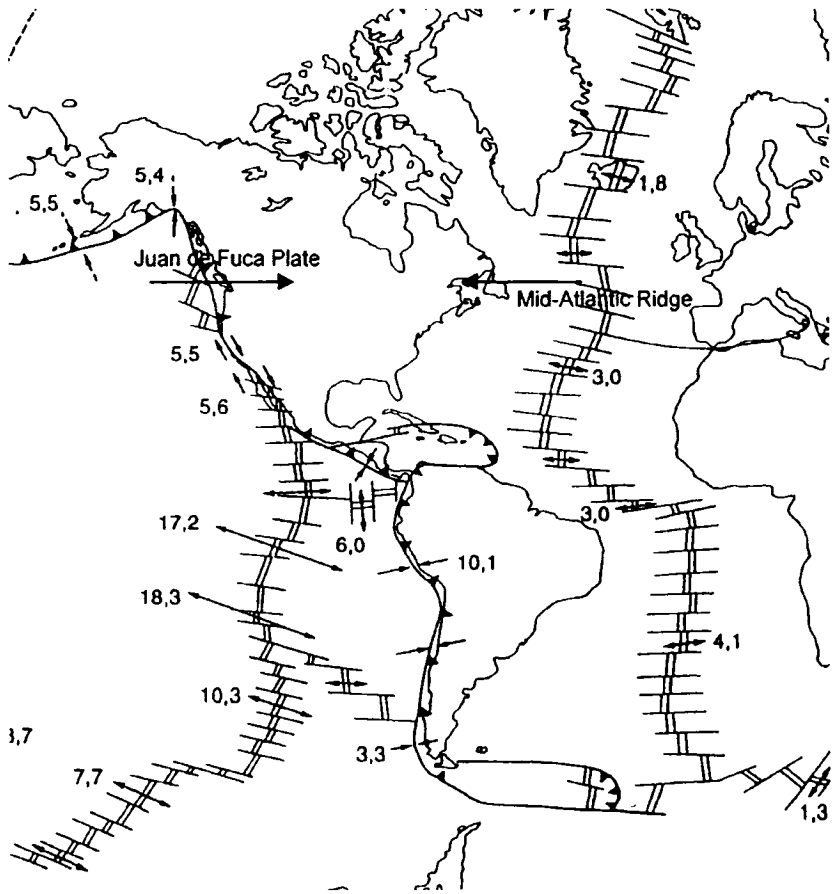

Figure 2.2 Relative Motions at Plate Boundaries (cm/year) (Earthquake design Course, Winter 2003)

Other sources of earthquakes that are not well documented and are generally of smaller magnitude are associated with: volcanic eruptions, collapses of mines, atomic explosions and stresses caused by large water reservoirs.

2.5 Seismic waves

Movement in the earth's crust causes vibrations which create seismic waves (Figure 2.3). There are various types of waves produced during an earthquake (Figure 2.4):

1. Body waves: waves travelling within the solid earth. The amplitude of this type of waves decreases as 1/d, where d is the distance to the focal point. There are two kinds of body waves:
    a. Primary waves (P-Waves): horizontal tension and compression waves, which travel in the direction of the wave front. They have a high frequency and are the first to reach a structure.
    b. Secondary waves (S-Waves): shear waves, which travel perpendicularly to the wave front. They have a lower frequency and greater amplitude than P-waves. From the engineering point of view, they are the most destructive waves.

2. Surface waves: waves travelling near the ground surface and having the ability to travel a great distance. Their amplitude varies as $1/\sqrt{d}$. There are two kinds of surface waves:
    a. Rayleigh waves: vertical waves travelling at the ground surface
    b. Love waves: horizontal waves travelling at the ground surface. This type of waves affect only layered solids.

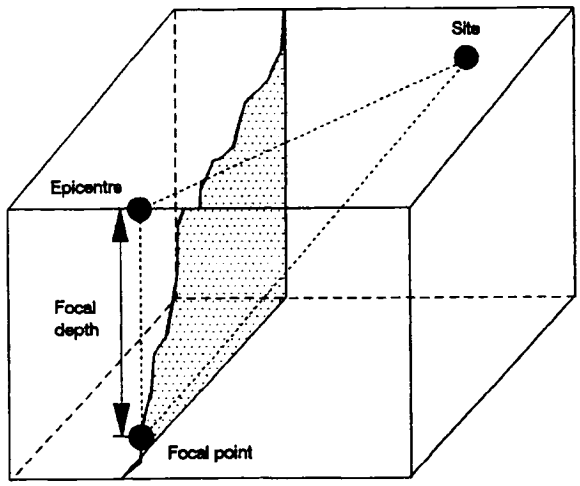

Figure 2.3 Seismic waves (Filiatrault, 2002)

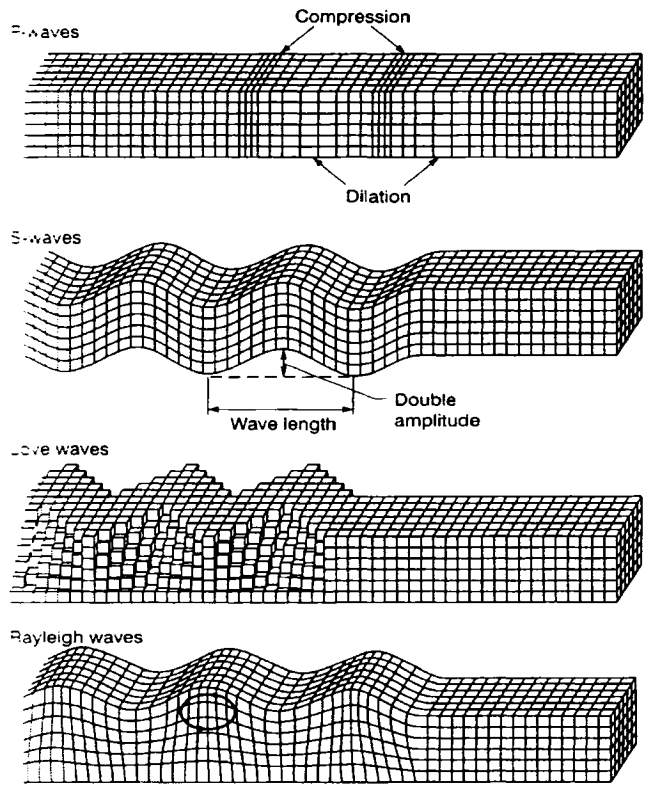

Figure 2.4 Deformations near the ground surface caused by seismic waves (Filiatrault, 2002)

A typical response spectra shows clearly the two body waves and the surface waves (Figure 2.5). The goal of the GAN technique is to calculate the frequency at which the maximum amplification takes place. The horizontal tremor may be considered to be amplified through multiple-reflections of the S-wave while the vertical tremor is comprised of multiple reflections of the P-wave (Nakamura, 1989).

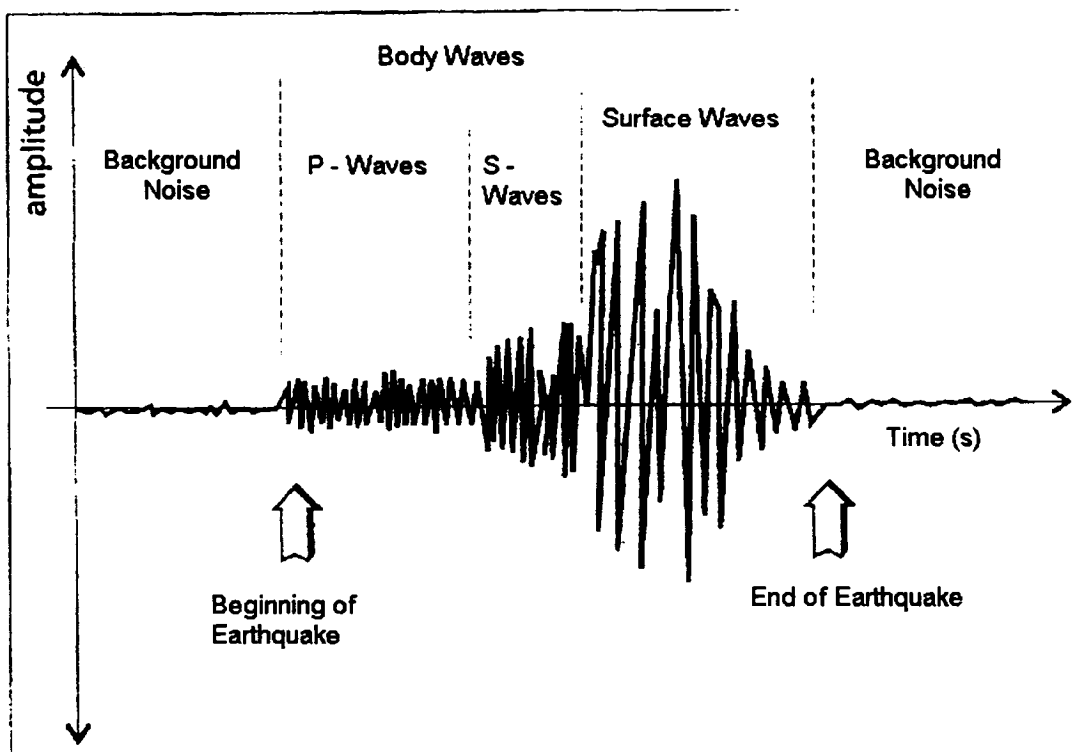

Figure 2.5 Typical Response Spectra (Earthquake Design Course CIVE 612, winter 2003)

Chapter 3 - Ground Ambient Noise (GAN) Technique

3.1 Introduction

Boring data is the best source of information on subsurface soil layers. The accurate representation of subsurface soil layers over a wide area requires a large number of boreholes and numerous analyses. Alternatively, microtremors can be used to identify the dynamic characteristics of surface layers. Most structures have a predominant frequency between 0.5 and 20 Hz; therefore, only microtremors with that frequency range will be considered in the analysis. This range comprises artificially induced microtremors, but they have to be small in amplitude in order to determine the characteristics of the surface layers. In consequence, measurements have to be carried out during periods when no single source of noise can dominate microtremors. Surveys are usually conducted at night time and when the wind is not too strong (Duval et al, 2004).

Nakamura (1989) developed a method to estimate the predominant frequency and the amplification factor from natural soil deposits from records of microtremors. The method is very popular for microzonation since it does not require data from actual seismic activity at the given site and at a reference site. Other existing techniques use microtremors to estimate the predominant frequency of a site, but the best results have been obtained with Nakamura's technique (Lermo and Chavez-García, 1994).

The response spectrum O*(f)* observed at a specific location is a function of wave motion radiation characteristic at the focal region F*(f)*, dynamic characteristic of the wave motion propagation up to the site T *(f)*, and the dynamic characteristics of the surface layers at the site S*(f)* (Nakamura, 1989).

Empirically, it has been observed that the seismic acceleration waveforms (O(f)) are very similar for different earthquakes at a given site (Figure 3.1). High frequency

tremors prevail (F(f), T(f)) when the magnitude of the earthquake is small and low frequencies prevail when the magnitude is large. Given that the observed seismic waveforms are similar for a given site, it implies that surface layer characteristics S(f) dominate, even when F(f) and T(f) are different. It can be concluded that the effect of the surface layer is the most critical factor for site response.

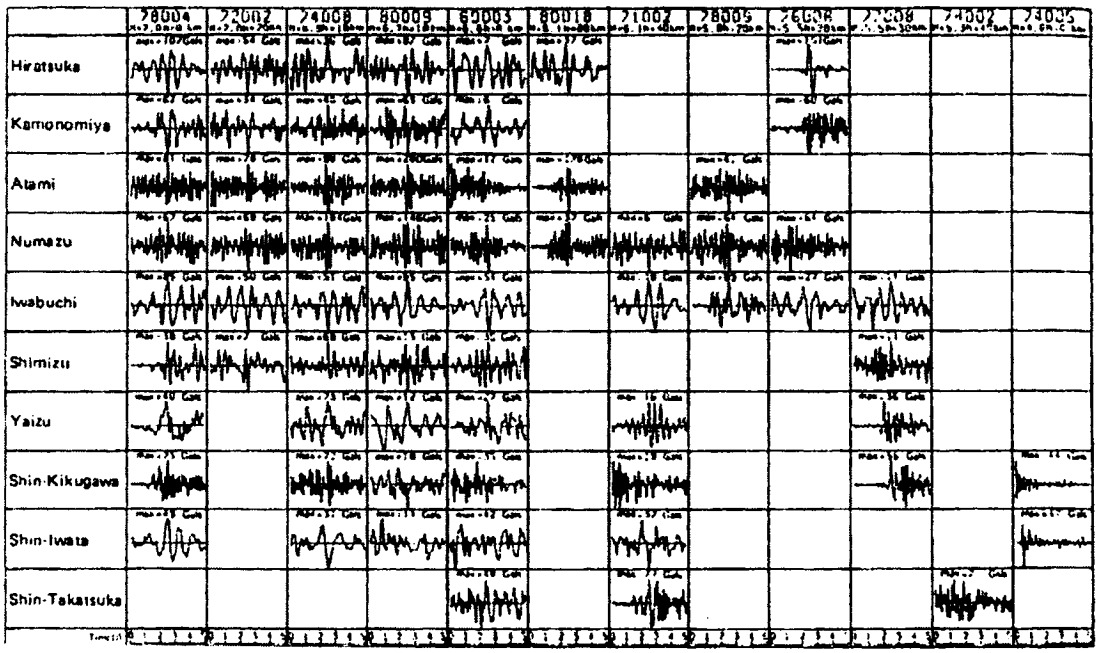

Figure 3.1 Difference in seismic waveform due to difference in earthquake and observation point (Nakamura, 1989).

3.2 Basic Concept of GAN Technique

Nakamura (1989) analyzed data from two locations in Japan where microtremor analysis had been done. By plotting the horizontal components of motion against frequency he concluded that a site specific frequency could not be found from a frequency analysis only. Microtremors consist of various wave forms. Figure 3.2 shows the ratio (H_S/H_B) of maximum motion between horizontal and vertical motions of earthquake for each observation location. A value of "1" is characteristic of a firm soil, which implies that the amplitude of the tremors is the same in all directions.

Nakamura's method relies in three main hypotheses (Rosset et al, 2002):

1- Ambient noise is generated by reflection and refraction of shear waves within superficial soil layers and by surface waves.
2- Local superficial sources of noise do not affect ambient noise at the level of the bedrock.
3- Soft soil layers do not amplify the vertical component of ambient noise. Therefore, the vertical component of the ambient noise has the same characteristics for the source ground motions and for the Rayleigh wave. On the other hand, the horizontal component has the same characteristics as the vertical component plus the effect of the surface layers.

The transfer functions for the horizontal and vertical components of the tremors are respectively defined as (Rosset et al, 2002):

$$S_E = \frac{H_S}{H_B} \qquad [3.1]$$

and

$$A_S = \frac{V_S}{V_B} \qquad [3.2]$$

Where H stands for the horizontal component, V stands for the vertical component and S and B stand for surface and basement responses (or strata) respectively for the tremor spectrum. The effect of Rayleigh waves is included in the surface waves, but not in the waves at the level bedrock.

Site effects that do not include source contributions are defined by S_m as (Rosset et al, 2002):

$$S_M = \frac{S_E}{A_S} \quad \leftrightarrow \quad S_M = \frac{H_S}{V_S}\frac{V_B}{H_B} \qquad [3.3]$$

Figure 3.2 shows the maximum (H/V) ratio for different earthquakes and locations. A value of "1" is related to rock or firm soil, since amplitudes are the same in all

directions. The ratio V_B/H_B becomes 1.0 for a wide frequency range and therefore (Nakamura, 1989),

$$\frac{V_B}{H_B} = 1.0 \quad \text{and} \quad S_M = \frac{H_S}{V_S} \qquad [3.4]$$

The value S_M is close to "1" in the frequency range of Rayleigh waves, and thus has a little effect on the estimated transfer function. Nakamura (1989) shows that S_M includes the effect to eliminate it.

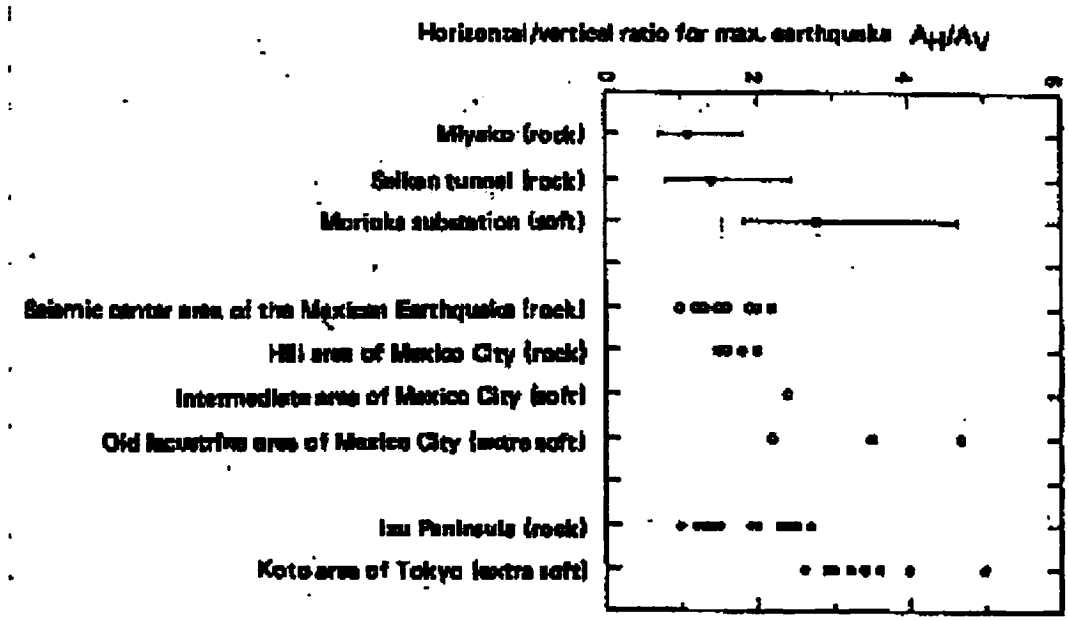

Figure 3.2: Ratio of maximum values between horizontal and vertical components of earthquake (Nakamura 1989)

Since H_S is affected by soft soil amplification, the source and the Rayleigh waves, and V_S is affected only by the latter two; S_m measure only the amplification of the soft soil. Therefore, the amplification of the horizontal motion by surface layers can be estimated from the ratio of the horizontal and vertical maximum values of the response spectra measured on the surface (Nakamura 1989).

Hence, it is possible to estimate the dynamic characteristics of surface layers using only microtremors observed on the surface by recording the ambient noise with a single 3-component seismometer, one vertical (up and down) and two horizontal (north-south and east-west).

3.3 Instrumentation and Data Processing Software

The field surveys were carried out using an ORION seismometer from Nanometrics LTD. connected to a Guralp CMG-40T velocimeter (Figure 3.3). Specifications for both instruments are shown in Table 3.1. The velocimeter meets the requirements for rapid installation, minimum set up time and optimum sensitivity and dynamic range.

Table 3-1: System specifications for the transducer GURALP CMG-T$) and the seismometer ORION (Modified from Rosset, 2003)

System Specifications	
Type of sensor	Triaxial velocimeter Guralp CMG-T40
Corner Frequency	0.033 Hz
Flat Response	0.03 to 50 Hz
Digitizer Resolution	24 bit
Sampling Rate	100 Hz
Dynamic Range	132 dB
Anti-aliasing filter	3rd order Bessel -3 dB at 3.7 kHz
Hard Drive	2 GBytes
ORION includes a built-in LCD display that provides information on instrument status and the incoming signal for the three components.	

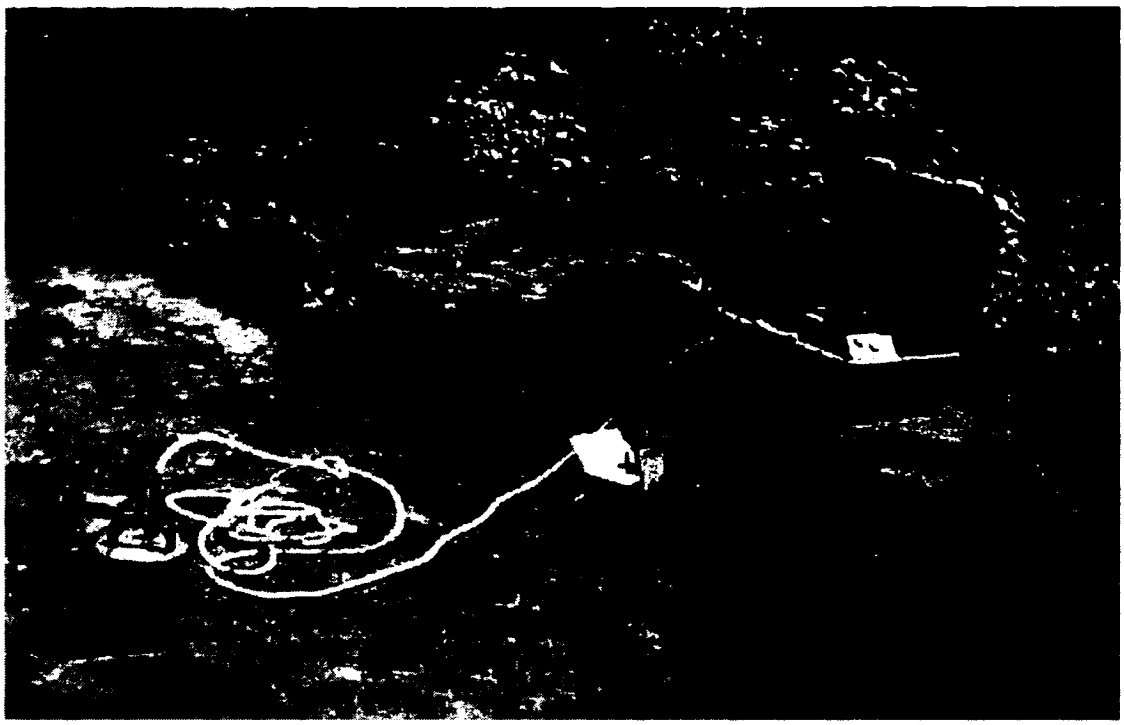

Figure 3.3: Seismometer ORION from Nanometrics LTD. connected to a velocimeter Guralp CMG-40T.

A user interface, SPCRATIO, was developed using Matlab (version 5.3 and updated in version 6) to process the data (Rosset, 2002; Gozenbach, 1997). A flowchart summarizes the procedures included in the software (Figure 3.4). The left side shows the steps of the spectral analysis from the ambient noise records to the H/V ratio. The right side illustrates: the recorded signal, the Fourier Spectra of the selected portion for the analysis, and the spectral ratio based on the segmented signal. The last figure at the bottom is the representation of the average and individual H/V ratios on a logarithmic scale.

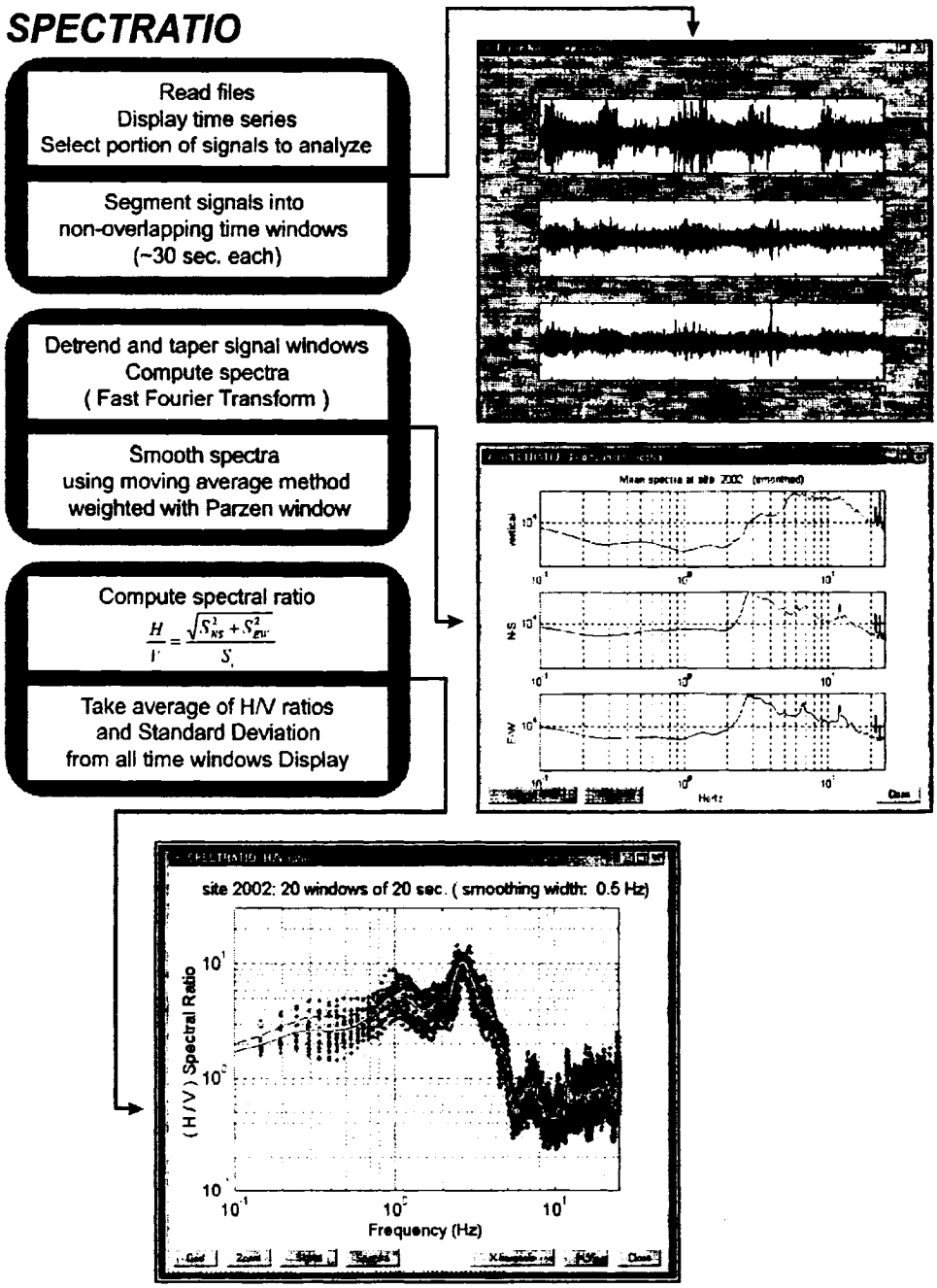

Figure 3.4: Procedure for calculating the H/V ratio from records of ground ambient noise (Rosset et al, 2002).

Chapter 4 - Numerical Approach – SHAKE®

4.1 Introduction

Shake® is the most widely used software for computing the seismic response of horizontally layered soil deposits. It provides estimates of the modes of resonance and amplification factor of soil deposits when appropriate soils properties and input rock motions are available. The results obtained from the numerical approach are used to validate the frequency found with the empirical approach (GAN method). The program computes the response of a semi-infinite horizontally layered soil deposit overlying a uniform half space subjected to vertically propagating shear waves. The computer program was originally written by Schnabel and Lysmer (1970).

The program has undergone many modifications to make SHAKE user friendly and usable with a personal computer. A few examples are: Shake91, Shakedit, ShakEdit32 or ProSHAKE. For the purpose of this project, Shake91 was used in conjunction with a custom program called Excel-Shake, for inputting the data (De la Puente and Rosset, 2002). The user is able to perform analyses step by step or in a batch mode by selecting a group of sites and input ground records.

4.2 Description of the Program SHAKE91

The soil profile is idealized as a system of homogeneous, visco-elastic sublayers of infinite horizontal extent. The algorithm is based on the solution to the wave equation, which was adapted for transient motions using the Fast Fourier Transform. An iterative procedure is used to account for the nonlinear behaviour of the soils, which is explained later in this chapter.

Input motions can be specified at the top of any layer within the soil profile or at the

bedrock, which is the usual case. Input bedrock motions should be representative of the study area. Typically, one would use the nearest and most recent seismic records for the region. Since no strong ground motions are available for Montreal, and since the source mechanisms of earthquakes are not completely known different seismic scenarios are required.

The program performs the analysis by using the following steps (Schanbel et al, 1972):

1. Determine the ground motions likely to develop at the site. The maximum acceleration, predominant period, and effective duration are the most important parameters of earthquake motion. Design ground motions with the desired characteristics can be selected from previous earthquakes or artificially generated.
2. Determine the dynamic shear modulus and damping ratio of the soil deposits.
3. A one dimensional analysis can be used to compute the response of the soil deposits to base rock motions if the soil profile is essentially horizontal.

An equivalent linear procedure is used to account for the nonlinearity of the soils using an iterative procedure with shear modulus and damping ratios that are compatible with the equivalent uniform strain induced in each sublayer. The initial input properties are the maximum shear modulus for each sublayer and a low value for the damping ratio.

The following assumptions are incorporated in the analysis (Schnabel et al, 1972):

1. The soil system extends infinitely in the horizontal direction
2. Each sublayer, m, is defined by its shear modulus, G_m, damping ratio, β_m, total unit weight, γ_{tm} (or corresponding mass density, ρ_m) and thickness, h_m (Figure 4.1). All the properties are independent of frequency.

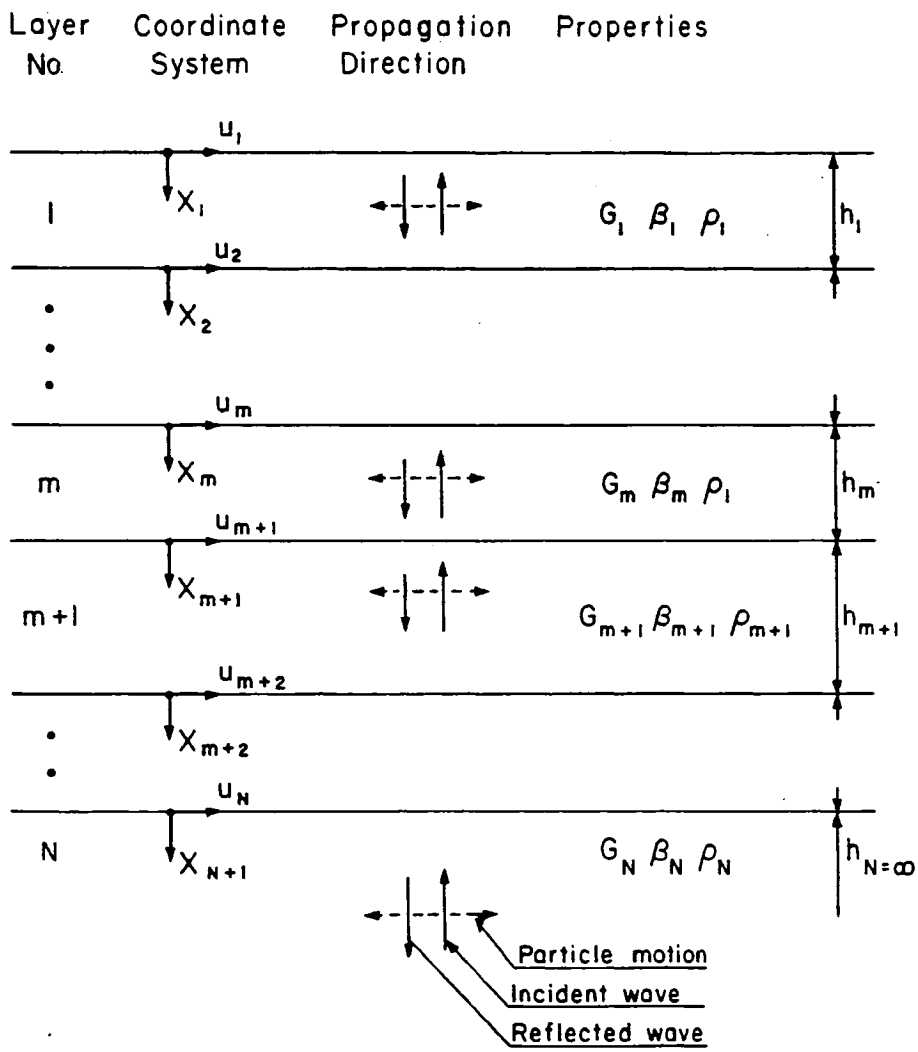

Figure 4.1: One-dimensional System (Schnabel et al, 1972.)

3. The response of the system is calculated considering vertically propagating shear waves from the underlying rock formation. The shear waves are propagating vertically from the underlying bedrock because inclined incoming seismic waves are refracted to a near vertical direction due to the decrease in velocities of waves in surface deposits.

4. The shear waves are specified as acceleration ordinates at equally spaced time intervals. (Cyclic repetition of the acceleration time history is implied in the solution).
5. The strain dependency of the shear modulus and damping ratio is accounted for by an equivalent linear procedure based on the equivalent uniform strain for each sublayer. The ratio of the equivalent uniform shear strain divided by the calculated maximum strain is specified by the user.

The program can compute the responses for a design ground motion specified anywhere in the system. The program also incorporates nonlinear soil behavior, the effect of the elasticity of the base rock and systems with variable damping.

4.3 One-dimensional Shear Wave Propagation

The system consists of N horizontal layers which extend to infinity in the horizontal direction and has a halfspace as the bottom layer. Each layer is homogeneous and isotropic and is characterized by its thickness, h, density, ρ, shear modulus, G, and damping factor, β, and viscosity, η.

The propagation of harmonic shear waves produces horizontal displacements (Schanbel et al, 1972)

$$u = u(x, t) \qquad [4.1]$$

which must satisfy the equation:

$$\rho \frac{\partial^2 u}{\partial t^2} = \frac{G \partial^2 u}{\partial x^2} + \eta \frac{\partial^3 u}{\partial x^2 \partial t} \qquad [4.2]$$

The harmonic displacement with frequency ω can be written in the form:

$$u(x,t) = U(x) \bullet e^{i\omega t} \qquad [4.3]$$

Substituting equation [4.3] into equation [4.2] results in an ordinary differential equation:

$$(G + i\omega\eta)\frac{\partial^2 U}{\partial x^2} = \rho\omega^2 U \qquad [4.4]$$

which has a general solution

$$U(x) = Ee^{ikx} + Fe^{-ikx} \qquad [4.5]$$

in which

$$k^2 = \frac{\rho\omega^2}{G + i\omega\eta} = \frac{\rho\omega^2}{G^*} \qquad [4.6]$$

where k is the complex wave number and G^* is the complex shear modulus. The critical damping ratio is related to the viscosity η by:

$$\omega\eta = 2G\beta \qquad [4.7]$$

Since G and β are almost constant for the frequency range of interest G^* can be expressed in terms of the critical damping ratio instead of the viscosity:

$$G^* = G + i\omega\eta = G(1 + 2i\beta) \qquad [4.8]$$

where G^* can be assumed to be independent of the frequency ω.

From [4.3] and [4.5], the wave equation for a harmonic motion of frequency ω, is

$$u(x,t) = Ee^{i(kx+\omega t)} + Fe^{-i(kx-\omega t)} \qquad [4.9]$$

where the first term is the incident wave traveling in the negative x-direction (upwards), and the second, is the reflected wave traveling in the positive x-direction (downwards) (Figure 4.1).

Using a local coordinate system for each layer (Figure 4.1), the displacements at the top and bottom of layer m are (Schnabel et al, 1972):

$$u_m(X=0) = (E_m + F_m)e^{i\omega t} \qquad [4.10]$$
$$u_m(X=h_m) = (E_m e^{ik_m h_m} + F_m e^{-ik_m h_m})e^{i\omega t}$$

The shear stress on a horizontal plane is:

$$\tau(x,t) = G\frac{\partial u}{\partial x} + \eta\frac{\partial^2 u}{\partial x \partial t} = G^*\frac{\partial u}{\partial x} = ikG^*(Ee^{i(kx+\omega t)} + Fe^{-i(kx-\omega t)})e^{i\omega t} \qquad [4.11]$$

and the shear stresses at the top and bottom of layer m are:

$$\tau_m(X=0) = ik_m G_m^*(E_m - F_m)e^{i\omega t} \qquad [4.12]$$
$$\tau_m(X=h_m) = ik_m G_m^*(E_m e^{ik_m h_m} - F_m e^{-ik_m h_m})e^{i\omega t} \qquad [4.13]$$

The shear stresses and the displacements have to be continuous, that means that:

$$u_{m+1}(X=0) = u_m(X=h_m)$$
$$(E_{m+1} + F_{m+1})e^{i\omega t} = (E_m e^{ik_m h_m} + F_m e^{-ik_m h_m})e^{i\omega t}$$
$$E_{m+1} + F_{m+1} = E_m e^{ik_m h_m} + F_m e^{-ik_m h_m} \qquad [4.14]$$

and

$$\tau_m(X = h_m) = \tau_{m+1}(X = 0)$$

$$ik_m G_m^*(E_m e^{ik_m h_m} - F_m e^{-ik_m h_m})e^{i\omega t} = ik_{m+1} G_{m+1}^*(E_{m+1} - F_{m+1})e^{i\omega t}$$

$$\frac{k_m G_m^*}{k_{m+1} G_{m+1}^*}(E_m e^{ik_m h_m} - F_m e^{-ik_m h_m}) = E_{m+1} - F_{m+1} \qquad [4.15]$$

Combining equation [14] and [15] will lead to the amplitudes of the incident and reflected wave in layer m+1, expressed in terms of the amplitudes in layer m:

$$E_{m+1} = \frac{1}{2} E_m(1 + \alpha_m)e^{ik_m h_m} + \frac{1}{2} F_m(1 - \alpha_m)e^{-ik_m h_m} \qquad [4.16]$$

$$F_{m+1} = \frac{1}{2} E_m(1 - \alpha_m)e^{ik_m h_m} + \frac{1}{2} F_m(1 + \alpha_m)e^{-ik_m h_m} \qquad [4.17]$$

where

$$\alpha_m = \frac{k_m G_m^*}{k_{m+1} G_{m+1}^*} = (\frac{\rho_m G_m^*}{\rho_{m+1} G_{m+1}^*}) \qquad [4.18]$$

The α_m is called the complex impedance ratio, which is independent of the frequency.

At the surface, $X_1=0$, there are no shear stresses, $\tau_1=0$; therefore, $E_1=F_1$. Starting at the surface and by repeating the use of the formulas [4.16] and [4.17], the following relationship is found (Schnabel et al, 1972):

$$E_m = e_m(\omega)E_1 \qquad [4.19]$$

$$F_m = f_m(\omega)E_1 \qquad [4.20]$$

Where e_m and f_m are the amplitudes for the case E1=F1=1. They can be determined by equations [4.16] and [4.17].

The transfer function of the displacements between layer m and n, $A_{n,m}$, can be found

by:

$$A_{n,m}(\omega) = \frac{e_m(\omega) + f_m(\omega)}{e_n(\omega) + f_n(\omega)} \qquad [4.21]$$

The strains and accelerations can be derived from the displacement function u(x, t). For the acceleration:

$$\ddot{u}(x,t) = \frac{\partial^2 u}{\partial t^2} = -\omega^2 (Ee^{i(kx+\omega t)} + Fe^{-i(kx-\omega t)}) \qquad [4.22]$$

and for the strains:

$$\gamma = \frac{\partial u}{\partial x} = ik(Ee^{i(kx+\omega t)} - Fe^{-i(kx-\omega t)} \qquad [4.23]$$

The microzonation shows the variation in seismic response as a function of the soil profile and identifies locations where motions may be amplified to a level which could damage existing buildings or other structures. Specific ground conditions may result in resonance and large amplifications of the seismic signal.

4.4 Reference earthquake records

The earthquake motions used as input for SHAKE for this project are those selected by Rosset, (2003). These consist of five different earthquake records and synthetics records provided by Atkinson and Beresnev (1999) (Table 4.1). Earthquakes are scaled to a PGA value of 0.16g to be consistent with the National Building Code of Canada (NBCC, 1985) (Rosset, 2003).

The Saguenay earthquake is characterized by a high frequency or low period (LP) (Figure 4.2). Five stations that recorded the earthquake were selected, which are

located around the epicenter at distances ranging from 50 to 150 km (Table 4.2). Montreal is located at a distance of 300 km from the epicenter. (Rosset, 2003)

Table 4-1: Principal characteristics of earthquakes considered as input ground motion in the analysis in SHAKE 91 (modified from Rosset, 2003).

Event	Date	Coordinates	Depth	Magnitude	Faulting type
Saguenay	1988/11/25 23:46:04	48.117 N. 71.183 W.	29 km	M_N=6.5 M_S=6.0 M_B=5.7	Thrust with a s-s component
Kocaeli	1999/08/17 03:02	40.70 N. 29.91 E.	16 km	M_W=7.4 M_S=7.8	Right-lateral s-s
Duzce	1999/11/12 16:57:20	40.768 N. 31.148 E.	14 km	M_W=7.1 M_L=7.2 M_S=7.3	Right-lateral s-s
Imperial Valley	1940/05/18 08:37	32.73 N. 115.50 W.	≈10 km	M_W=6.9	Right-lateral s-s
Loma Prieta	1989/10/18 00:05	37.040 N. 121.877 W.	17 km	M_W=6.9 M_L=6.7 M_S=7.1	Right-lateral s-s and reverse slip

The Kocaeli and Duzce earthquakes (Table 4.1) correspond to the second scenario, with earthquake motions with intermediate periods (IP) (Figure 4.2 and 4.3). The events are associated with intraplate tectonic movements which are similar to the Western Quebec seismic zone movements (Rosset, 2003).

The third scenario corresponds to high period (HP) earthquakes. Two earthquakes from California with similar periods have been chosen: Imperial Valley earthquake (1940) and Loma Prieta earthquake (1989) (Table 4.2). Their accelerograms and response spectra are shown in Figure 4.2 and 4.3 (Rosset, 2003).

Table 4-2: List of seismic stations selected for each of the seismic events (modified from Rosset, 2003).

Event	Station ID	Latitude	Longitude	Type	Epicentral distance (km)
Saguenay	Chicoutimi-Nord	48.4902 N.	71.0123 W.	Rock	43
	St-André	48.3248 N.	71.9917 W.	Rock	64
	La Malbaie	47.6553 N.	70.1527 W.	Rock	92
	Tadoussac	48.1432 N.	69.7189 W.	Rock	109
	Québec	46.7782 N.	71.2749 W.	Rock	150
Kocaeli	Gebze, Kocaeli	40.820 N.	29.440 E.	Rock	42
Duzce	Murdunu, Duzce	40.463N.	31.182 E.	Rock	34
Imperial Valley	Diamonds Hts, 1940	--	--	Rock	--
Loma Prieta	Belmont, BES, 1989	37.518 N.	122.267 W.	Rock	64

The last scenario consists of synthetic earthquakes (Figure 4.4), made specifically for the Montreal area (Atkinson et al, 1998). This scenario is referred to as the Broad Period Scenario (BP).Since the synthetic records are for stiff rock, the input motions have to be placed at the top of the basal till formation. Two sets composed of 4 signals each were selected for the analysis. The first set consists of a magnitude 6 earthquake 30 km from the epicenter and the second set is a magnitude 7 earthquake, at an epicentral distance of 70 km (Rosset, 2003).

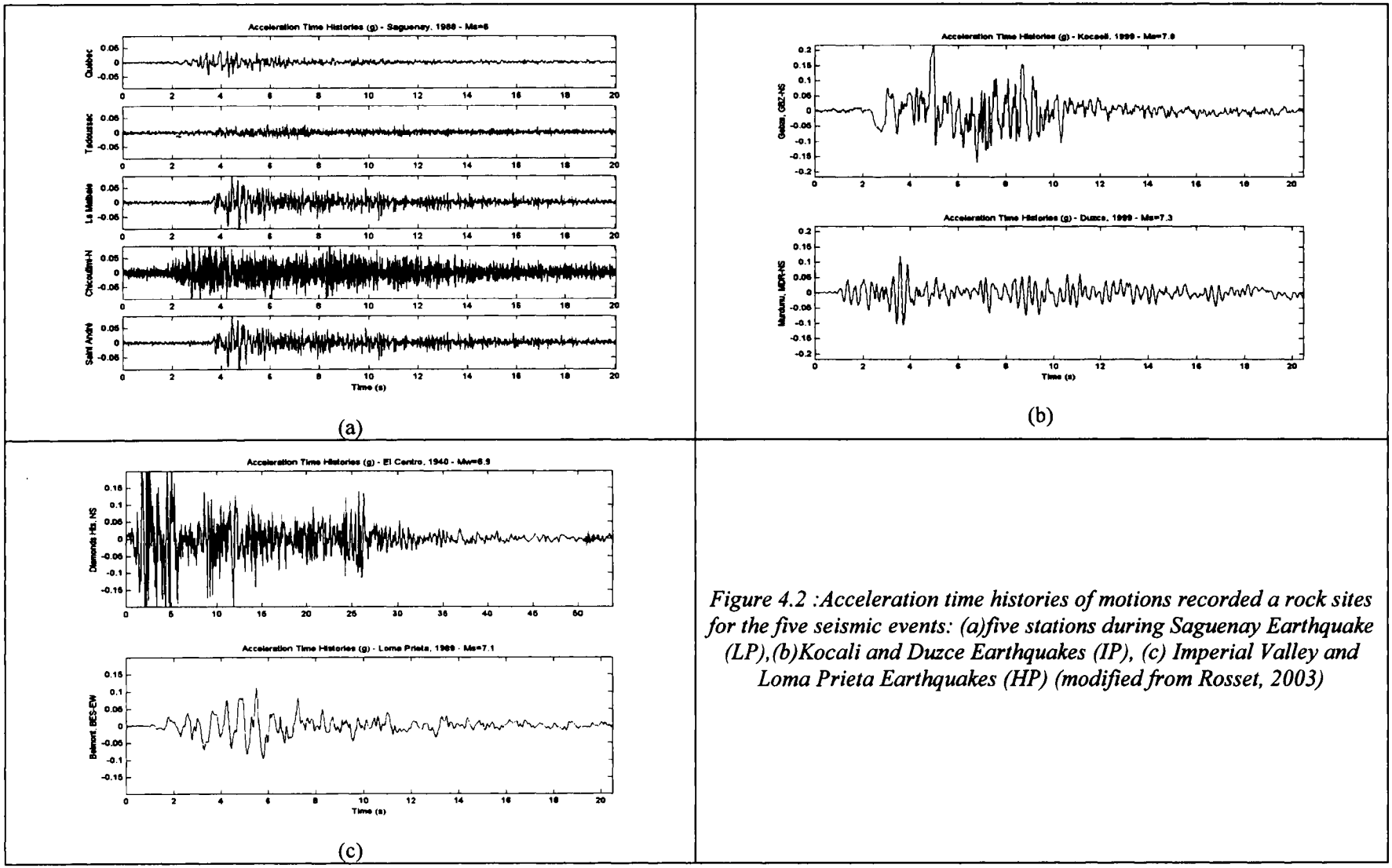

Figure 4.2 :Acceleration time histories of motions recorded a rock sites for the five seismic events: (a)five stations during Saguenay Earthquake (LP),(b)Kocali and Duzce Earthquakes (IP), (c) Imperial Valley and Loma Prieta Earthquakes (HP) (modified from Rosset, 2003)

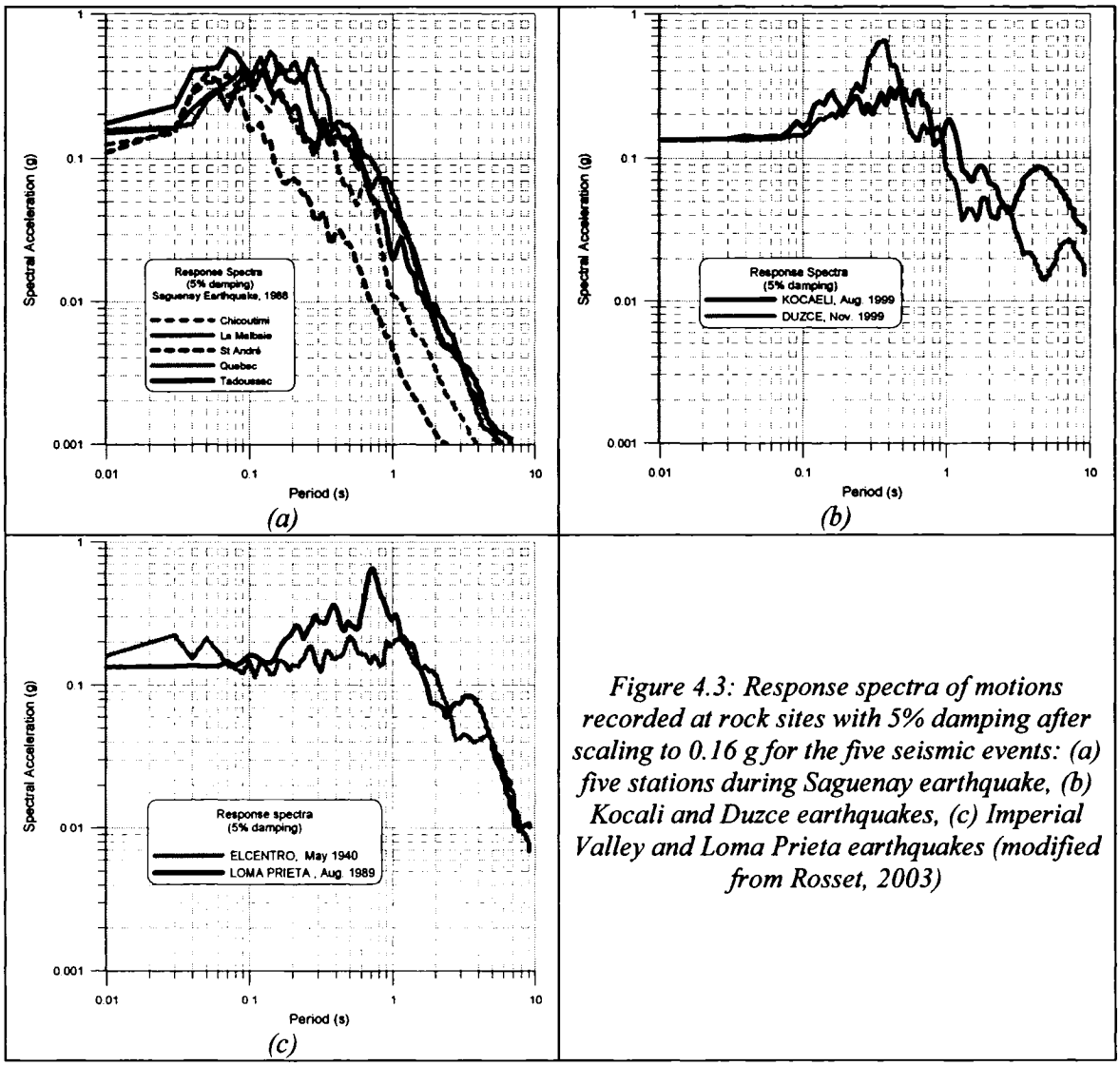

Figure 4.3: Response spectra of motions recorded at rock sites with 5% damping after scaling to 0.16 g for the five seismic events: (a) five stations during Saguenay earthquake, (b) Kocali and Duzce earthquakes, (c) Imperial Valley and Loma Prieta earthquakes (modified from Rosset, 2003)

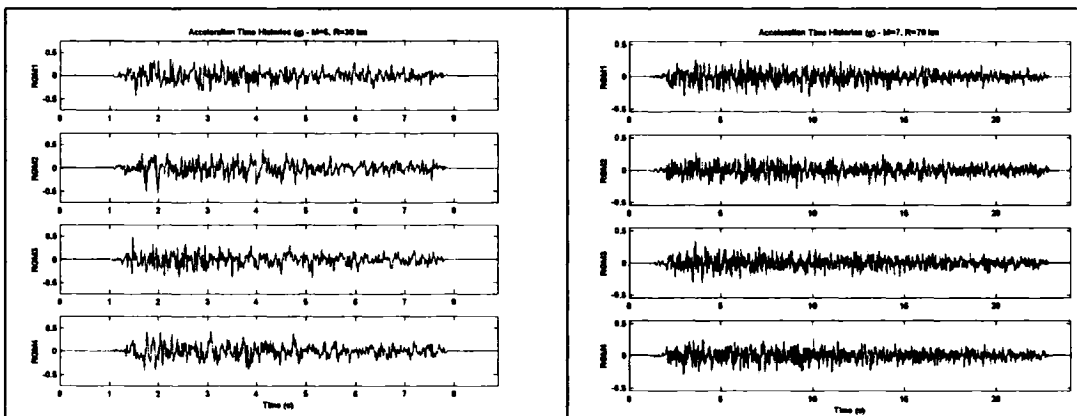

(a)

(b)

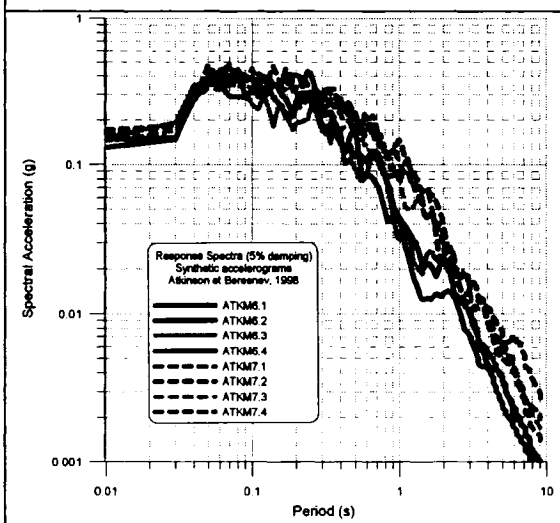

(c)

Figure 4.4 : : Input Ground Motions for the Broadband Period scenario. Simulated signals (in g) for the (a) M=6, d=30 km and (b) M=7, d=70 km. (c) shows the response spectra with 5% damping after scaling to 0.16 g (Rosset, 2003)

Chapter 5 - Quaternary Deposits of Montreal

5.1 General Geology of Montreal

A basic knowledge of geological periods affecting the Montreal area is useful in characterizing the properties of surface deposits. Information on soil properties are obtained from available test results and from the literature. A compilation of the properties is used as a guide for the input database for Shake.

The Montreal area is underlain predominantly by sedimentary rocks belonging to the upper Cambrian and Ordovician series, which are mainly Limestone of Trenton and Utica Shale resting on the Precambrian basement. Table 5.1 summarizes the formation of soils in Montreal according to time period (Prest et al, 1962).

The soils that overlie the bedrock formations of the island of Montreal were formed during the Wisconsinan glacial event of the Quaternary period and of more recent deposits (Prest et al, 1962). Some rocks off the island are Precambrian and range in age from 3500 million to 600 million years. However, these rocks are covered mainly by younger sedimentary deposits. An occurrence of a Precambrian ultramafic igneous rock was observed west-northwest of Mont Royal. This occurrence was the hilltop of the old basement surface that was covered with sandy, muddy and limy sediments during the Palaeozoic era (Prest et al, 1977). The sediments, mainly of Cambrian and Ordovician age, became the sandstone, shale, limestone and dolomite that now make up the main part of the island and its surroundings (Prest et al, 1962).

Mont Royal is a stock of alkaline igneous rock and it is part of a chain of hills known as the Montregian hills. The Montregian intrusions were emplaced 120 million years ago (Prest et al, 1977).

Table 5-1: Geological Time and Rock Units – Montreal Area (Prest, 1977)

TABLE 1
GEOLOGICAL TIME AND ROCK UNITS - MONTREAL AREA
(not to scale; see "years" column)

EON	ERA	PERIOD	STAGE	SUBSTAGE	YEARS B.P.[1]	GEOLOGICAL UNIT
PHANEROZOIC	CENOZOIC	QUATERNARY	HOLOCENE (Recent)	(Present) Postglacial	0	Bog, pond, river deposits
			PLEISTOCENE	WISCONSINAN (Glacial)	10 000	Champlain Sea deposits
					12 500	Fort Covington Till
					25 000	Middle-till complex
					55 000	Malone Till
					70 000	
					125 000	
				SANGAMON (Interglacial)	250 000	(deposits presumably removed by successive glaciations and erosion)
				(Other glacials and interglacials)	1.8 million	
		TERTIARY			6.5 million	
	MESOZOIC	CRETACEOUS			135 million	Monteregian intrusives
		JURASSIC			195 million	
		TRIASSIC			225 million	
	PALEOZOIC	PERMIAN			280 million	
		PENNSYLVANIAN			325 million	
		MISSISSIPPIAN			345 million	
		DEVONIAN			395 million	Limestone blocks in breccia
		SILURIAN			440 million	
		ORDOVICIAN				Trenton, Black River, Chazy, Beekmantown — Mainly limestone, dolomite and shale
		CAMBRIAN			505 million	
					570 million	Potsdam sandstone
(PRECAMBRIAN)	PROTEROZOIC				2500 million	Anorthosite - (in Cartierville) Granitic and other gneisses, schist, crystalline limestone, slate, etc. - (in Oka area and the Laurentians to the north) Some of these rocks have been folded and metamorphosed several times)
	ARCHEAN[2]				3700 million	(oldest dated rocks in the world)
					4500 million	(presumed age of the earth)

[1] B.P.-"Before Present." The ages given are those generally accepted by the Geological Survey of Canada; they are based on a variety of radiometric-age determinations (^{14}C, K/Ar, Pb/Sr, U/Th/Pb) and partly on biochronological evidence.

[2] Subdivided by some authors into Pre-Archean and Archean, the latter being applied to the time of dated rocks only.

There is little information about the limestone of Trenton and the Shale of Utica. The limestone consists of thin bioclastic shelly layers usually separated by thin layers of clays, arranged in coarsening and shallowing upwards cycles deposited on a wide

carbonate ramp. The Utica Shale is a soft rock made up of thin layers of organic rich sediments interrupted by several light coloured layers (Rosset, 2003).

The main mechanical properties of the Limestone of Trenton and Shale of Utica are summarized in Table 5.2.

Table 5-2 Unit weight and S-wave velocity for bedrock formations (Rosset, 2003).

	Unit Weight (Kg/m^3)			S-wave Velocity (m/s)		
	Min	Max	Mean	Min	Max	Mean
Limestone of Trenton	2620	2777	2730	-	-	2300
Shale of Utica	2640	2710	2670	-	-	2100

5.2 Glacial Deposits

All surface deposits in the Montreal Island are considered to be of Wisconsinan age. The oldest soil deposit is considered to be a lodgement of till deposited by glaciers during the Laurentide and Appalachian ice age which moved south-westward up the St. Laurent River valley. Overlying this, lake glacial deposits and ice contact deposits are present. When the ice started melting, ice flowed along the St. Laurent lowland and a thin layer of till with a layer of clay content was deposited (Fulton, 1989). The deposits resemble the ones found in New York State. The glacial deposits found on the Island of Montreal, starting from the older to the younger, are named Malone till, Middle till, and Fort Covington till.

5.2.1 Malone till Deposit

The deposition of all the older tills and ice contact deposits occurred during the last part of the Wisconsinan glacial stage. The glacier advanced south-westward up the St. Laurent valley, passed into the lower Great Lakes basins and reached its terminus south of the basins. The ice from the St. Laurent region was fed by ice from the north.

At the end of this glacial period the direction of the ice flow shifted to the south-east (Prest et al, 1977).

The Malone till in the Montreal area is well graded, it is generally stony and has a variable silty to sandy matrix. The clay-size fraction is lower than expected in view of the glacier (Prest et al, 1962). The stones range in size from tiny pebbles to boulders. Generally the boulders are limestone or dolomite derived from the local lowland strata. Usually, it is located directly on top of the bedrock and is commonly 1 to 3 m thick. Laboratory and *in situ* test results are shown in Figure 5.1. Blow counts from the standard penetration tests are usually higher than 30 blows/ft. The unit weight ranges from 2160 to 2480 Kg/m^3 and the average strength, from 320 to 430 KN/m^2 (Rosset, 2003). Malone till has a water content below optimum and therefore can be used as a backfill. It is practically impossible to compact this type of till when the optimum water content is reached (Prest et al, 1977). For those reasons Malone till could be considered equivalent to bedrock when confined and not overly wet (Rosset, 2003).

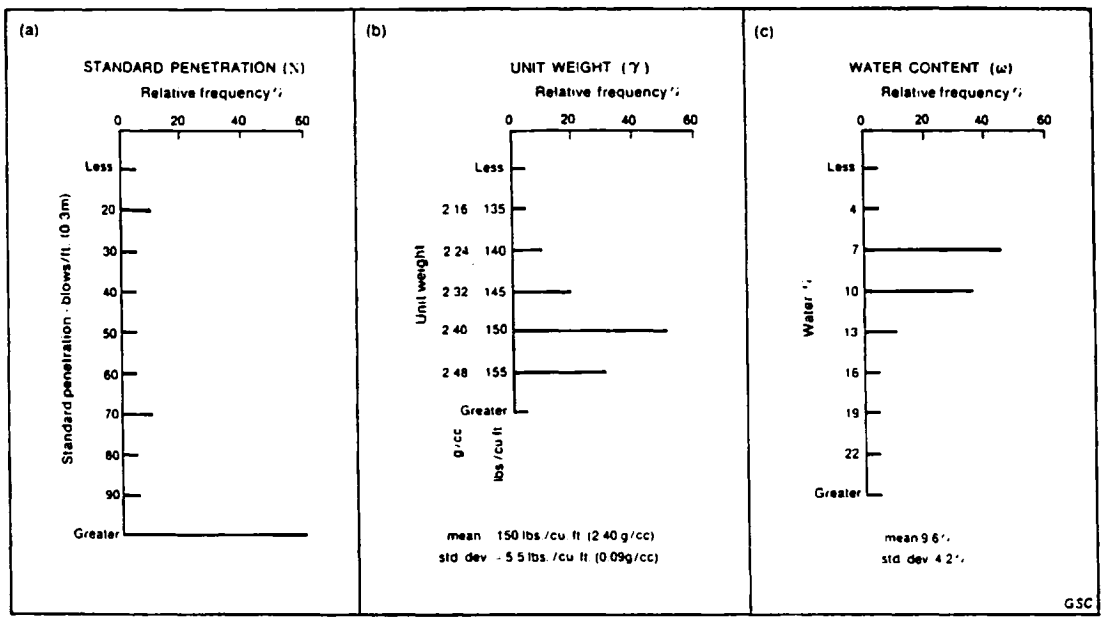

Figure 5.1: In-situ Properties of Malone Till. (Prest, 1977)

5.2.2 Interstadial Episode and Middle Till Complex

The Interstadial episode occurred during the retreat of the Malone ice. Mont Royal was above the glacial surface as a nunatak (a hill or mountain completely surrounded by glacial ice). Around Mont Royal, especially on the south west side, gravel and sandy sediments were deposited from meltwaters (Prest et al, 1977).

Some of the meltwaters found their way into crevasses carrying a mix of sediments, including gravel, sand and till. A tunnel carried meltwater, from the Malone ice, and deposited sand and gravel in Dorval, forming an esker (a long narrow ridge or mound of sand, gravel and boulders deposited by a stream, beneath the stagnant glacier) (Prest et al, 1977).

It is believed that glacier ice, glacial streams and glacial lakes were present in Montreal at some point. The glacier started to melt and the ice margin retreated from New York City up to the Hudson-Champlain valley and across the St. Laurent lowland creating a lake, which drained eastward to Maine and New Brunswick (Prest et al, 1977).

The ice front must have fluctuated in the glacial lake as several layers of till were deposited in the Montreal area. Therefore, after the ice withdrew from Lake Champlain and receded to the Montreal area, a short-lived glacial lake occupied much of the St. Laurent valley that discharged southward via the Lake Champlain Hudson valley. The sea could not invade the St. Laurent lowlands because ice was blocking the drainage on the east side (Prest et al, 1977).

The "Middle till complex" is a mixture of stony, silty, and sandy tills interlayered to well stratified gravelly to silty sediments with silt and fine sand lenses. Middle till is only identifiable by the presence of stratified sediments separating one or more till units from the lower, basal (Malone) till (Prest et al, 1962). Sometimes, it is predominately stony and may be confused with Malone till. In other parts, the till

layers may be found to be stone-poor and highly variable in composition and shape over short distances, or even composed almost entirely of silt and a few stones (Byers, 1949). Its thickness ranges from a few meters to tens of meters. This complex may be divided in upland and lowland phases (Prest et al, 1977). Both of them contain a high percentage of shale and limestone particles, which impart a grey color to the till. The terms "black sand' or "grey sand" are often used to describe this till deposits (Prest et al, 1962). The silty sands usually are medium to fine in size with less than 10% of silt particles. Sandy silts, on the other hand, are composed of fine sands and silt particles; more than 80% of the particles passing the #200 sieve. Figure5.2 shows that in the upland phase of the middle till complex, the shear strength decreases with increasing water content. The properties of middle till are shown in Figure 5.3, which shows that the blow count from the standard penetration test are most likely to be between 10 and 80 blows/ft, with an average of 38 blows/ft. The unit weight ranges from 2000 to 2240 kg/m^3, with an average value of 2160 kg/m^3. Figure 5.4 shows the influence of water content on the standard penetration test (Prest et al, 1977) and a linear relationship can be calculated.

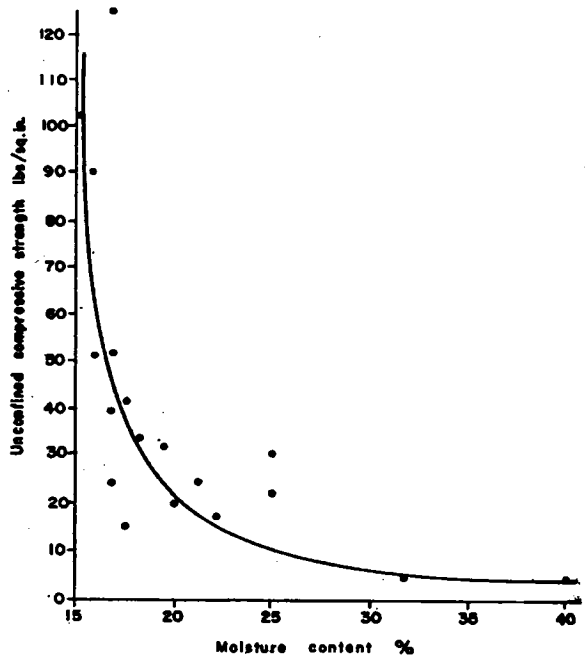

Figure 5.2: Shear strength of upland phase decreases when water content increases (Pres et al, 1962)

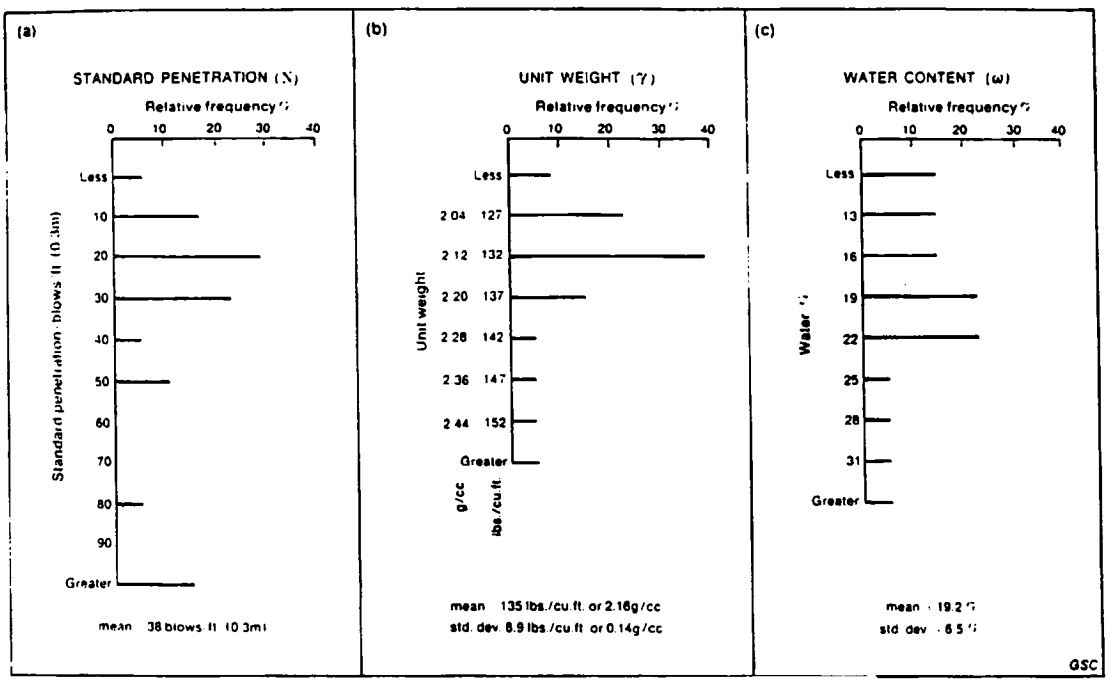

Figure 5.3: in situ properties of Middle till Complex (Pres et al, 1962)

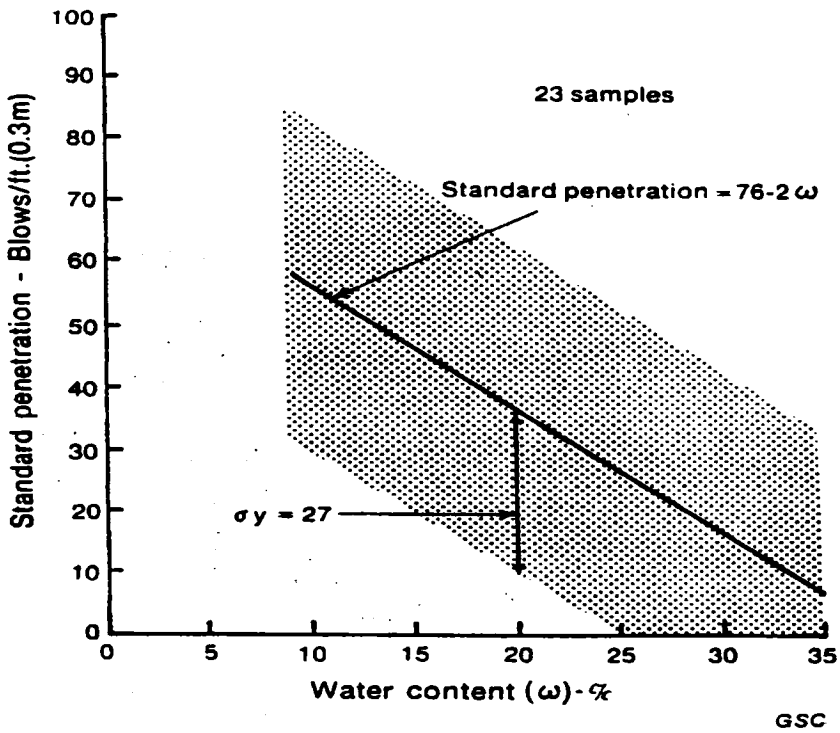

Figure 5.4: Influence of water content on Standard Penetration tests (SPT). (Prest, 1977)

5.2.2.1 Upland phase

The Upland phase is composed of well stratified silt, sand and gravel. It can be found abundantly on the north, west, and south sides of Mont Royal, and reaches about 53 m in elevation over sea level on the terrace of the Turcot scarp, which is a typical place to find "grey sand and gravel"(Prest et al, 1962).

5.2.2.2 Lowland phase

The Lowland phase is composed mainly of rhythmically bedded finer sediments, massive silt and fine sand, and interlayered till. It closely resembles the basal (lodgement) Malone till. The individual till layers range from 0.3 to 2 m. Massive silt and sand units may be up to 10 m thick and when located beneath the local water table, and they can become "quicksand". The term "quicksand" implies that the material is saturated and it will run or flow when subjected to vibration. The clayey silt layers of

the lowland phase are rarely more than 2 m thick (Prest et al, 1962).

5.2.3 Fort Covington Glacial Episode

During the recession of the Laurentide ice, a climatic change took place and caused a renewed glaciarization. The new glacial period and till deposits related to it are named Fort Covington (Clark, 1972). The ice sheet reoccupied the St. Laurent lowlands and extended until southern Ohio at its maximum point. The glacier covered both Lake Ontario and Lake Erie basins, the Appalachian Mountains, the Champlain-Hudson Valley and New York City. The last Laurentide ice did not last long due to rapid climatic changes (Prest et al, 1977).

The deposits consist mainly of clayey silt till that is seldom stony. Ice advanced into a glacial lake, and then deposited the substratified drift before overriding the area and depositing the upper lodgment till (Prest et al, 1977). Generally, the stones found in this type of till are small pebble to cobble size. When the Fort Covington ice was deposited on top of the Malone till or the bedrock, it scoured the material below and made it remarkably bouldery, which could be mistaken for Malone till. The till is generally fine grained, and it has a few particles greater than 20 mm in size. The particles retained in the No. 10 sieve are less than 20% and there are more than 60% of particles passing the No. 200 sieve (Prest et al, 1962). A summary of the in situ properties is shown in Figure 5.5. The unit weight of this till varies from 1640 to 2380 kg/m^3, with an average value of 2080 kg/m^3 (Rosset, 2003). There is no indication which could be the predominant value for the SPT blowcounts.

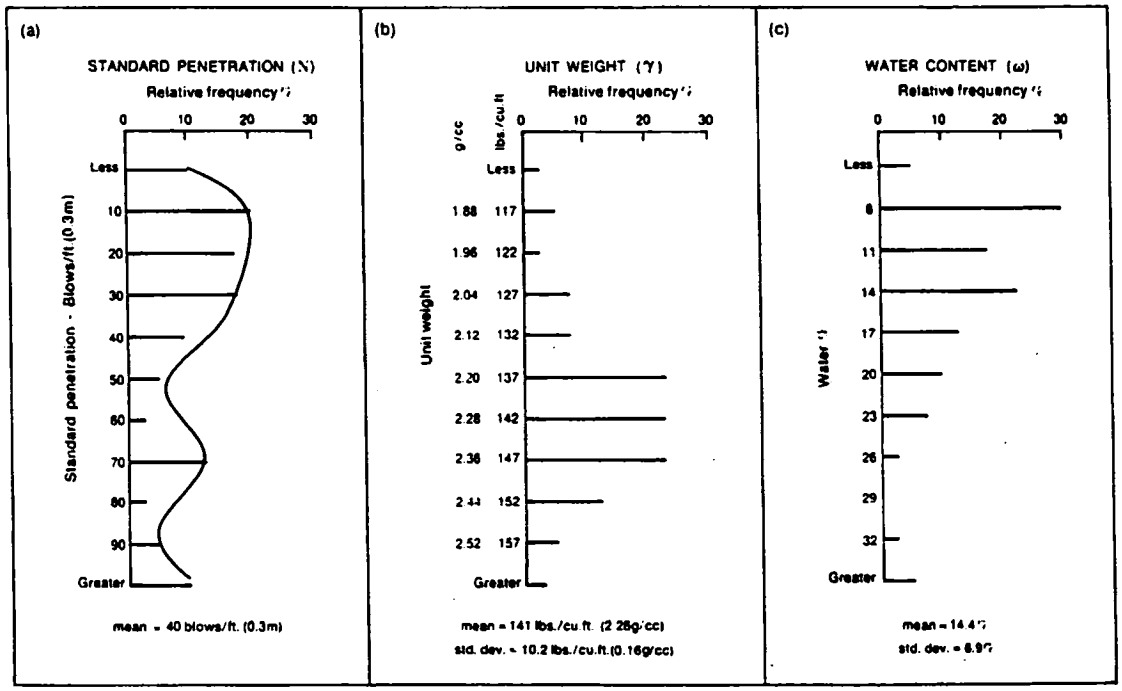

Figure 5.5: In-situ Properties of Fort Covington Till. (Prest, 1977)

The influence of water content on standard penetration tests is shown in Figure 5.6 and resembles the distribution in Figure 5.4.

The relationship between the blowcounts (N) and the unit weight of silt, and upper and lower tills are shown in Figure 5.7 (Prest et al, 1977). Blowcounts increases with stone content. For example, the blowcounts for coarse grained till are mostly influenced by unit weight, whereas blowcounts of dense glacial lake silt are practically unaffected by it (Prest et al, 1977).

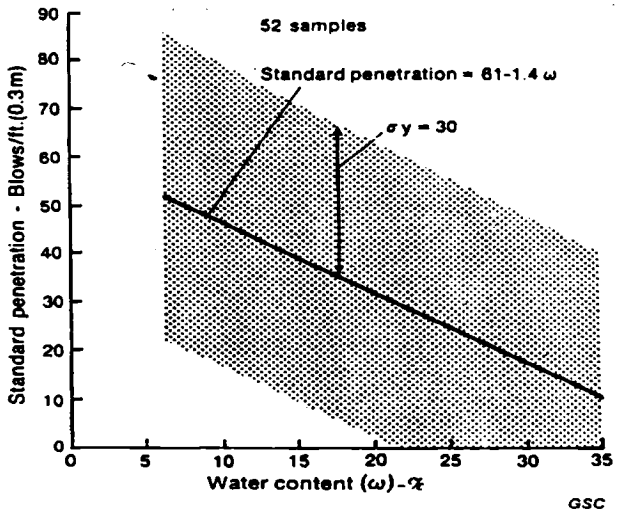

Figure 5.6: Relationship between SPT and Water Content for Middle Till Complex (Prest at al, 1977)

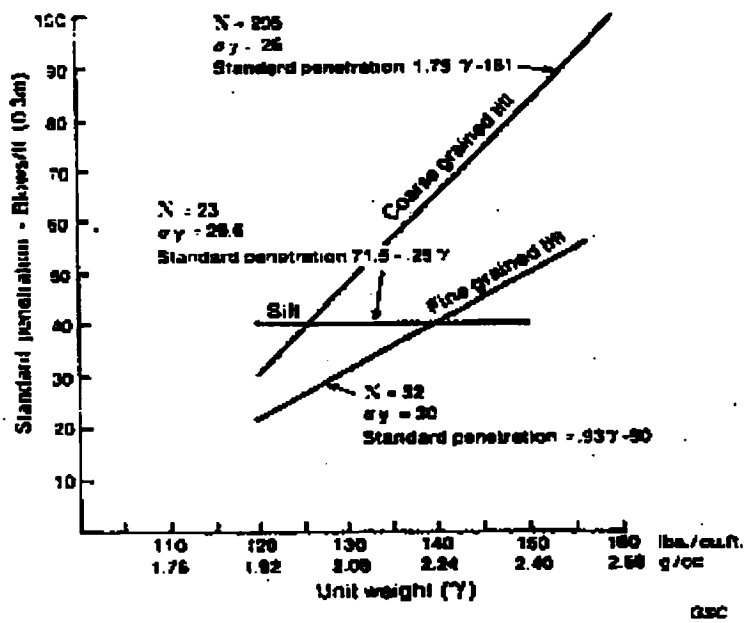

Figure 5.7: Relationship between SPT values and unit weight for silt and coarse and fine grained till. (Prest, 1977)

5.3 Late-Glacial and Postglacial Events

The Champlain and Upper St. Laurent valleys were occupied by a succession of glacial lakes (3). The phases of these lakes are poorly represented in stratified silt and

clay deposits in the Montreal area. These deposits are well bedded, light grey in color and not as well compacted as the middle till complex. They can be found in the Cote-Saint-Luc area, Ville LaSalle and south of the Dorval International Airport. In some places, the deposits are overlain by sticky, unctuous, marine clay (Prest et al, 1977).

Due to the weight of the glacier and the rapid deglaciation, the land surface did not recover rapidly from its depressed position; hence, the bottom was several hundred feet below sea level at that time. Therefore, the sea waters flowed in and occupied much of the former lake basin and large area that had been covered with ice. The sea extended westward following the St. Laurent Valley to beyond Brockville, but not into lake the Ontario basin, and up Ottawa valley to near Petawawa. The body of sea water west of Quebec City is referred to as the Champlain Sea (Prest et al, 1977).

Champlain sea deposits occurred while ice was still present in the region. A readvance of Laurentide ice constructed an end moraine (an accumulation of earth and stones carried and finally deposited by the glacier) in the north and northeast of Montreal (Prest et al, 1977). The deposits are limited mostly to ice-rafted boulders and pods, or pockets of till and till-like materials which were emplaced in marine clays as debris laden icebergs and shore ice melted in the sea. The till was deposited as flowtill; it came from glacial debris that was slid from the glacier and transported to the bottom of the sea as slurry (Prest et al, 1962).

5.3.1 Saxicava Sand

The uplift of the land and the direction of flow of the ice retreat tilted the land surfaces northward, elevating the shorelines of the Champlain Sea. The sea overlapped to Mont Royal to a maximum elevation of 170 m. During the transition from open sea to estuarine, Mont Royal rose above the sea level at a present elevation of 50 m. Therefore, erosional features on Mont Royal between those elevations are marine littoral (Prest et al, 1977). As the lifting of the St. Laurent lowland took place, the

Champlain Sea was increasingly restricted and shorelines developed at successively lower elevations (Prest et al, 1962).

Shorelines are responsible for shells, sand and gravel deposits. These deposits are restricted to elevations of 170 m on Mont Royal with the marine limit to 52 m on Hampstead west of Mont Royal, and 41 m of its north eastern side. The near shore, wave sorted, gravelly to sandy deposits related to this period are called Saxicava sand (Prest et al, 1977). The Saxicava sand deposited on Mont Royal is generally less than 3 m thick, but locally it can be as much as 15 m thick. Some of their engineering characteristics are: uniform grading, high water content, lack of compaction, and interbbeded beds of clay in some localities (Prest et al, 1977).

5.3.2 Leda Clay

Some soil was also deposited offshore in the island of Montreal, in quiet waters. They have the characteristic of being silty to clayey deposits, and are known as Leda clay. Locally, the marine clay is fossiliferous and especially shells can be found (Prest et al, 1962). This type of deposits have been observed from a maximum elevation of 112 m on Mont Royal down to present river levels around the island and even below sea level as noted in some borings.

Marine clay varies considerably. In deep water, it is massive, fatty or unctuous clay; but in shallow waters, it is well laminated and silty (Prest et al, 1977). Clay can be found in three different colors: unweathered clay has a dark bluish grey to medium grey color; thin beds of clay may have a pink hue and are referred as "red clay"; and, the upper surface of the Leda clay is sometimes oxidized to brown or yellow clay to a small depth from the surface. The boundary between oxidized and unoxidized clays is uneven. The bluish color depends on the amount of silt and clay encountered in the sample of clay. The red pink color, however, is considered to be due to (Stansfield, 1915):

a. an influx of red mud (most likely source of red materials)
b. oxidation of local water embayments of the Champlain sea during deposition of the clay
c. Influx of partly oxidized clay from land or water.

The unit weight may vary from 1520 to 1920 kg/m^3, with an average value of 1720 Kg/m^3. The water content ranges from 30 to 80%. An instrumented borehole in the vicinity of Ottawa indicated that values of the S-wave velocity were between 150 to 300 m/s down to a depth of 40 m (Rosset, 2003).

5.3.3 River and Stream Deposits

Land rose above the sea level from the time when the town of Hampstead was about 52 m in elevation. The withdrawal of the sea and the uplift of the surface created an estuary, creating an island at the highest part of Montreal and at the mouth, the beginning of the St. Laurent River. As the land continued to rise, the interface between salt waters and fresh waters migrated north-east. By the time the land surface at 30 m reached sea level, most of the Montreal Island was exposed and only narrow rivers occupied the valleys of Montreal. Estuarine conditions terminated when the north eastern tip of the Montreal Island rose above sea level; the surface has risen since another 6 m (Prest et al, 1977). Interbedded river sand and gravel with grey and pink clay are associated with this phenomenon. All the erosional features from elevations 52 to 6 m are the work of the rivers rather than the sea (Prest et al, 1962).

The largest river deposit is a long strand of fine to medium sand with scattered pebbles which extends near Boulevard Decarie and the Canadian Pacific railway to Montreal west. Its maximum thickness is about 1.5 m. On the west side of the Island of Montreal the sandy deposits lie mainly between an elevation of 51 and 40 m. Also all the way to Lac des Deux Montagnes it has been down cutting and the elevation of the deposits is at 22 m and as thick as 6 m. However, at the western end the sand deposit

is a patchy mantle, more than 0.5 to 1 m thick (Prest et al, 1977).

Prominent river scarps may be found in different parts of the island. The most prominent one is the Turcot scarp. It was formed by river erosion. Other scarps are found on Ile Perrot, in Pointe- Claire, Ville LaSalle, Montreal North and Sherbrooke Street east of Mont Royal (Prest et al, 1977).

The early rivers generally contained coarse sand and gravel. These deposits can be found on both sides of the island and below an elevation of 30 metres and may contain some clay or even clay balls. The stones are mostly subangular to subrounded and range greatly in size (Prest et al, 1962).

The river clay deposits are widely spread and hardly distinguishable from marine clay. They are around a meter thick and have a looser texture than the marine clay. The deposits may be seen to be stratified in the thicker sections.

The unit weight is in between 1780 to 2360 kg/m^3 with an average value of 2050 kg/m^3. Measurements from a borehole indicate an average value of 400 m/s for the S-wave velocity.

5.3.4 Bogs and Swamp Deposits

Numerous ponds and bogs areas remained when the rivers started to dry and pond clay, marl and peat were deposited. The peat can rest on rock, glacial till, marine clay, or on pond clay or marl. The only deposits younger than the peat deposits are the present day deposits due to erosion, rivers and streams. Generally, the thickness of the deposits ranges from a few centimetres to a few metres and, locally, peat may fill deeper parts of abandoned river channels attaining a thickness of more than 5 m. The material is very compressible when allowed to drain. For construction purposes the material is usually replaced by a more appropriate material (Prest et al, 1977).

5.4 Summary of Results

A model for the layers has been chosen as input for SHAKE91 (Table 5.3). The model is based on the observations made by Prest and Hode-Keyser (1977). It follows the chronological order described and it is in accordance with models proposed for other regions of the St. Laurent Valley (Rosset, 2003).

Table 5-3:Compilation of engineering characteristics for quaternary deposits of the Island of Montreal (Rosset, 2003)

	SPT, Blows (N)			Comp. Strength (kN/m^2)			Shear Resistant (kN/m^2)			Water Content (%)			Dry Unit Weight (kg/m^3)			Density		
	Min	Max	Mean	Min	Min	Max	Mean	Max	Min	Mean	Max	Mean	Min	Max	Mean	Min	Max	Mean
Malone Till			>50	320							430					6	14	9.6
Middle Till Complex	10	80	38										41	860		14	32	20
Fort Covington Till	10	100	40													7	25	14.4
Leda Clay								2.6	2.74							30	80	
River Sand																		
Peat					192	240												>200

S-wave Velocity (m/s)			Liquid Limit (%)			Plasticity Index (%)			Unit Weight (Kg/m^3)		
Min	Max	Min	Max	Mean	Min	Max	Mean	Mean	Min	Max	Mean
		1.8	4.8	3.2	2160	2480	2400	1000[f]	13.2	22.4	15.4
		0	5		2000	2240	2160	800[f]	18	21	
360	760	< 10	> 100		1640	2380	2080[b]	600[a]	24	38	32
150	300				1520	1920	1720	150[c]			
350	600				1780	2360	2054[a]	400[e]			
							2000	300			

Chapter 6 - Results

6.1 GAN Technique Results

The island of Montreal was divided in 70 regions of equal area (3000 x 3000 m^2) (Figure 6.1). Each region was assigned a specific number of field tests. The number of field tests depended on the type of surficial deposits and the depth to bedrock estimated from the maps of Prest and Hode-Keyser for the cell (1977) (Figure 6.2). A total of 703 field tests were conducted. Cells where the type of soil is predominately clay or sand usually have a larger number of field tests; whereas, cells with this soil covers and shallow regions with stiff soils, like basal till, have fewer field tests, since they usually have high predominant frequencies and small amplification factors. Nevertheless, if a cell is comprised mainly of till deposits and depth to bedrock is greater than 30 ft (10 m) more tests were performed since predominant frequencies are lower and amplification factors higher.

Figure 6.1: 70 Regions selected on the surficial deposits map (modified from Hode et al. 1977)

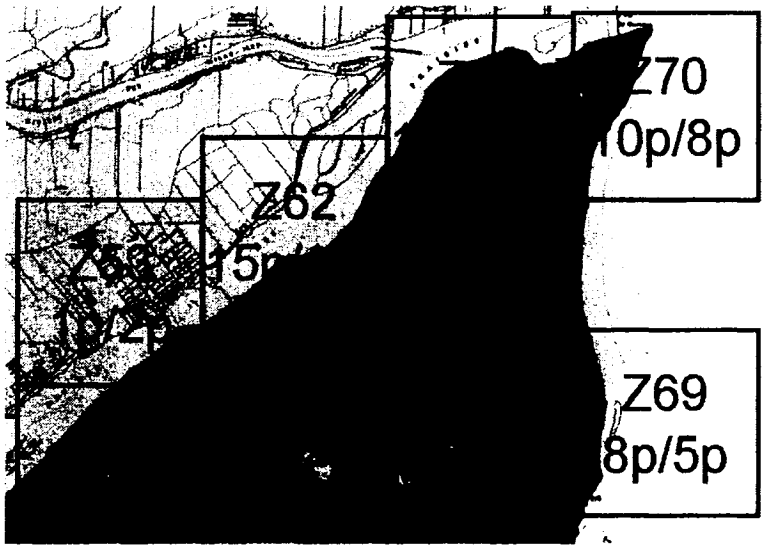

Figure 6.2: Close-up of Regions with the field investigations. The first number is the planned number of tests, the second, is the actual number done in the region.

The spectra obtained from the H/V method have multiple shapes and sometimes the interpretations of the results are not clear. A qualitative criteria was established to describe the overall quality of the results. The criteria depends on the shape of the H/V spectra. Table 6.1 summarizes the characteristics of the spectra for each category of results. Figure 6.3 shows typical shapes for each shape category.

Table 6-1: Qualitative criteria for the GAN Results

Characteristics of the H/V Spectra	Category
One peak, or a very high peak compared to the others	1
One peak with a flat top. Wide range of values as is possible the predominant frequency	2
One peak, but not well defined	3
Flat shape. Most likely it is a rock site.	4
Presence of two clear peaks, one a little higher than the other one.	5
Two peaks with at least one with a wide crest.	6
A 0.7 is added to any of the above number to indicate that an increase in the signal is present at the end of the results and it could indicate a higher predominant frequency.	+ 0.7

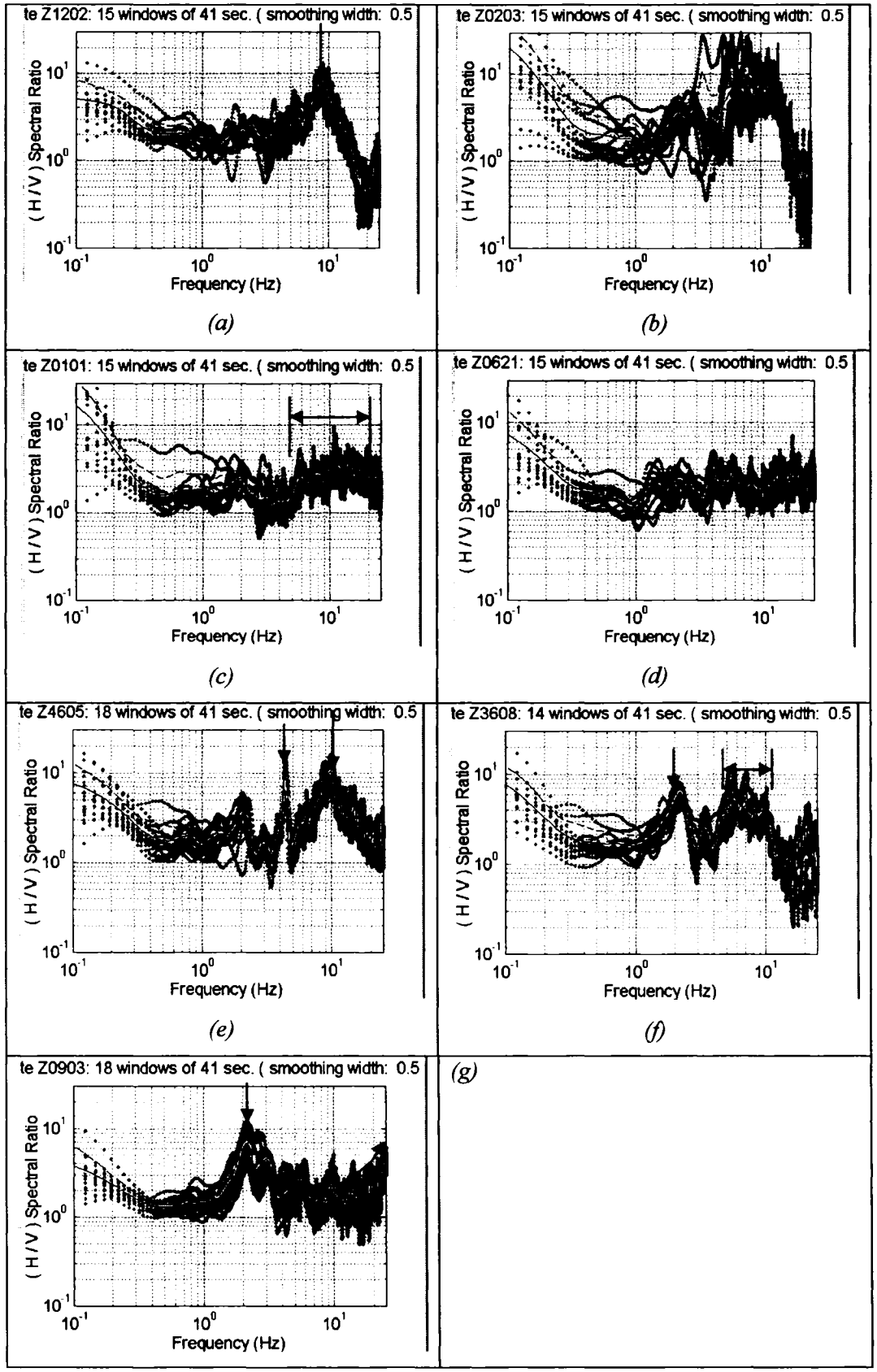

Figure 6.3: Examples of the Spectra Categories: (a) 1, (b)2, (c)3, (d)4, (e)5, (f)6, (g)#.7

All of the results obtained from GAN should be validated with results from Shake 91 analysis (Rosset, 2003). As shown in Figure 6.4, about 40% of the samples have one clear accurate peak and 31% of the field tests have two peaks. Usually the highest frequency is predominant, but there can be exceptions. A preliminary map of non-validated predominant frequencies from GAN is shown in Figure 6.5.

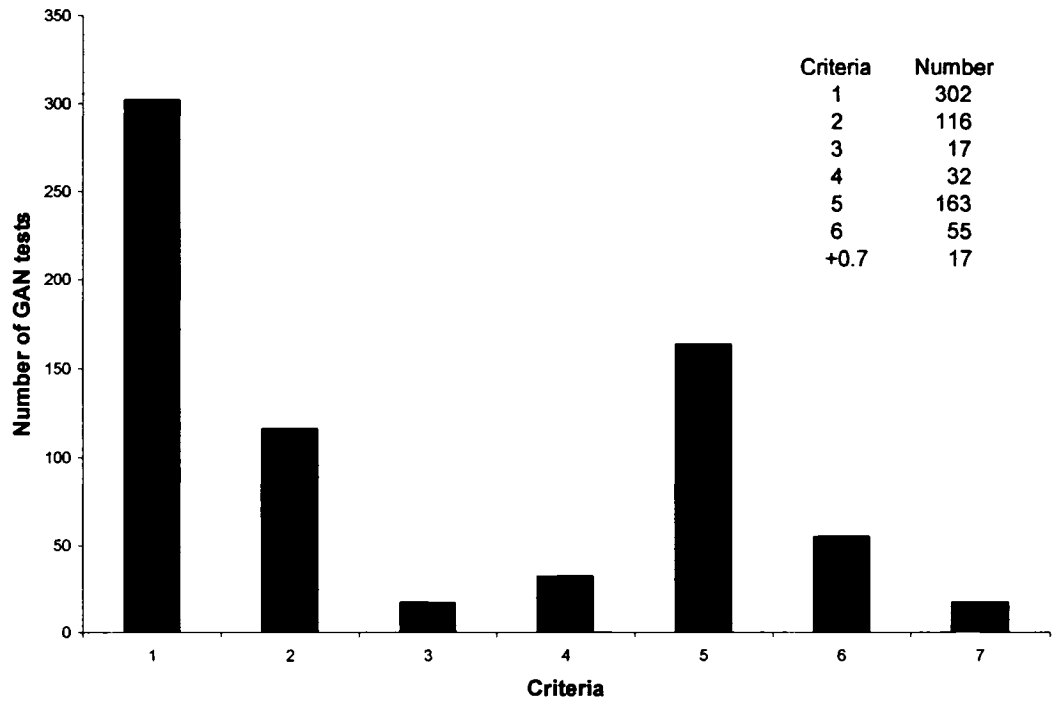

Figure 6.4: Classification of GAN tests using the qualitative Criteria

The map shows that the predominant frequencies are lower frequency regions near the St. Laurent River or where rivers existed at some ancient time (Figure 6.5). In the eastern part of the island, results are fairly homogeneous, while in the western part, results are much more variable. A probable explanation is that bedrock may be much more irregular in the western part of the island. This is partially verified by examining the map for depth to bedrock derived from the analysis of more than 2000 boreholes (Figure 6.6). Another possible explanation is that the soil column is much more variable in the western part of the island.

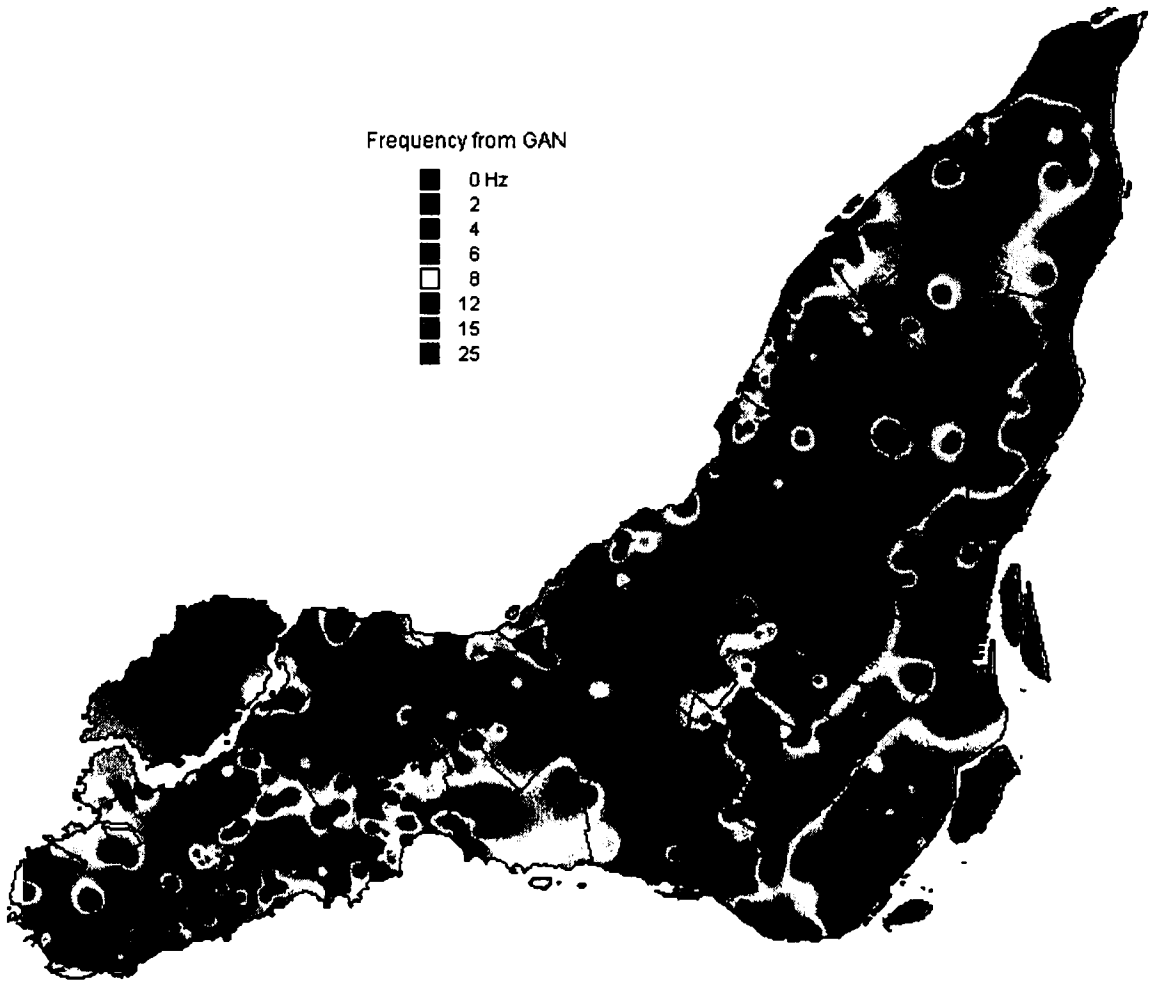

Figure 6.5: Preliminary map for the predominant frequencies for the island of Montreal

6.2 Analysis using SHAKE 91

A digital database of borehole locations of boreholes and depth to bedrock was provided by the Ville de Montreal. The database consists of more than 26000 boreholes, but less than 14000 reach the bedrock and have a complete description of the soil column. The database is divided in two types of boreholes depending on the government branch that provided them. Municipal boreholes have an ID of the form: 80F001-2653 and the federal government boreholes: 56OTTA-02429. The database provides locations and depths of all the boreholes, but only the municipal boreholes have descriptions of the type of soil, grain size and origin. The federal government boreholes were obtained from microfiches at the Ville of Montreal office. When the origin of the layer is provided in the soil description of the soil (i.e. river deposit or glacial deposit) the identification of the soil becomes easier, and the risk of wrongly identifying the soil type is minimized.

The distances from the location of each GAN field test with each the boreholes was calculated. Only boreholes that are less than 100 m from a GAN test were included in the Shake analysis because soil column descriptions vary widely over small distances. For the analysis, the boreholes are divided in three different groups depending on the distance from the locations of a GAN field test:

1. Less than 30 m (30)
2. Between 30 m to 60 m (60)
3. Between 60 m to 100 m (100)

A total of 67 boreholes satisfy the criteria of group 1, 100 those of group 2 and 207 those of group 3; for a total of 374 boreholes. Only 51 GAN field test locations have boreholes at the distance less than 30 m. 70 GAN field tests are within 30 and 60 from a borehole and 106 within 60 to 100 from a borehole. In consequence, only 227 GAN tests out of the 703 have at least one borehole close enough to validate the predominant frequency and obtain a "validated" amplification factor from Shake.

Since only average values for the soil properties are presently available and only 30% of the GAN field tests have boreholes to validate the frequency and calculate the amplification an interpolation technique is currently required to create a complete microzonation map for the island.

6.3 Comparative Analysis between the results of GAN and SHAKE

To facilitate the understanding of the results, a map of the depth to basement was created with all the boreholes in the database (Figure 6.6). The objective is to identify the locations were the GAN tests that are located on shallow soil should have very high frequencies.

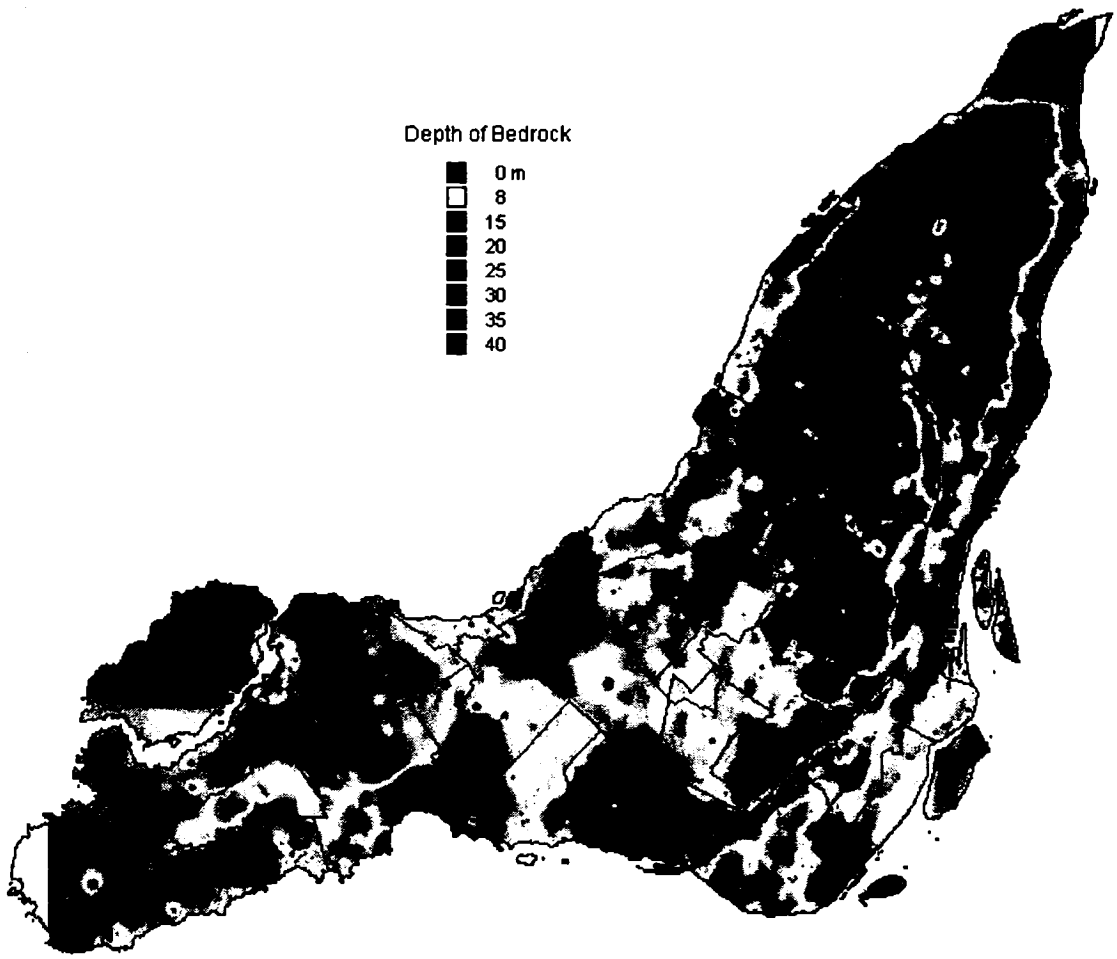

Figure 6.6: Map of the depth of the basement of the Island of Montreal

The locations of low frequencies (Figure 6.5) coincide with locations where the distance to bedrock is more than 20 m (65 ft) (Figure 6.6). The patterns of depth to bedrock in the western part of Montreal are similar to that of the predominant frequency from GAN tests. There are few locations with spurious changes in depth and should be verified in the future. Note that a large part of the island has shallow bedrock.

The predominant frequencies estimated by the analytical approach and GAN are compared in Figure 6.7 for all tests in the three groups. The results vary widely and indicate that the frequency found with SHAKE 91 is usually higher than the one from the GAN field tests. Note that the maximum frequency value that can be obtained by the analytical approach is 24.88 Hz.

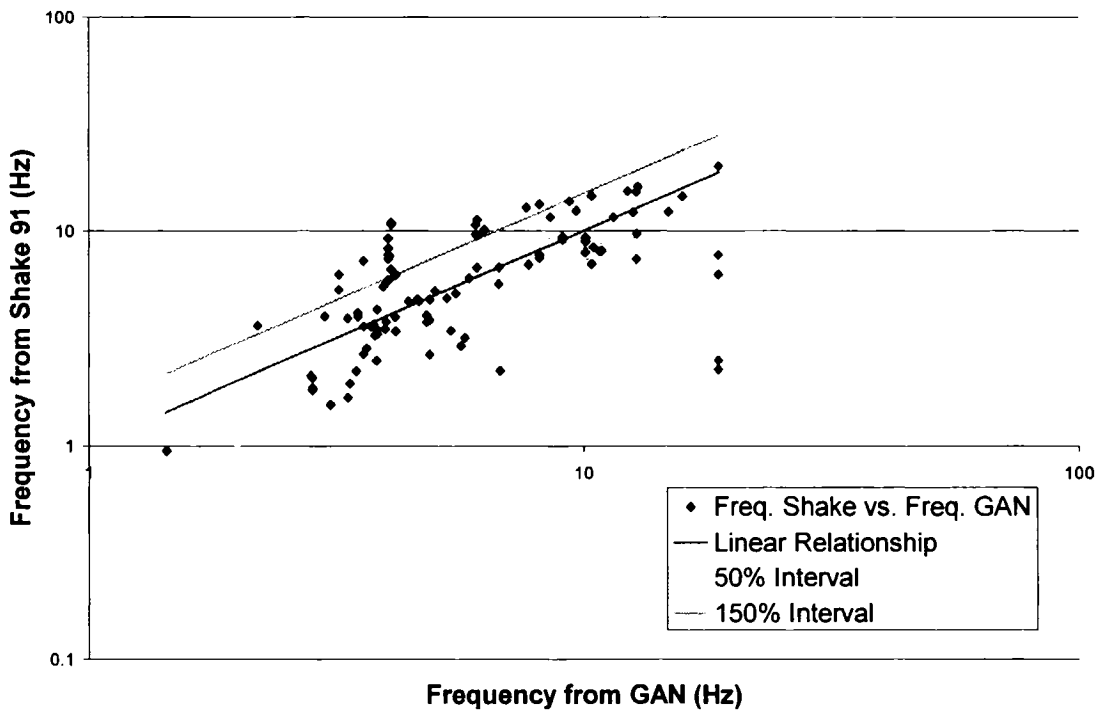

Figure 6.7: Predominant Frequency of Resonance calculated from SHAKE91 vs. Frequency found from GAN field Tests. The 50% and 150% interval are also shown in the graph.

Figure 6.8 shows the results for a column of soil composed of one type of the six possible soils in Montreal. From the figure it can be concluded that if the bedrock is 3 m (10 ft) or less from the surface, the predominant frequency calculated with Shake 91 will always be 24.88 Hz. Since the difference of shear wave velocity greatly affects the predominant frequencies it is be better to analyze boreholes in groups with the similar soil characteristics. For example, all locations with a clay layer of 3m or higher is classified as clay since it has very low shear wave velocity. Ideally, boreholes should be divided in 6 different groups: peat, sand, clay, and the three basal tills. However, peat is usually at the surface and has practically no effect on frequency. Also, none of the boreholes have significant quantities of sand. Those that have sand are usually underlain by a layer of Malone till (BT2) twice as thick. As a consequence, boreholes are classified in 4 groups:

1. Clay: when at least 10% of the soil column consists of clay.
2. BT3: when the highest proportion of basal till is Fort Covington till
3. BT2 or BT1: when the till is predominantsince they are hard to differentiate and very stiff, both of these tills are classified in one group.
4. Rock: when the soil column is less than 3m (10 ft) thick.

6.3.1 Boreholes classified as Clay sites

Figure 6.9 shows the relationship of the predominant frequency from Shake 91 versus the GAN field tests for boreholes classified as clay sites. The soil properties assumed in Chapter 5 are used in Shake and give very good agreement with GAN frequencies. As the distance between borehole and GAN tests location increases, the difference between the results obtained in Shake and GAN field tests results also increases, but remains good up to distances of 100 m.

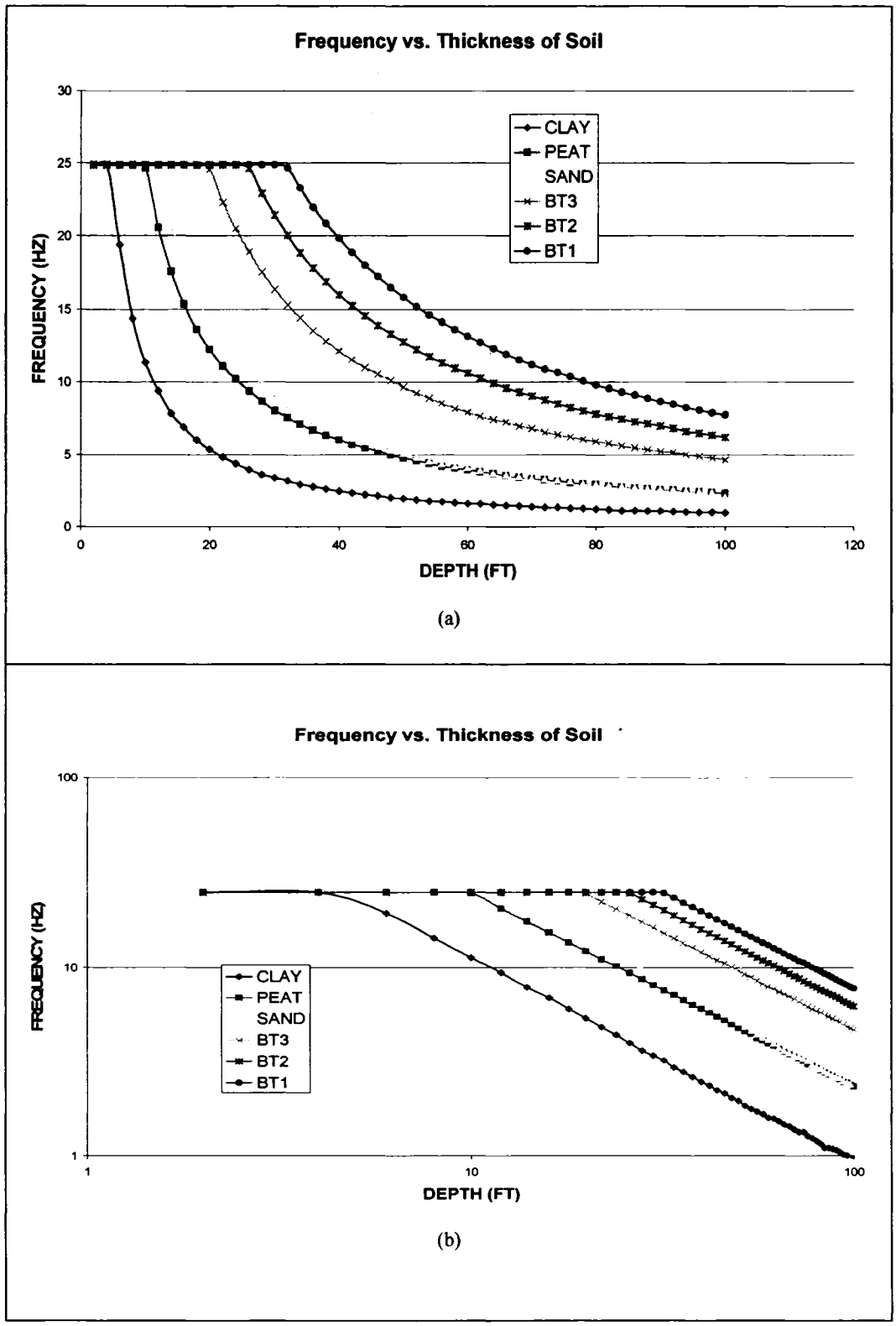

Figure 6.8: Frequency vs. depth for a soil column consisting of only one layer of soil. Figure (a) shows the relationship on a standard scale and (b) shows the relationship on a logarithmic scale

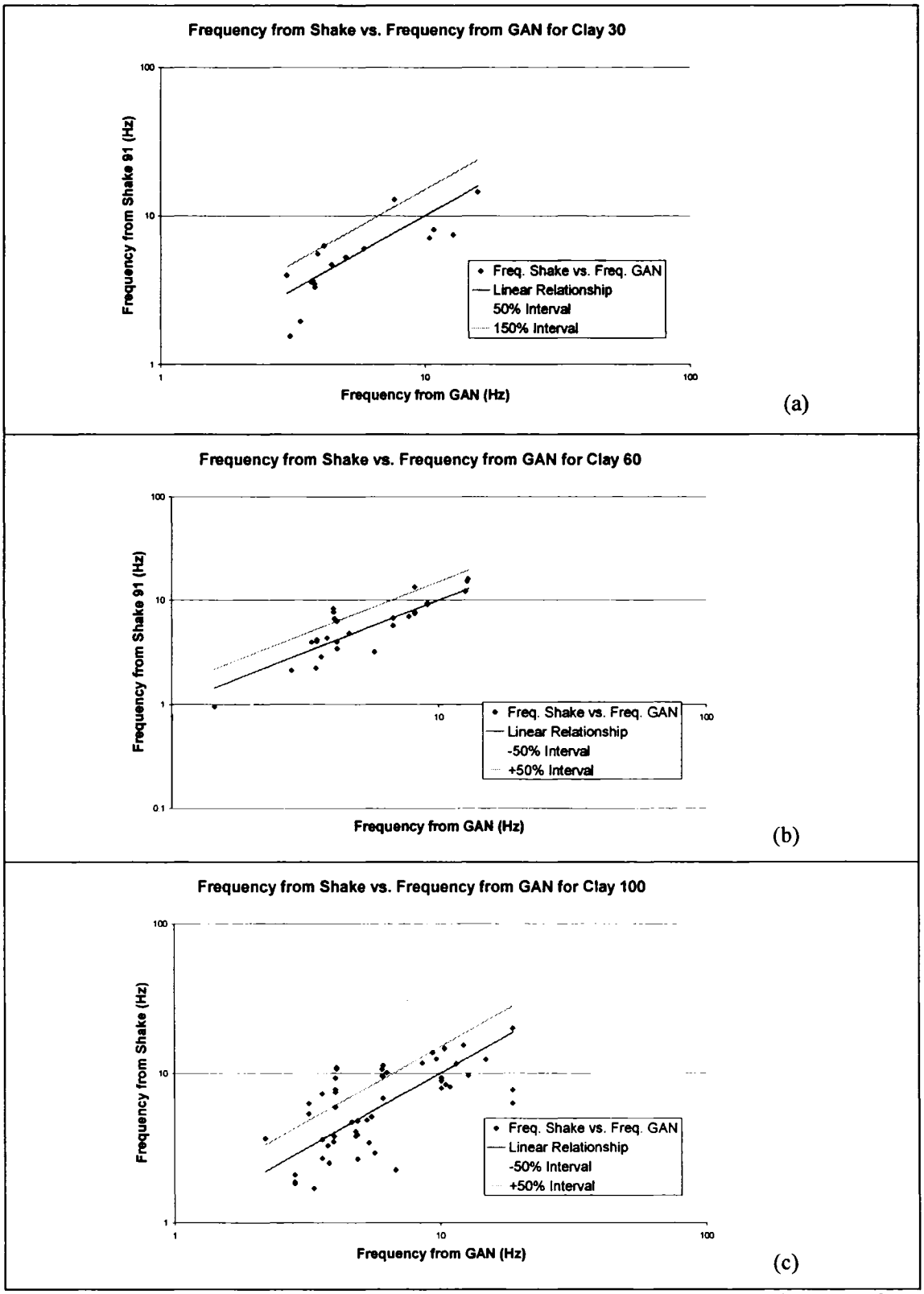

Figure 6.9: Frequency found in Shake 91 vs. Frequency found in the GAN field tests for the Clay group (a) 30, (b) 60 and (c) 100.

Nakamura (2000) proposed the following empirical equation to predict the predominant frequency as a function of shear wave velocity and soil thickness:

$$F=V_s/4h \qquad [6.1]$$

where Vs is the shear wave velocity and h is the thickness of the layer (Nakamura, 2000). Rosset (2004) proposed an empirical equation for Montreal that is only a function of soil thickness for clay (Figure 6.10):

$$F=24/(h^{0.8}) \qquad [6.2]$$

Based on the current results a new empirical equation is proposed for clay sites in Montreal:

$$F=30.9/(h^{0.65}) \qquad [6.3]$$

The previous relationships are compared in Figure 6.10.

Multiple peaks can occur in some instances, for example, with 5 m (16 ft) clay layer and a depth to bedrock of 22 m (70 ft) Shake 91 finds a predominant frequency of 5.63 Hz for the first record of the Saguenay earthquake. However, the third record of the Saguenay earthquake gives a frequency of 12.5 Hz. The frequency found from the first record is the closest to the one from GAN field investigations. The explanation for this result is that Shake 91 identifies the second frequency as the dominant frequency since the amplification factor is slightly greater for the second peak (Figure 6.11). This type of result is described as a "borehole with multiple peaks" in the following paragraphs. In this case, the Shake 91 frequency that is retained is the one that is the best match to the GAN frequency.

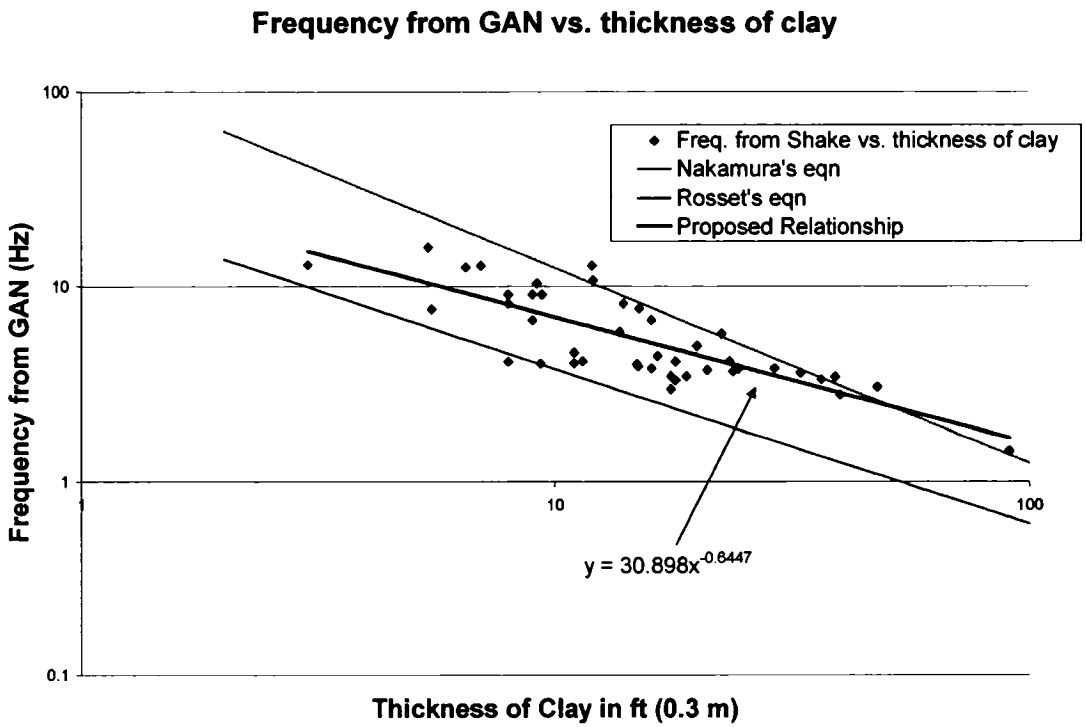

Figure 6.10: GAN frequency vs. Thickness of the layer of clay. The relationships between frequency and Thickness are shown in each graph.

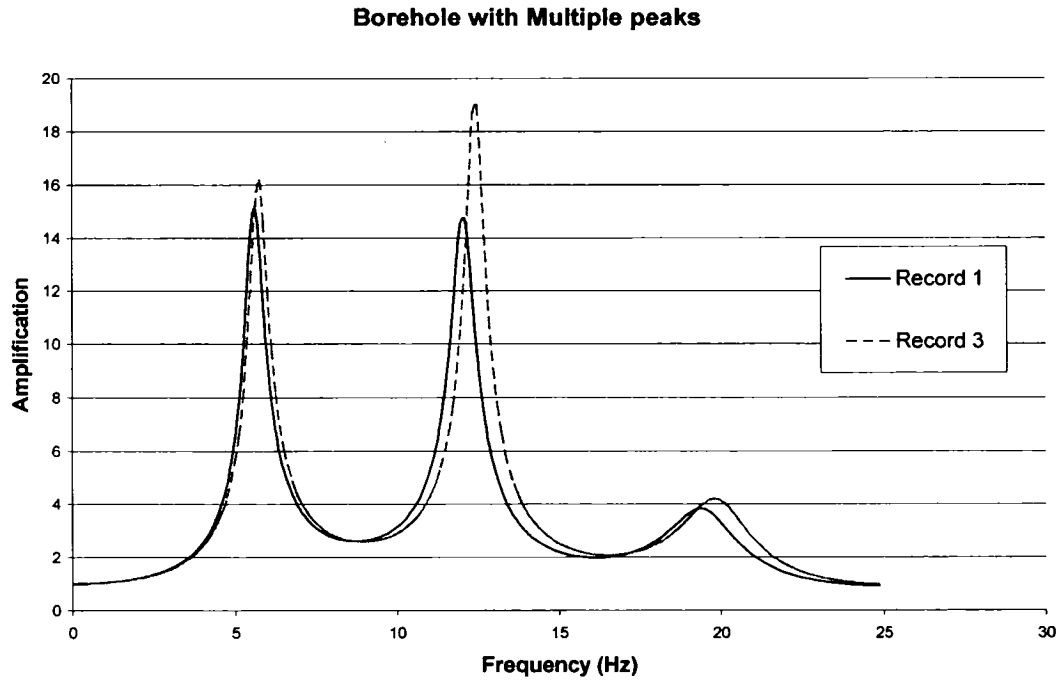

Figure 6.11: Borehole with multiple peaks. It clearly shows the closeness of the amplification for the two frequencies of resonance.

6.3.2 Boreholes with BT3 layers

When the soil column consists mainly of basal till, the predominant frequency is usually high. The average values presented in the previous chapter for basal tills are those for deep layers. Only one borehole in the database provided a value for the shear wave velocity of BT3 soils of 1500 ft/s (~450m/s). The value of 1500 ft/s is 25% less than the average value proposed by Rosset (2003).

Figure 6.12 compares the predominant frequencies derived from the GAN field investigations and from the analytical approach. It is clear that the frequencies found with Shake 91 are higher than the ones from GAN field tests. A reason could be that the average shear wave velocity might be too high compared to the actual values for BT3. The shear wave velocity obtained from one of the boreholes (1500 ft/s (~450 m/s)) gives a better relationship to the GAN values, but these are still a little high. Figure 6.13 shows the gradual effect of lowering the shear wave velocity even further. The frequencies found in Shake 91 are best matched to the value of the GAN tests when the shear wave velocity is 1300 ft/s (~400 m/s), which is close to 50% of the average value originally proposed by Rosset (2003).

6.3.3 Boreholes with BT2 layers

This type of basal till is very hard to differentiate from BT1. Both of them are very stiff and the only practical difference is that BT1 may contain boulders. Both tills are very stiff with average values for the shear wave velocity higher than 800 m/s (2600 ft/s). Usually, this type of soil has a very high predominant frequency, but as Figure 6.8 shows, when the thickness of till is greater than 9 m (~30 ft) the frequency drops to 15 Hz, thick and to 10 Hz around 18 m thick (60 ft). There are several boreholes with basal till layers thicker than 18 m (60ft) and predominant frequencies as low as 6 Hz.

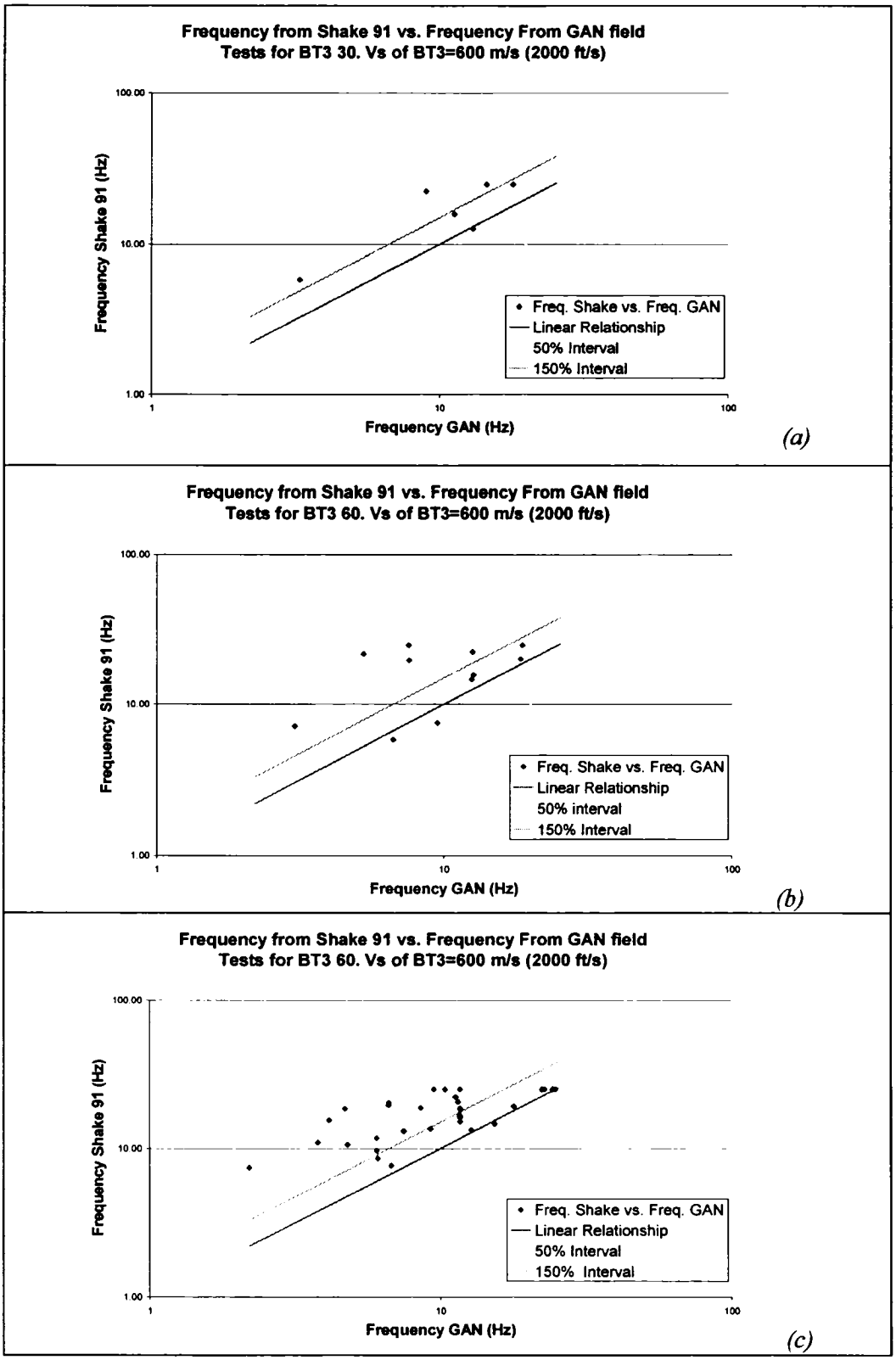

Figure 6.12: Predominant Frequencies from Shake 91 and GAN field tests. (a) BT3 30, (b) BT3 60, (c) BT3 100.

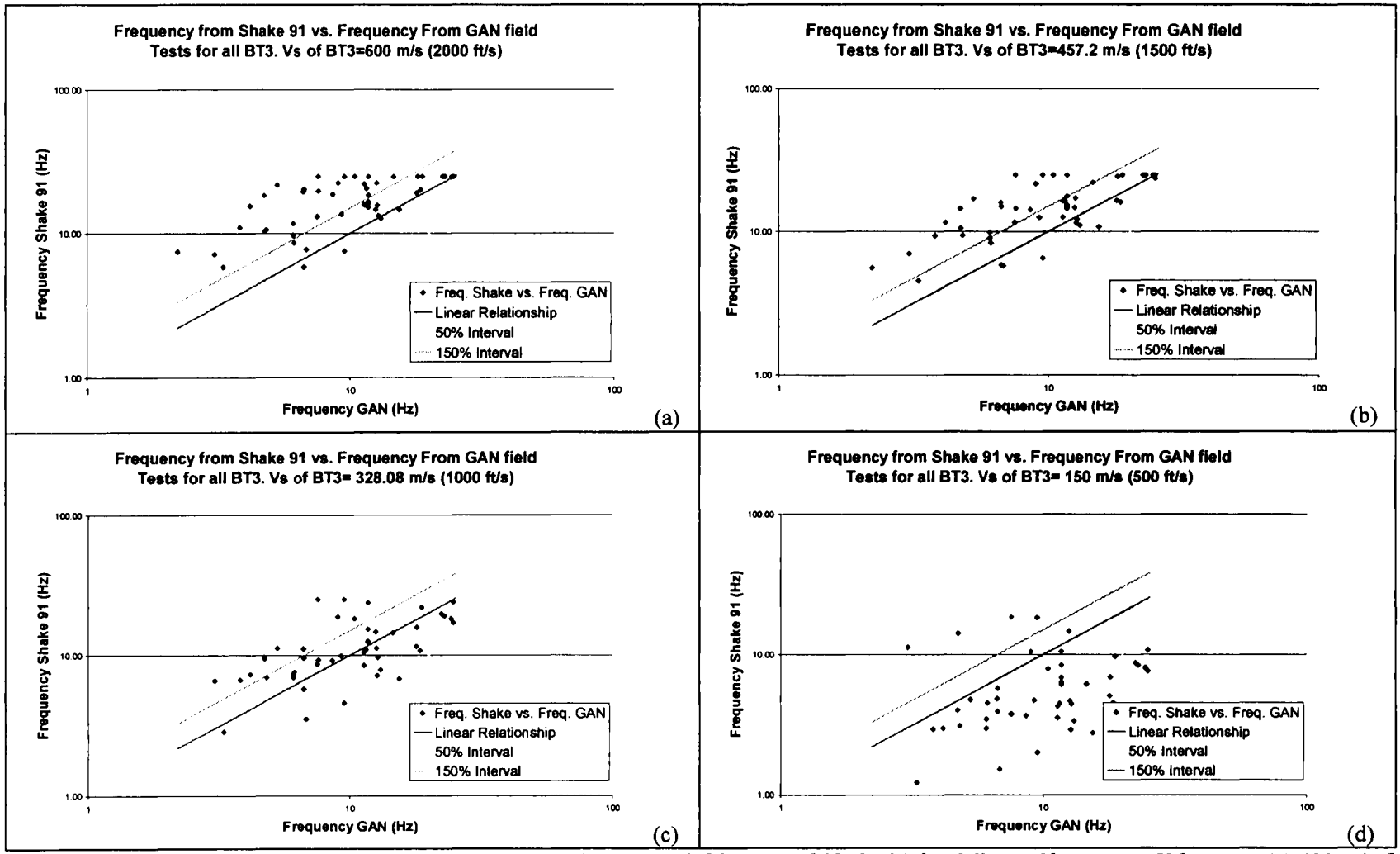

Figure 6.13: Relationship between predominant Frequency from GAN field tests and Shake 91 for different Shear wave Velocities: (a) 600 m/s (b) 457.2 m/s, (c) 328.1 m/s and (d) 150 m/s

Boreholes with only sand are classified into this category since the origin of the deposits is not specified and they could be either sand or BT2. BT2 is a mixture of stony, sandy, silty tills, which could be almost entirely of silt and sand. Usually BT2 is covered by a layer of sand or sand and clay.

The frequencies found in Shake 91 versus GAN frequencies are shown in Figure 6.14. As with BT3, the average shear wave velocity suggested by Rosset (2003) gives high frequencies compared to the ones found by the H/V Method (GAN field tests). If lower shear wave velocities are used, the frequencies of GAN become much closer to the Shake 91 frequencies (Figure 6.15). However, lowering the frequencies to a value which will satisfy the linear relationship requires a shear wave velocity close to that of sand (Vs= 400 m/s). Figure 6.16 shows the relationships between frequency and the thickness of the BT2 layer. From 6.16c, it can be concluded that there exists a good relationship if the thickness of BT2 is greater than 15 m (~50 ft).

6.3.4 Boreholes for Surface deposits of 3 m or less

These boreholes are expected to yield high frequencies since the depth to bedrock is shallow. Only boreholes with 1.5 m (~5 ft) of clay have a frequency lower than 24 Hz. The original frequencies found from the numerical analysis are shown in Figure 6.17. Most of the results found in Shake 91 give the default frequency 24.88 Hz, which is usually higher than the frequency found in GAN tests.

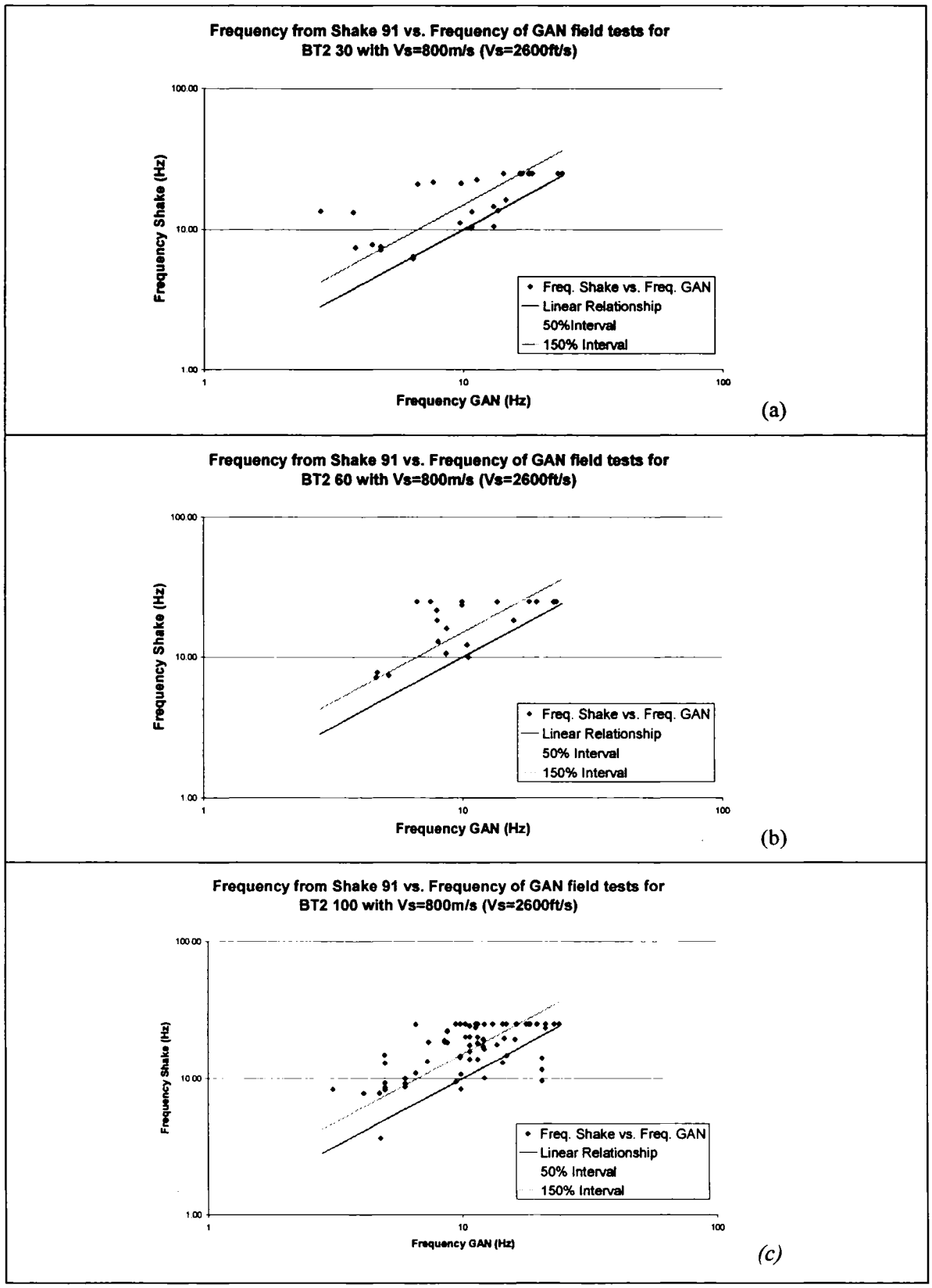

Figure 6.14: Frequency found in Shake 91 vs. Frequency from the GAN tests: (a) BT2 30, (b) BT2 60, (c) BT2 100. The intervals (50% and +150%) are shown in each figure

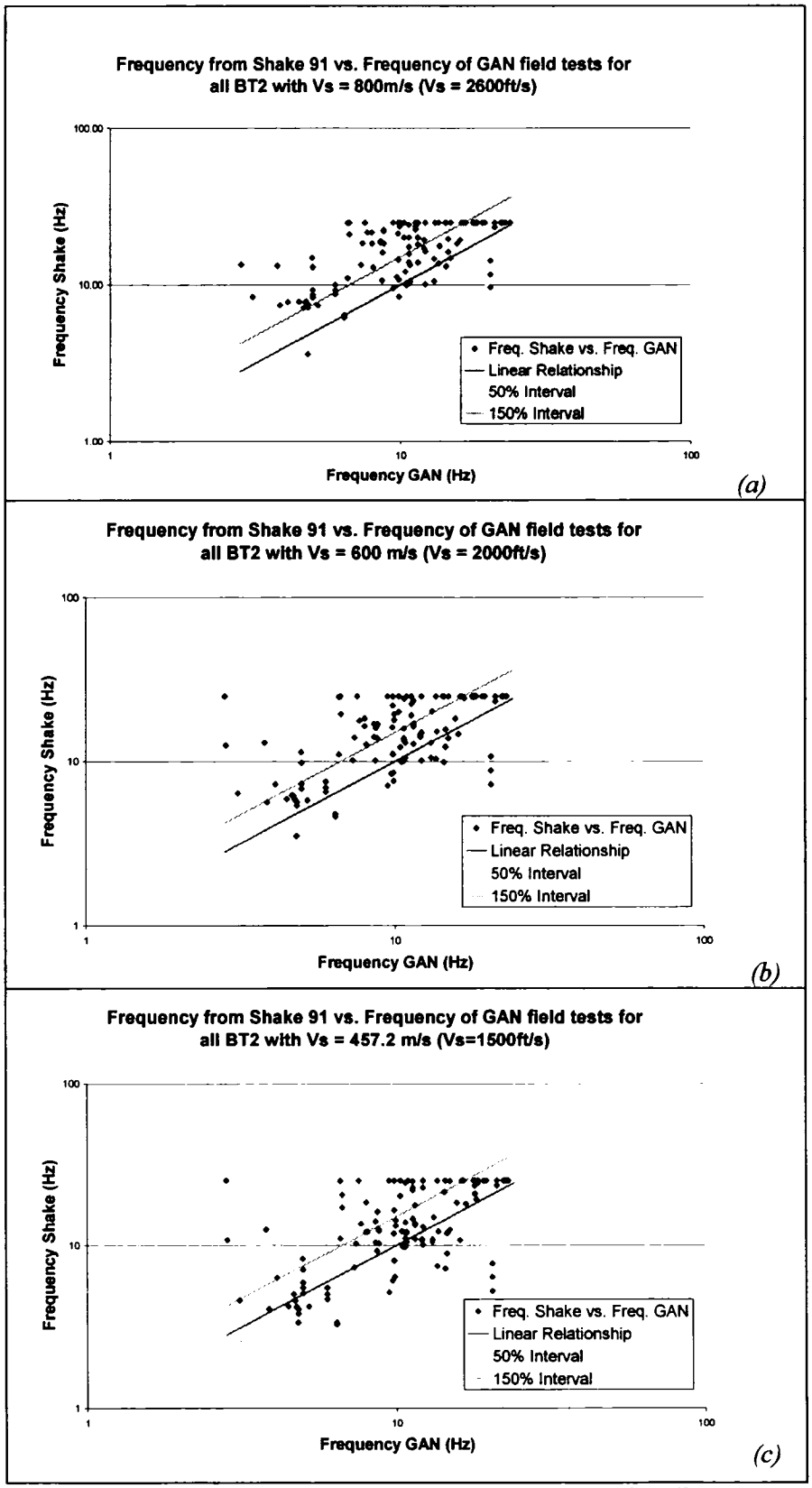

Figure 6.15: Frequencies from Shake vs. Frequencies from GAN for all BT2: (a) Original Vs=800 m/s, (b) Vs=600 m/s (c) Vs=457.2 m/s

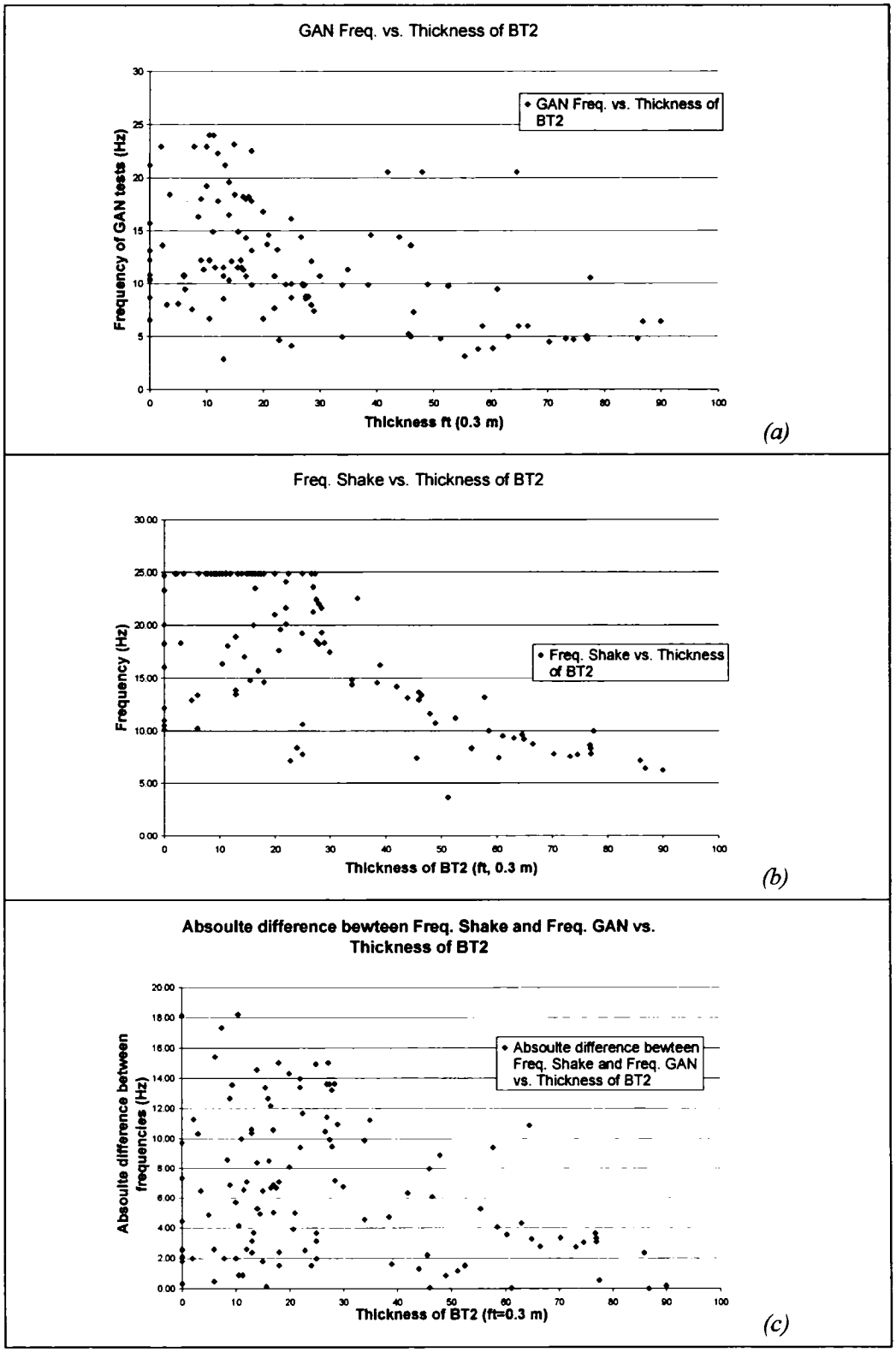

Figure 6.16: (a) Frequency of GAN vs. Thickness of BT2 soil (b) Frequency of Shake vs. Thickness of BT2 soil and (c) Absolute difference between the two frequencies vs. Thickness of BT2 soil.

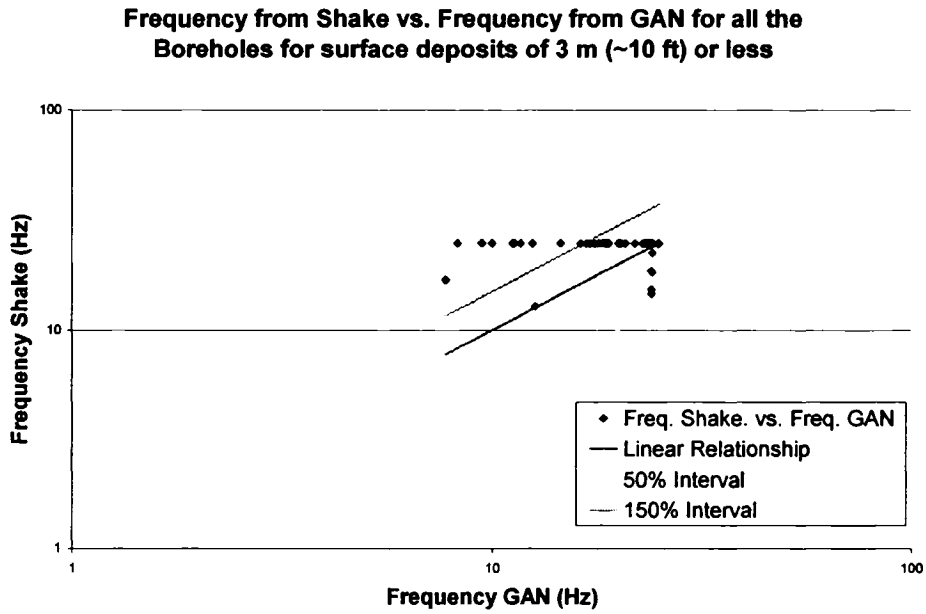

Figure 6.17: Frequency found in Shake 91 vs. Frequency from the GAN field tests.

6.4 Amplification factors

The PGA amplification factors are a function of the frequency content of the input motions and of the thickness (h), mass density (ρ), shear modulus (G), viscosity (η) and damping ratio (β) of each soil layers. Figure 6.22 shows the amplification factors versus depth for the four earthquake scenarios described in Chapter 4 (low period (LP), intermediate period (IP), high period (HP) and broad period (BP) scenario) for four soil types: (a) clay, (b) sand, (c) BT3 and (d) BT2.

The first seismic scenario results in high amplification factors at shallow depths for clay (Figure 6.18 (1)). Then, the amplification factors decrease gradually. Amplification factors between 1 and 2 units are calculated for clay at depths higher than 40 ft (~12 m). Therefore, boreholes with thick clay layers have small amplification factors if the first earthquake scenario is considered. There is no correlation between the amplification factor and the thickness of the clay layer for the second and third earthquake scenarios (Figure 6.18 (2) and (3)). The maximum

amplification occurs at a thickness between 20 (~6 m) and 40 ft (12 m) for the IP scenario, and between 40 and 60 ft (~20 m) for the HP scenario. The last scenario (BP) has the same characteristics as the first one. For layers thicker than 60 ft (~20 m) all seismic scenarios have a similar amplification factor between 1 and 2 units.

The amplification factors for the LP and BP seismic scenarios for sand (Figure 6.19 (1) and (2)) are similar to the ones from clay. Although, the amplification factors for layers thicker than 40 ft are between 1 and 3 units. The second seismic scenario (IP) for sand (Figure 6.19 (2)) shows a very different behavior for the Kocaeli and Douzce earthquakes and the HP scenario shows no correlation between depth and amplification factor for sand.

Both basal till behaves similarly for all the seismic scenarios (Figures 6.20 and 6.21). The LP and BP reach a maximum amplification factor close to 6 units when the thickness of basal till is close to 20 ft (6 m). The amplification factor decreases at a slow rate as the thickness of basal till increases, with an amplification factor of 3 on very deep basal till. For the second and third scenarios, there is no correlation between the amplification factor and depth.

According to the previous sections, the only soil that shows a good correlation between GAN and Shake frequencies is clay. Figure 6.22 shows amplification factors for the four different seismic scenarios for clay. There is good correlation between amplification factors and depth for first and fourth scenarios and no correlation for the second and third scenario.

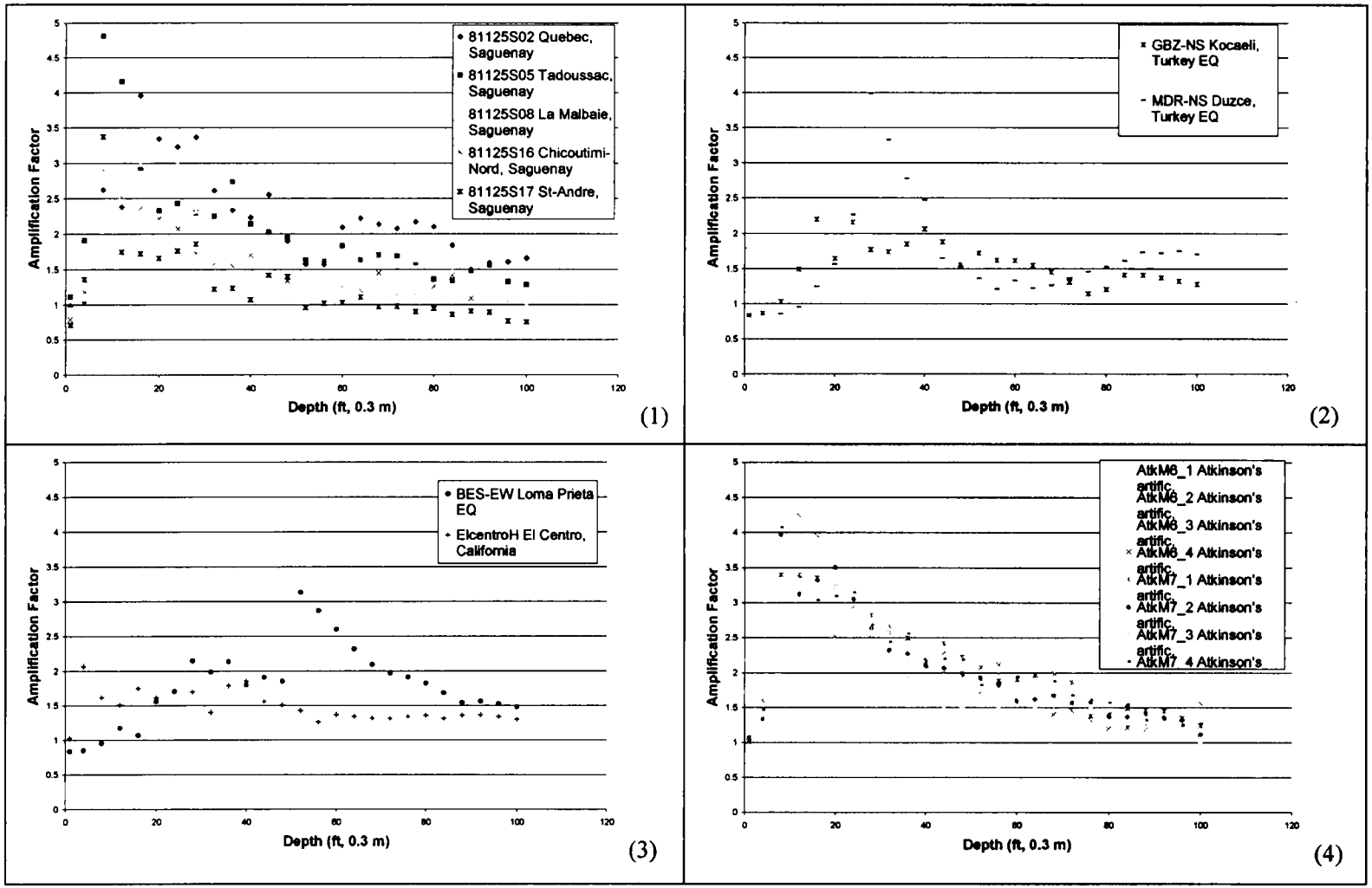

Figure 6.18: Amplification factor vs. Depth of soil for clay for the four earthquakes scenarios: (1) Saguenay earthquake (LP), (2) Kocaeli and Duzce earthquakes (IP), (3) Imperial Valley earthquake and Loma Prieta earthquake (HP) and (4)Artificial earthquakes (BP).

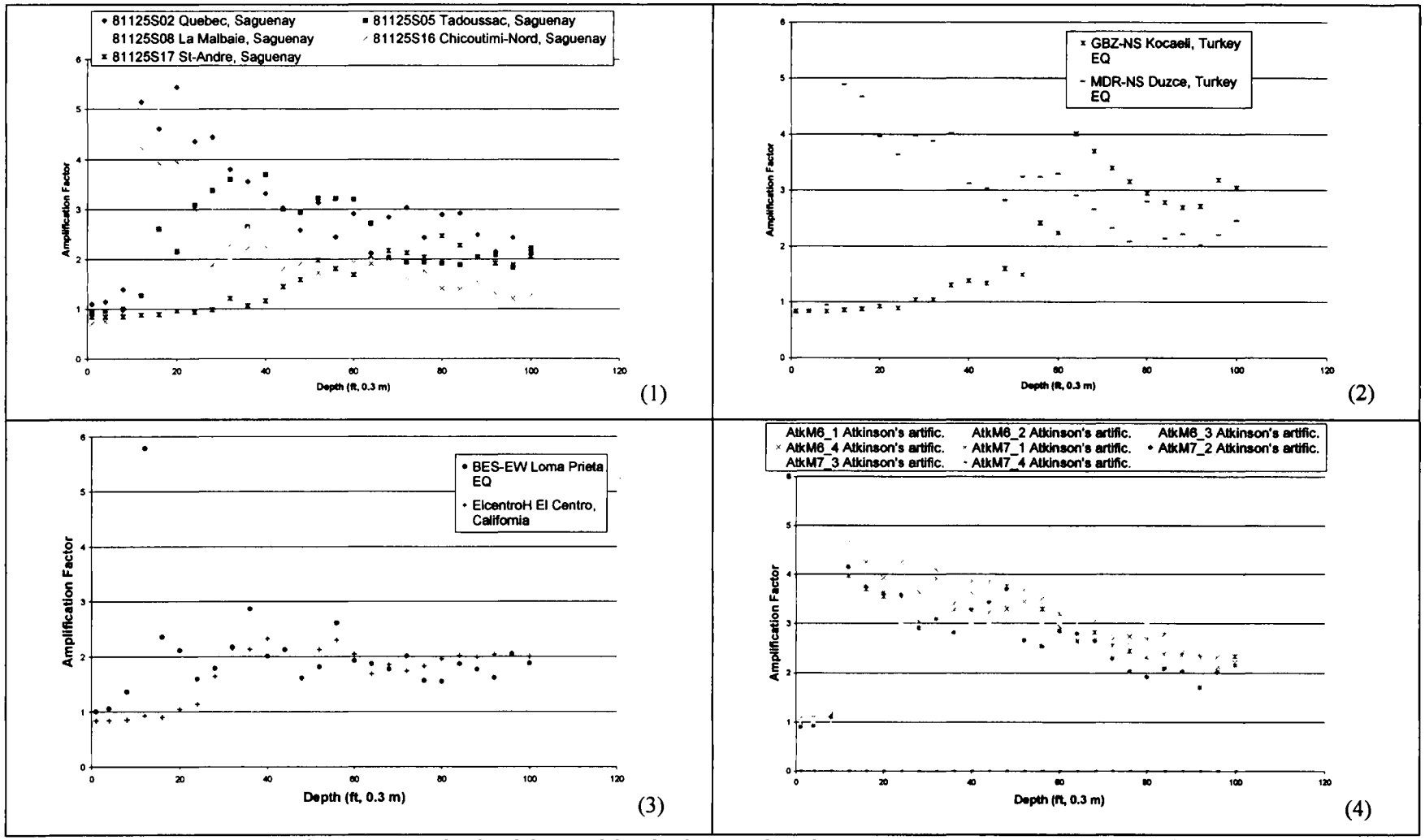

Figure 6.19: Amplification factor vs. Depth of soil for sand for the four earthquakes scenarios: (1) Saguenay earthquake (LP), (2) Kocaeli and Duzce earthquakes (IP), (3) Imperial Valley earthquake and Loma Prieta earthquake (HP) and (4)Artificial earthquakes (BP).

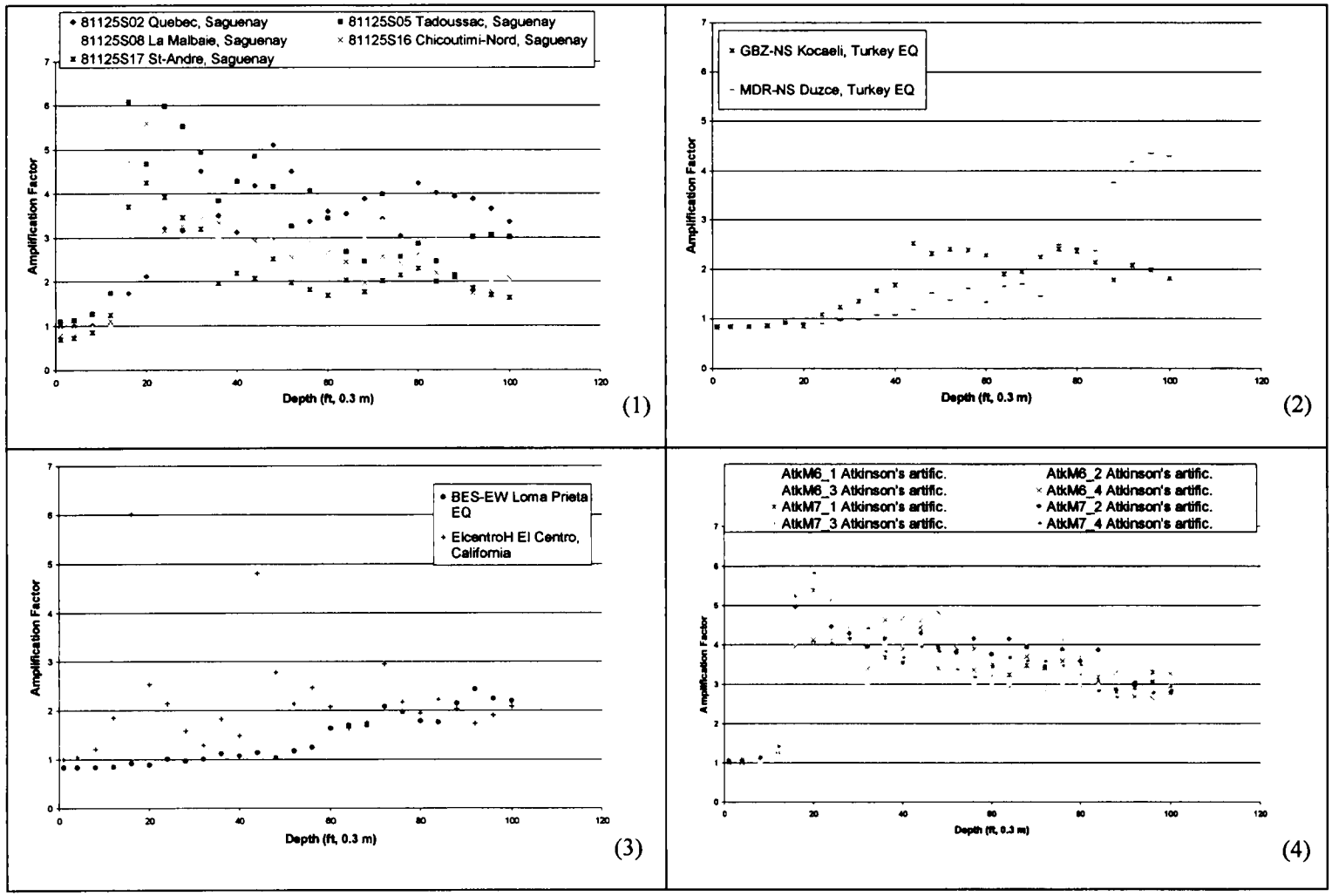

Figure 6.20: Amplification factor vs. Depth of soil for BT3 for the four earthquakes scenarios: (1) Saguenay earthquake (LP), (2) Kocaeli and Duzce earthquakes (IP), (3) Imperial Valley earthquake and Loma Prieta earthquake (HP) and (4) Artificial earthquakes (BP).

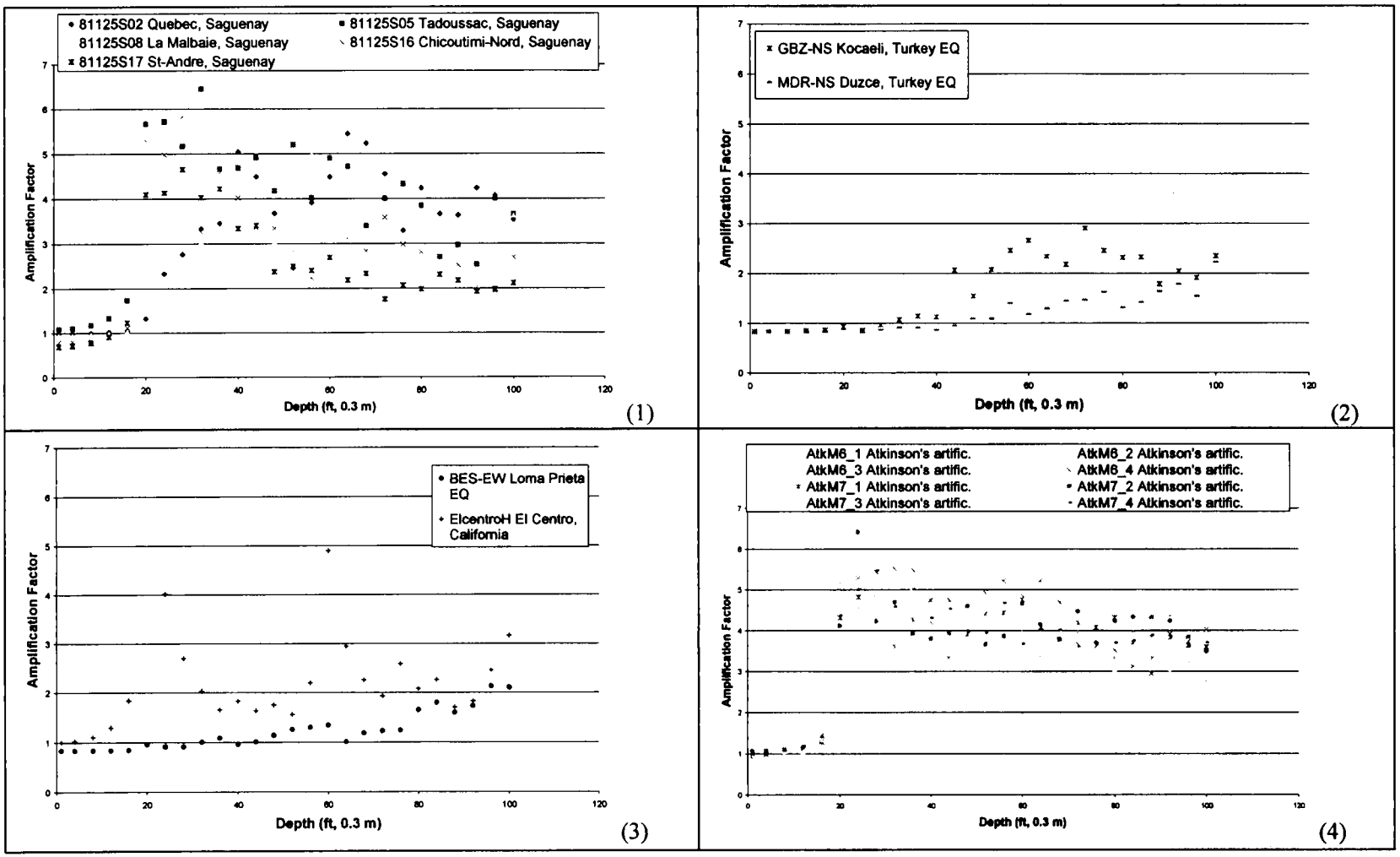

Figure 6.21: Amplification factor vs. Depth of soil for BT2 for the four earthquakes scenarios: (1) Saguenay earthquake (LP), (2) Kocaeli and Duzce earthquakes (IP), (3) Imperial Valley earthquake and Loma Prieta earthquake (HP) and (4) Artificial earthquakes (BP).

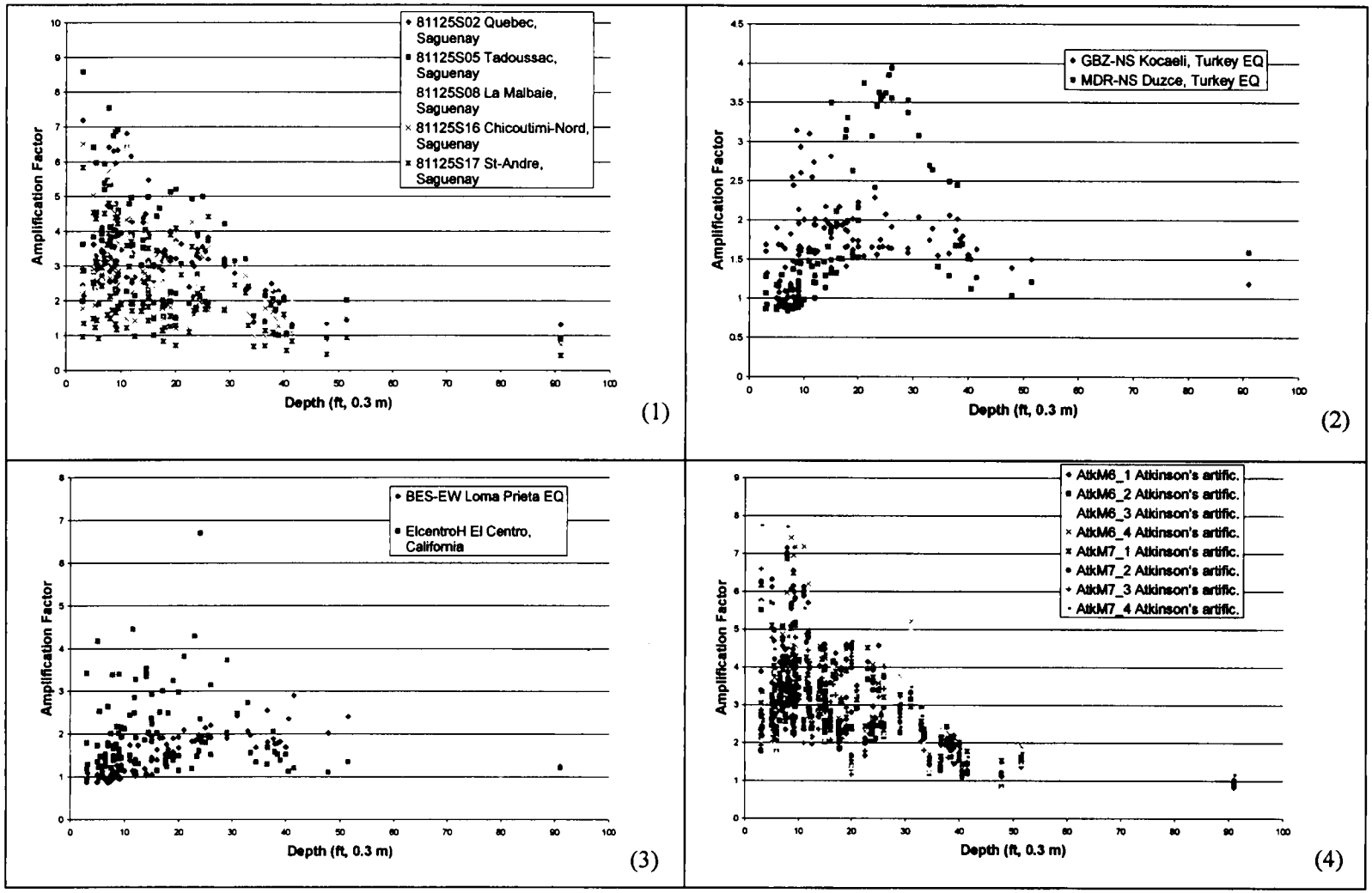

Figure 6.22: Amplification factors for the four seismic scenarios for Clay

Chapter 7 - Recommendations for new values of Shear Wave Velocities

7.1 Introduction

In the previous chapter, boreholes were divided in 4 groups according to the type of soil that controlled the analysis in Shake. The first and last groups, clay and boreholes with basement near the surface, exhibited a good correlation between frequencies calculated in Shake and the frequencies found from the ground ambient noise (GAN) field investigations. The other two groups, BT2 and BT3, exhibited Shake frequencies higher than expected; therefore, some adjustments to soil properties are required to obtain a better match between Shake and GAN frequencies.

The model presented in Chapter 5 is based on the suggestions of Rosset (2003) which assumed an average value for the shear wave velocity of each type of soil deposit. This is an approximation since the shear wave velocity usually increases for a soil deposit as a function of depth. Adjustments to the average shear velocity values are proposed to account for changes in shear wave velocity as a function of depth and to improve the match between Shake and GAN frequencies.

7.2 Boreholes with BT3 layers

The shear wave velocity of any soil increases as a function of depth. BT3 is comprised of clayey silt with few stones and is similar to marine deposits. If all BT3 layers less than 3 m (10 ft) thick are treated as clay, frequencies found in Shake are closer to the

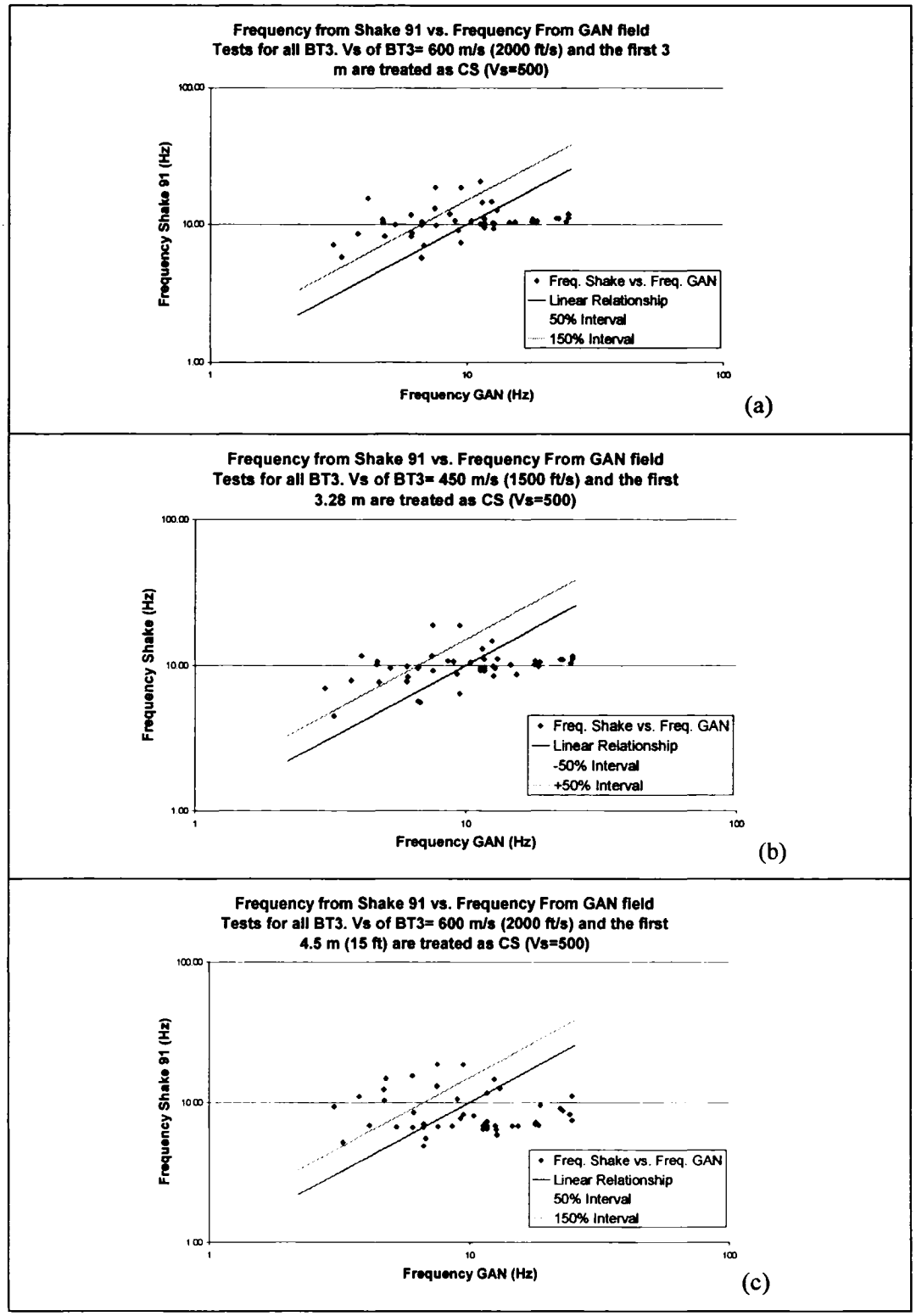

Figure 7.1: Frequency found in SHAKE 91, vs. Frequency from GAN field investigations for all the BT3: (a) BT3 Vs=600 m/s and the first 3 m are taken as Clay, (b)Vs of BT3 = 450 m/s and clay thickness of 3 m and (c) Vs of BT3 of 600 m/s with a thickness of clay of 4.5 m

ones found from the field investigations (Figure 7.1). Those boreholes are reclassified as clay sites since at least 10% of the thickness of the soil column is now treated as clay. When the 3 m (10 ft) adjustment is taken into account there is not much difference between the results using a shear wave velocity for the BT3 of 600 m/s (2000 ft/s) or 457.2 m/s (1500 ft/s) (Figure 7.1 (a) and (b) respectively). If the clay layer is assumed to be thicker, the frequencies are underestimated (Figure 7.1 (c)). The closest match is obtained for a shear wave velocity of 450 m/s (1500 ft/s) for BT3 and the first 3 m (10 ft) of BT3 are assumed to behave as clay.

A statistically significant relation between the GAN results and the thickness of the BT3 layers could not be found (Figure 7.2). This can be explained by the fact that boreholes with a BT3 designation are comprised of many different soils, such as CS or BT2 which can have a significant effect on the frequency.

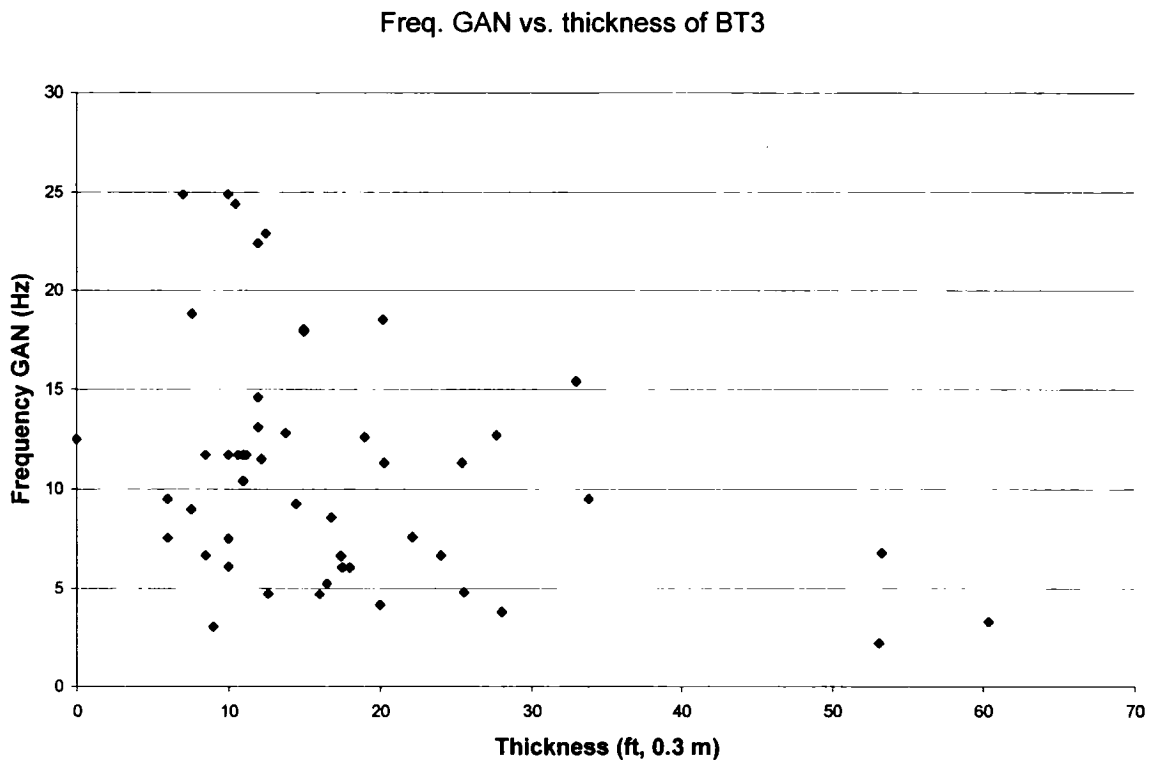

Figure 7.2: Frequency from GAN tests versus thickness of BT3.

7.3 Boreholes with BT2 layers

Sites with BT2 layers less than 50 ft (15m) thick exhibit a wide range of Shake frequencies, some are close to GAN frequencies while and others do not match them at all. In latter case, BT2 layers are usually very close to the surface and the shear wave velocity may be lower than what is assumed in the Shake analysis. If the BT2 close to the surface is similarly to sand, the match between Shake and GAN frequencies is improved (Figure 7.3). The closest match is obtained for a shear wave velocity of 600 m/s (2000 ft/s) for BT2 and by assuming that the first 6 m (20 ft) of the layer behaves as sand with a shear wave velocity of 400 m/s (1300 m/s).

7.4 Summary of Changes

According to the previous analysis, the shear wave velocities suggested by Rosset (2003) are adequate for clay, sand and peat. For the basal tills, it has to be reduced by 25% to obtain an adequate match to GAN frequencies. Also, when BT3 is present near the surface the first 3 m (10 ft) are treated as clay; and, when BT2 is near the surface, the first 6 ma re treated as sand. Table 7.1 summarizes the shear wave velocities used for the analysis. Figure 7.4 shows the new frequencies calculated in Shake 91 vs. the Frequencies from GAN field tests after adjustments.

Final adjustments to the shear wave velocities were done to clay peat and sand to further improve the match in frequencies. The changes do not exceed more than 15% from the original average value suggested by Rosset (2003). Finally Figure 7.5 shows the final match between GAN and Shake frequencies.

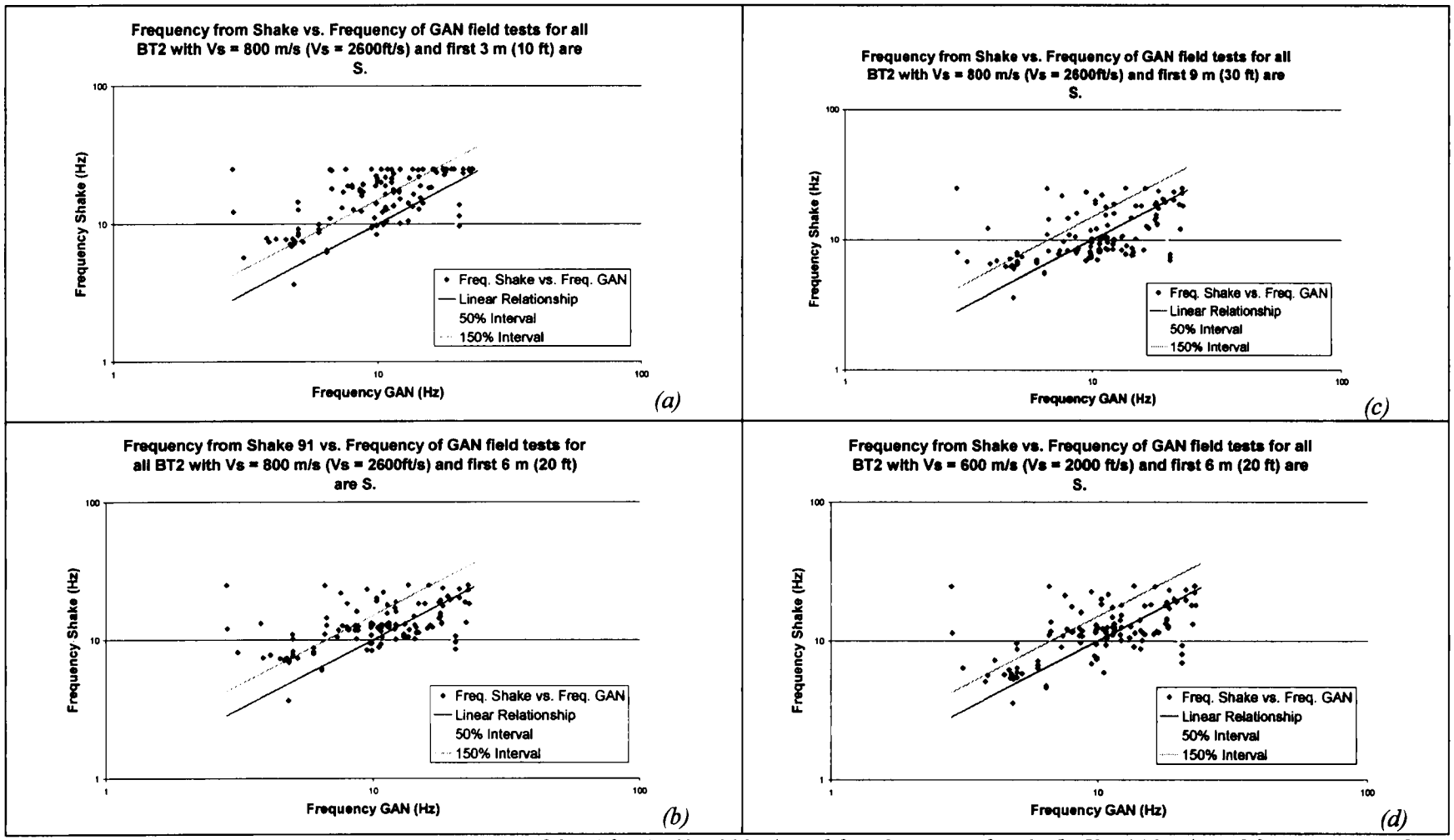

Figure 7.3: Frequency of SHAKE 91 vs. Frequency of GAN for (a) Vs=800m/s and first 3 m treated as S, (b) Vs=800 m/s and first 6 m treated as S, (c) Vs=800 m/s and first 9 m treated as S and (d) Vs=600 m/s and first 6 m

Table 7-1: Summary of the shear wave velocities for the final analysis

Soil	Shear Wave Velocity, Vs (m/s)	Shear Wave velocity, Vs (ft/s)
P	300	1000
S	400	1300
CS	150	500
BT3	460	1500
BT2	600	2000
BT1	730	2400

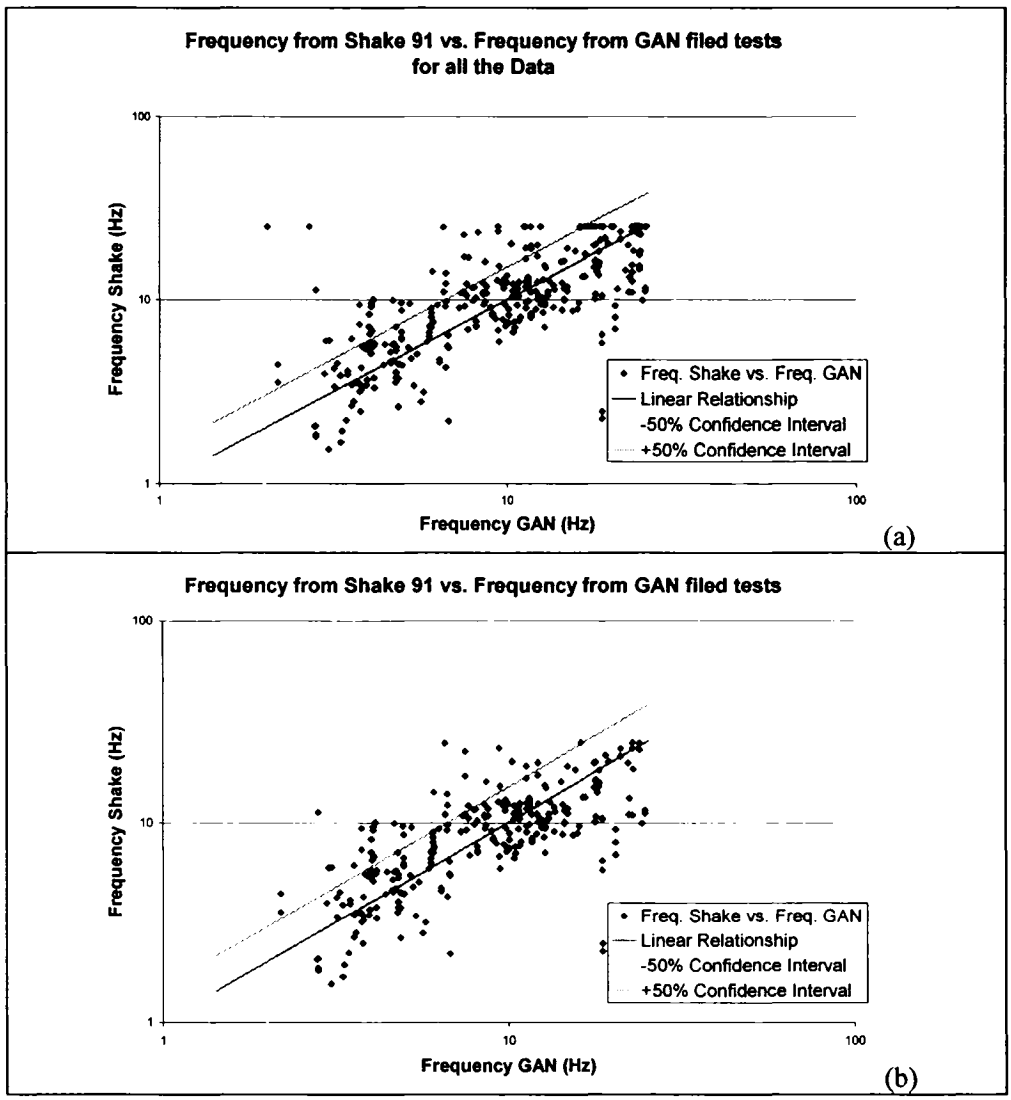

Figure 7.4: Frequency from Shake vs. Frequency from GAN tests for all the results with the new shear wave velocities. (a) Includes the last group of boreholes, less than 10 ft (3.28 m) deep. (b) Disregards the group of less than 10 ft deep.

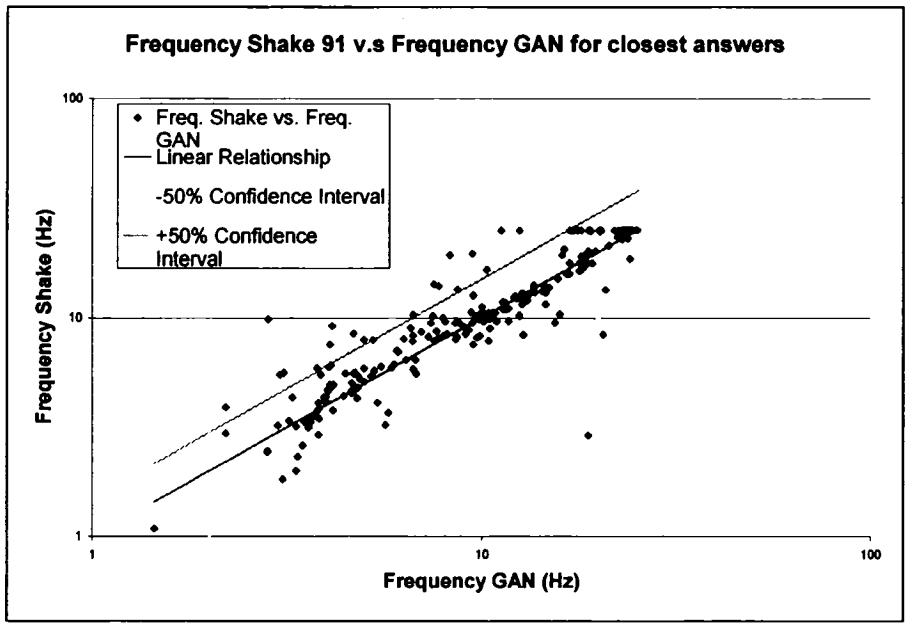

Figure 7.5: Frequency SHAKE vs. Frequency GAN for the best approximation using a variation of 15% for the shear wave velocity of clay, peat and sand is included.

For the 227 GAN sites with a borehole within 100 m, only 39 (16.7%) boreholes show a difference between the GAN and Shake frequencies greater than 3 Hz. Half of those cases improve when the shear wave velocities of Rosset (2003) are adjusted. In Figure 7.5 only the boreholes with the closest shake and GAN were chosen. Table 7.2 explains how widely frequencies can vary on a function of location by comparing frequencies at 3 GAN sites with Shake frequencies from neighboring boreholes.

Table 7-2: Examples of boreholes with different frequency values obtained in SHAKE 91 for the same GAN site.

	ID	Freq. (Hz)	ID	Freq. (Hz)	ID	Freq. (Hz)
GAN	Z1305	14.4	Z2204	18	Z4001	22.9
Boreholes	84F001-4658	9.28	60F001-0005	12.35	67OTTA-16016	12.66
	74F078-0426A	14.03	59F013-0001	18.98	95F002-0005-15	22.78
			60F001-0006	19.27	64F046-0001-15	21.4

7.5 Final Amplification Factors

Amplification factors are calculated using shear wave velocities that give the best match of frequencies. Figure 7.5 shows the average amplification factors for the four earthquake scenarios (LP, IP, HP and BP) as a function of depth to bedrock. The scenario that gives the highest correlation is the IP scenario (Table 7.3). These amplification factors are smaller than the ones found for the other scenarios. All of the scenarios exhibit a large amplification between 3 and 10 Hz, but only the BP and LP have a high amplification factor for the rest of the frequencies. Table 7.4 summarizes the amplification factors for the four scenarios. The IP and HP scenarios do not have a very large amplification for most of the sites (Figure 7.7 (b) and (c)); therefore, if earthquakes in Montreal are similar to those seismic events, the PGA would have a small amplification. On the other hand, the first (LP) and fourth (BP) scenarios have a fair quantity of sites with amplifications between 3 and 5 (Figure 7.7 (a) and (d)).

Table 7-3: Correlation coefficients for all the earthquake scenarios with respect to Shake frequency and Bedrock depth

	LP	IP	HP	BP
Shake Frequency	-0.50501	-0.80488	-0.20015	-0.45368
Depth to bedrock	0.512521	0.798433	0.344146	0.453499

Table 7-4: Amplification Factors for all the scenarios considered

	LP Scenario (Saguenay Eqs)	HP Scenario (California Eqs)	IP scenario (Turkey Eqs)	BP Scenario (Artif. Eqs)
Max	5.826125	6.70	3.35	6.40
Min	0.894375	0.92	0.83	0.95
Avg.	2.924222	1.79	1.46	3.30

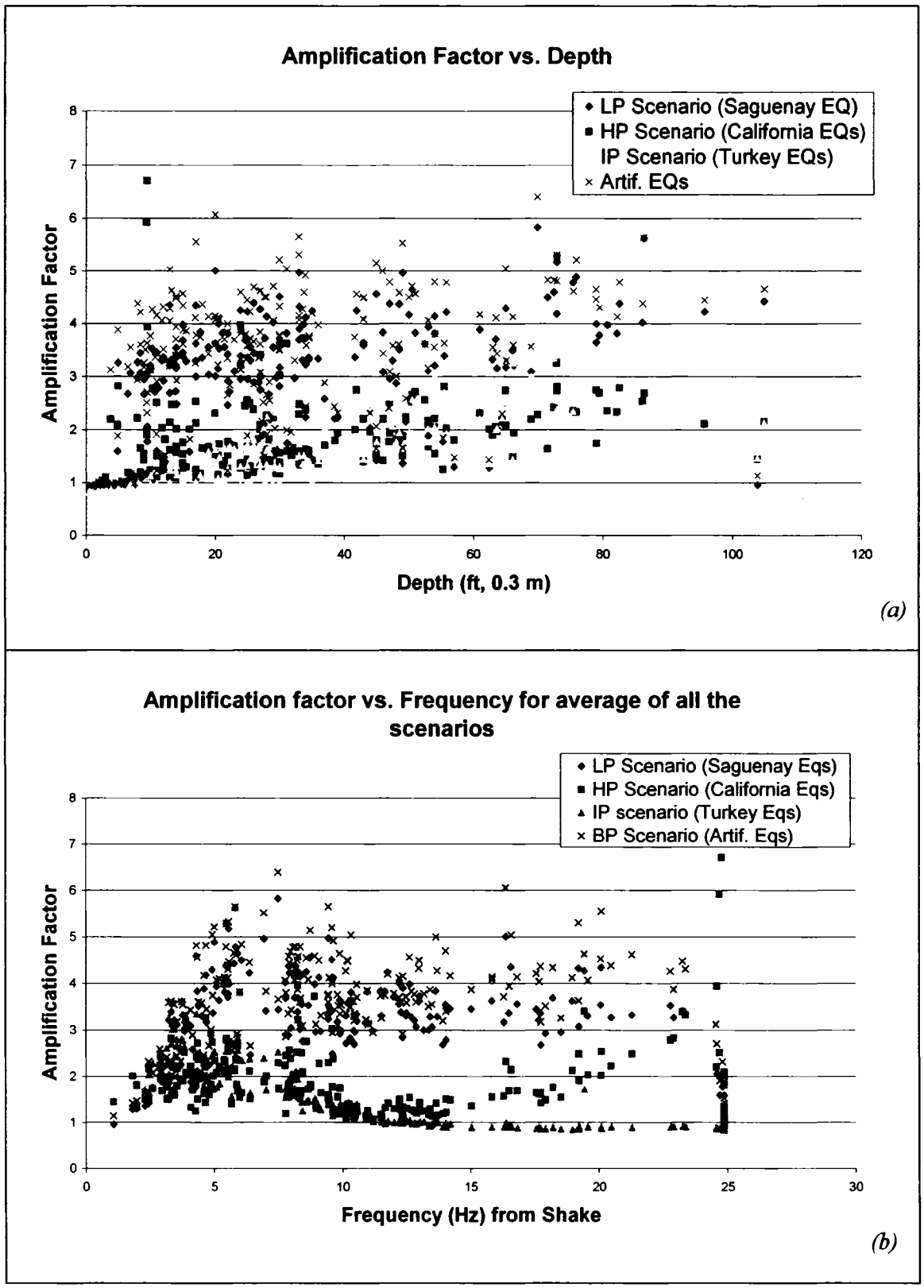

Figure 7.6: : Amplification Factors for the four scenarios: (a) Amplification Factor vs. Depth of Basement and (b) Amplification factor vs. Frequency.

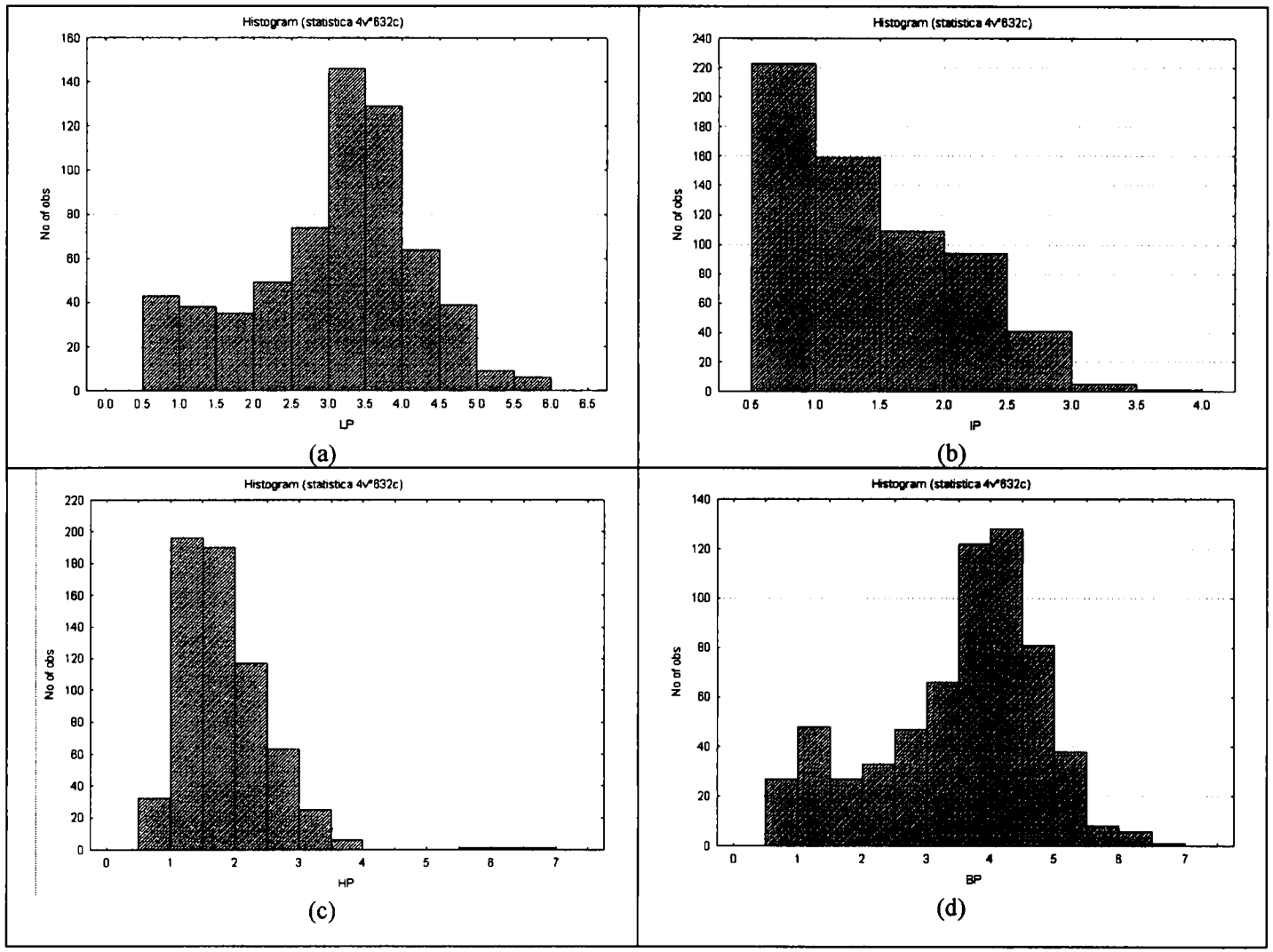

Figure 7.7: Histograms for the four earthquake scenarios: (a) LP, (b) IP, (c) HP and (d) BP.

There are some amplification factors less than 1 (Figure 7.7) but all of these are higher than 0.85. Amplification for seismic scenarios 1 and 4 are very similar, andhave a correlation of 0.9 (Figure 7.8 (1D and 4A)). The amplification factors for other seismic scenarios do not show good correlations. Since the artificial earthquakes (BP scenario) are very similar to the Saguenay earthquake (LP), the broad band scenario could also be treated as an LP scenario.

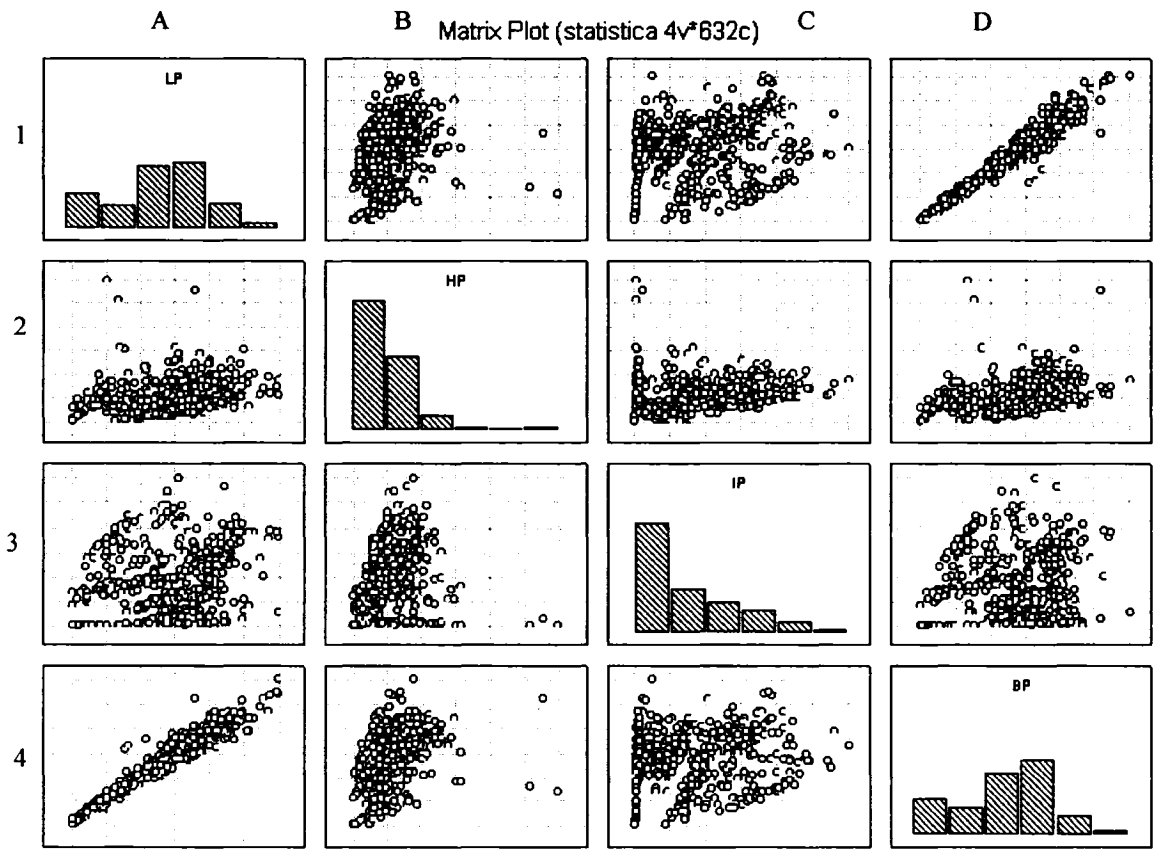

Figure 7.8: Matrix Correlations between the Amplification Factors for the four Seismic Scenarios. The Diagonal shows the histograms for each scenario, starting from upper left corner: LP, HP, IP and BP .The other plots are the correlations between the scenarios.

7.6 Conclusions on the validation of GAN field tests results using boreholes and Shake Analysis

The conclusions on the qualitative analysis of the GAN results set from Chapter 6 (Figure 6.3 and Table 6.1) and the final frequencies found in Shake 91 are the following:

- All GAN results classified in group 4 are on rock sites
- Only one of the category 0.7 for the GAN tests is not rock, which is less than 6% of the tests in the group
- When GAN results have two peaks, the predominant frequency is assigned to the second peak.
- GAN results classified as group 2 have large uncertainties and any value in the plateau is equally probable. The frequency in the plateau that is closest to the GAN frequency is selected.
- No general conclusions could be obtained for results classified as group 3 since only 3 boreholes are close to the GAN tests.

The rules above are applied to the GAN field results that could not be directly validated with a borehole.

Chapter 8 - Microzonation Mapping

8.1 Introduction

The main goal of this thesis is to perform a microzonation of Montreal and to present the results in a form that can be used as input to vulnerability studies. Since only 227 GAN sites out of 703 are close enough to a borehole to validate the predominant frequency, an interpolation technique had to be developed to validate the other GAN frequencies and estimate the amplification factors. First, a study of the spatial variability of the data was performed to determine the accuracy for the spatial interpolation of the predominant frequency. A widely used interpolation technique for spatial data is kriging, which first requires the estimation of a covariance function.

8.2 Variogram

Intuitively, two neighboring points should share similar values if they are representative of similar physical conditions. On the other hand, conditions are more likely to be different for points located at long distances from each other (Chiles et al, 1999). The dissimilarity ($\gamma^*_{\alpha\beta}$) between two values at two points X_α and X_β, is defined as [Wackernagel, 2003]:

$$\gamma^*_{\alpha\beta} = \frac{(Z_\alpha - Z_\beta)^2}{2} \qquad [8.1]$$

where Z_α and Z_β are values at points X_α and X_β respectively. Using all the possible sample pairs in a data set, a plot of dissimilarities against the spatial separation (h) is produced which is called the variogram cloud (Wackernagel, 2003). Figure 8-1

shows a typical variogram cloud. The variogram cloud is a powerful tool for exploring features of spatial data. If the variogram is bounded by a finite value $\gamma(\infty)$, a covariance function can be found such that:

$$C(h) = \gamma(\infty) - \gamma(h) \qquad [8.2]$$

where h is the distance between the sample points (Wackernagel, 2003).

When a variogram does not vary with direction, it is said to be isotropic. Otherwise, if the experimental variogram changes with variations in the azimuth of the vector connecting to points, it is considered to be anisotropic [3]. In practice, anisotropies are detected by inspecting experimental variograms in different directions.

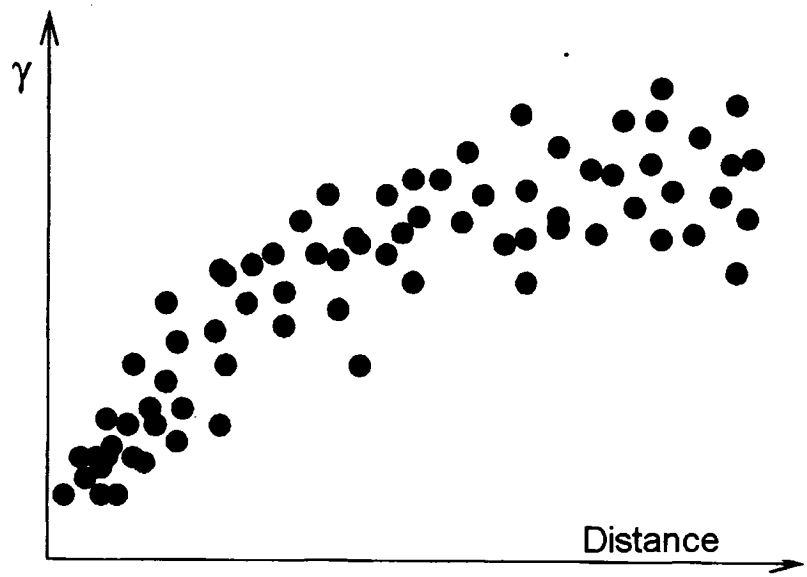

Figure 8.1: Example of variogram cloud (Wackernagel, 2003)

First, a test of the first order variability of the borehole data was performed by calculating the variogram of the depth to basement. Only the closest 100 boreholes which are located at a maximum distance of 1000 m from a point are included in the calculation. Figure 8.2 shows the region selected (Z6518) for a typical GAN test and the corresponding isotropic variogram. The variogram does not show a strong relationship between distance and dissimilarity and a function for the covariance can

not be estimated. All the other regions defined around locations of GAN test exhibit similar variograms.

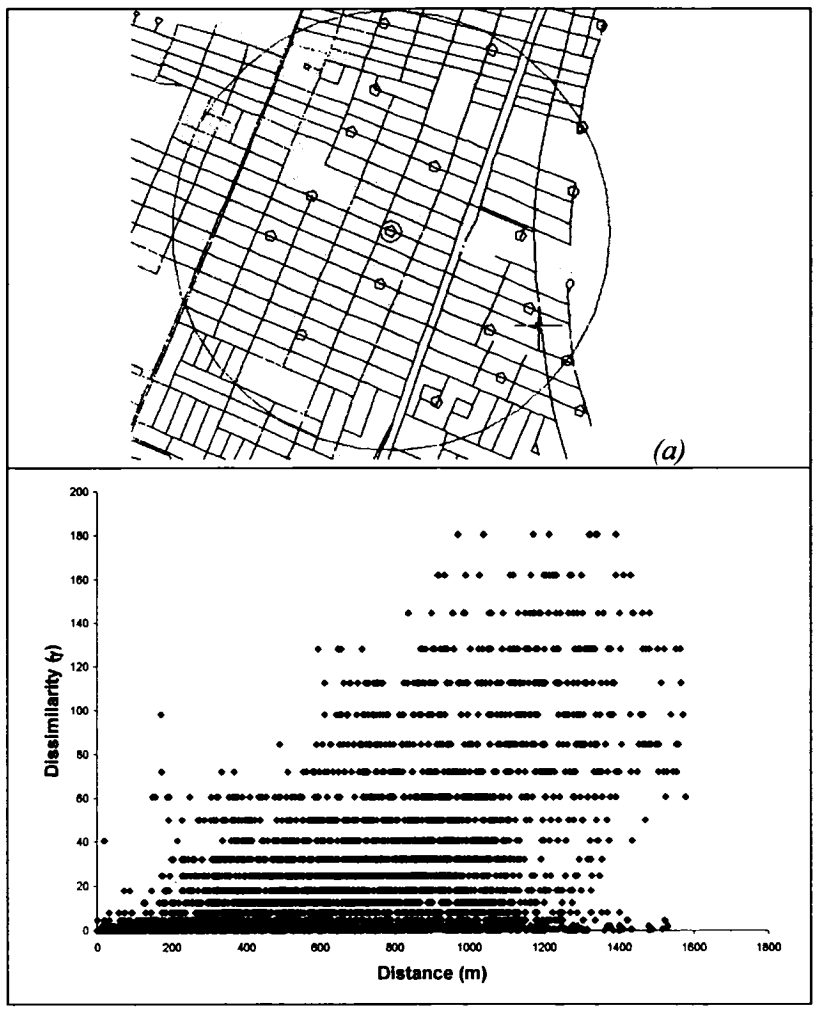

Figure 8.2: Sample region for the variogram based on the closest 100 boreholes (isotropic) located less than 1000m from the reference point (a) Shows the location of Z6518 and (b) shows the variogram for Z6518.

Since soil the deposits in the island of Montreal are usually in a direction parallel to the St. Laurent River, depth to bedrock is also anisotropic. If the region is divided in 16 quadrants, of 22.5° each as shown in Figure 8.3 (a), the relationship is improved and estimation of covariance functions can be achieved (Figure 8.3 (b)). Since the variogram has to be done for each of the 16 sectors and the relevant equations have

also to be estimated, the procedure becomes unfeasible if applied to each GAN tests that does not have a borehole nearby for validation and another procedure has to be devised.

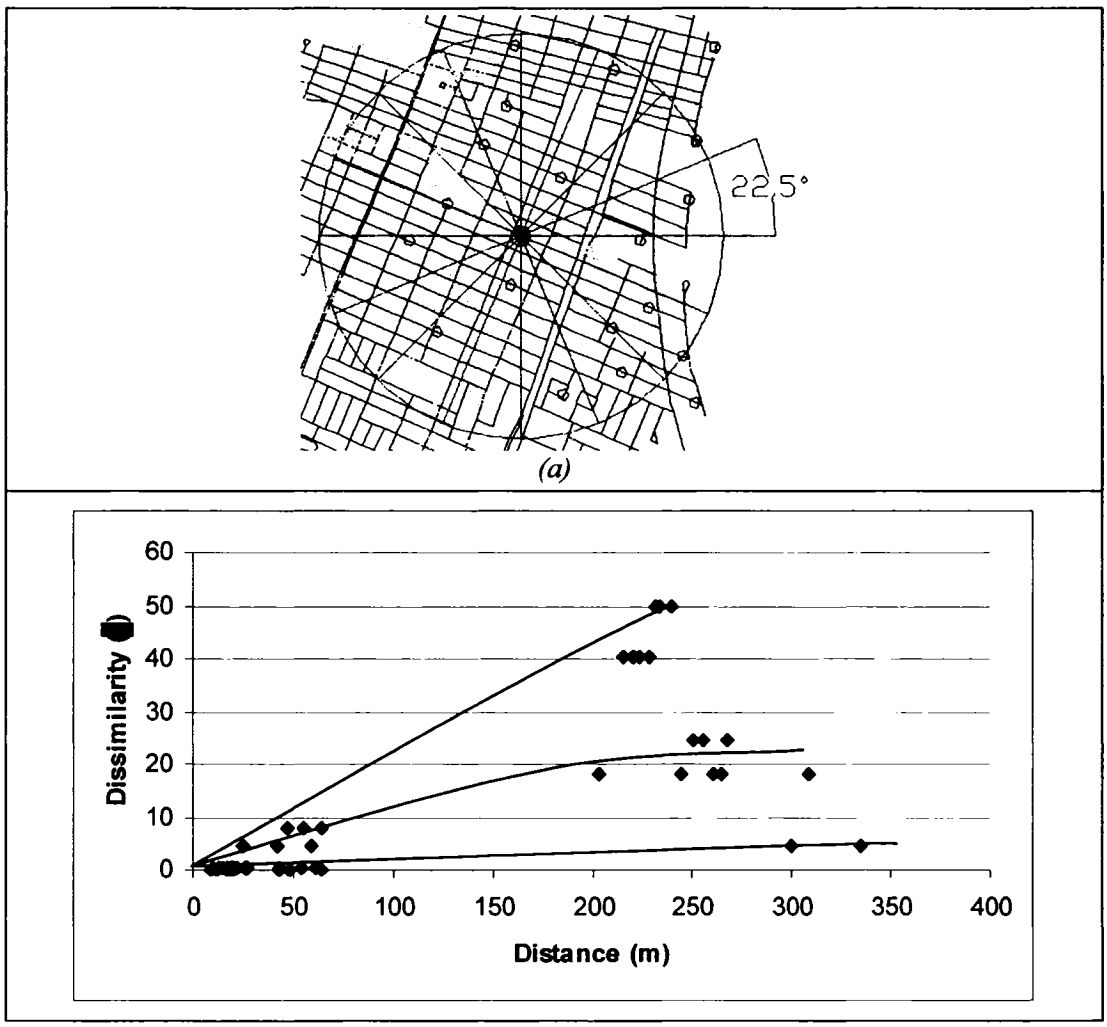

Figure 8.3: (a) Division of each region for directional variogram and (b) Variogram for one of the regions using only the closest 10 boreholes.

8.3 Final Results

The procedure retained to validate the predominant frequency of GAN tests not located close to a borehole consists of taking the closest 10 boreholes to a GAN test location, use the soil properties and shear wave velocities recommended in Chapter 7 for Shake 91, and obtain frequencies and amplification factors. The frequencies from

the borehole are compared to the GAN frequency. The borehole that provides the closest match between Shake and GAN frequencies is identified and the Shake 91 amplification factor for the borehole is assigned to the GAN test location. The relationship between the frequencies of the 10 closest boreholes vs. GAN frequency is shown in Figure 8.4. The figure indicates that the Shake frequency can be very different from the GAN frequency. Selecting only frequencies that offer the best match improves the results considerably (Figure 8.5). Table 8.1 summarizes the results for the 475 GAN tests.

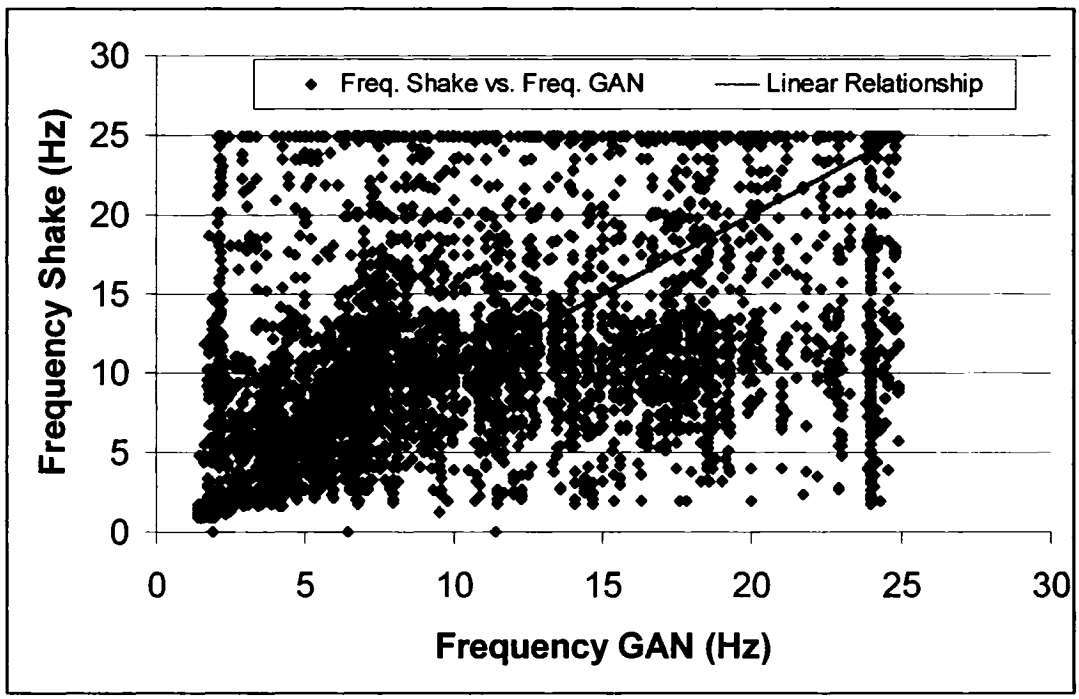

Figure 8.4: Figure 8.4: Frequency of Shake vs. Frequency of GAN for the closest 10 boreholes for each GAN test.

Table 8-1: Results for the 475 boreholes.

Criteria (Difference between Shake and GAN Frequencies)	Number of GAN tests	% GAN Tests
Less than 1 Hz	323	68%
Between 1 and 2 Hz	81	17.1%
Between 2 and 3 Hz	23	4.8%
Larger than 3 Hz	48	10%

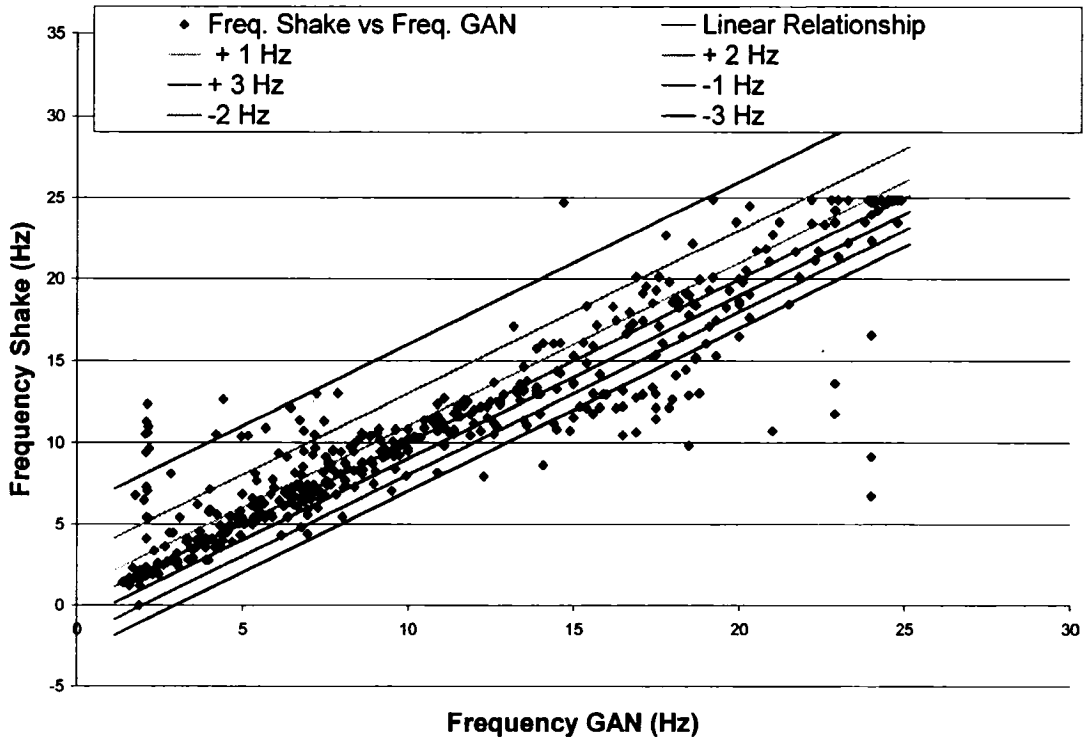

Figure 8.5: Final Results for the 475 GAN tests.

Note that the locations where the difference between the Shake and GAN frequencies is higher than 3 Hz are very few (Figure 8.6).

8.4 Microzonation Mapping

Microzonation maps are created using only the locations where the frequency could be validated (i.e. matched within 3 Hz). Maps for the predominant frequency calculated in GAN and Shake are provided in Figures 8.7 and 8.8. The locations of the boreholes used for the analysis with Shake are provided in Figure 8.9. The amplification factors for the corresponding predominant frequencies for the four scenarios (LP, IP, HP and BP) are shown in Figures 8.10, 8.11, 8.12 and 8.13. The maps include the sites investigated by Rosset (2003).

Figure 8.6: Difference between Shake and GAN frequencies

As expected the maps of the Shake and GAN frequencies are very similar since only the data with less than 3 Hz in difference were used.

The four maps for the amplification factor use the same color scale to facilitate the comparison between results. As in Figure 7.5 (b), the largest amplification factors for the LP and the BP scenarios are at locations of high predominant frequencies. The average amplification factor is 3 for the Island, even at locations where the rock is a few meters from the surface. Note that at locations with 30 m of clay, at the tip of the island, the amplification factors drop to 1 or 2 for these scenarios (Figures 8.10, 8.11, 8.12 and 8.13). As explained in Chapter 6, amplification factors in deep clay areas are expected

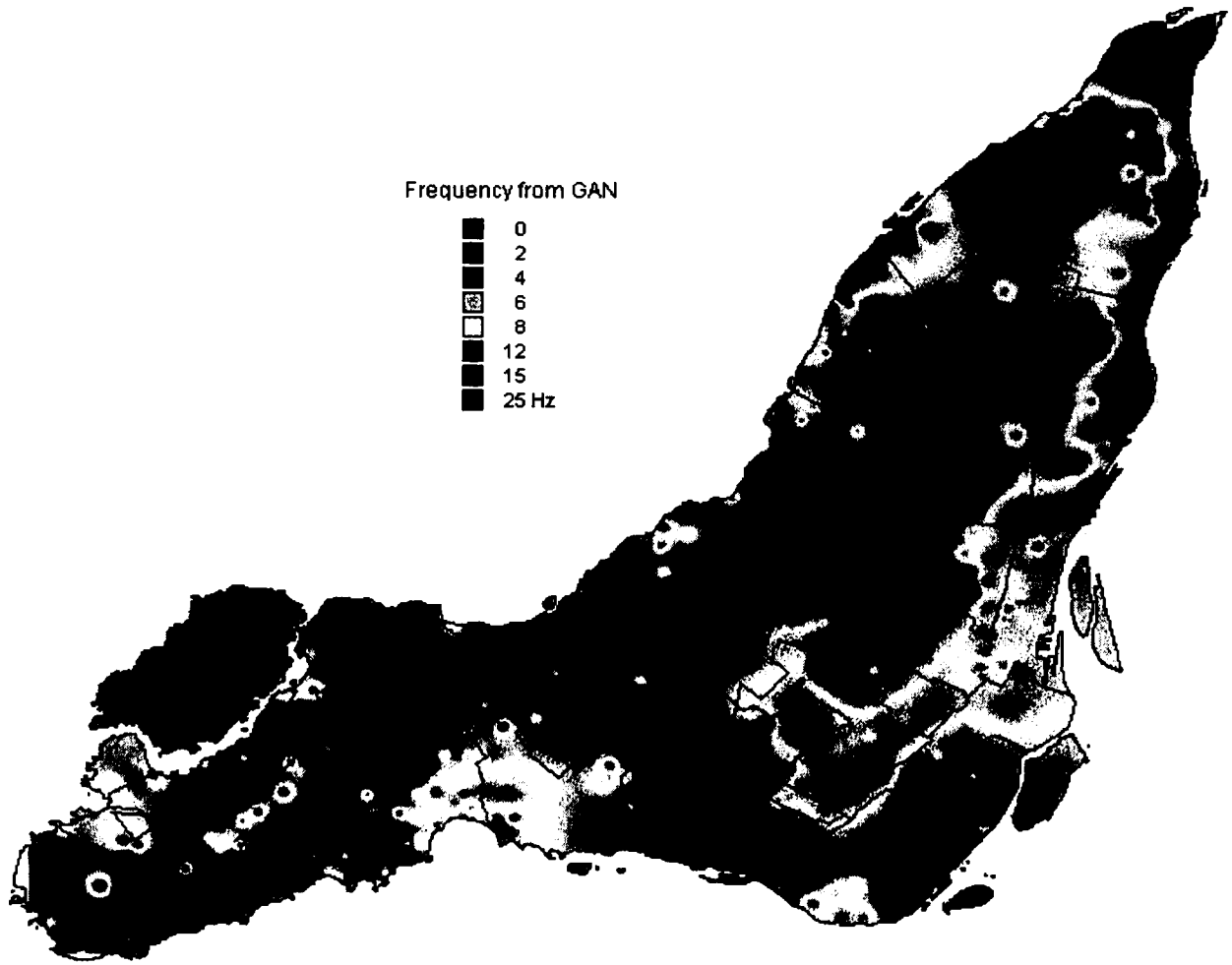

Figure 8.7: Frequency calculated from GAN technique

Figure 8.8: Predominant Frequencies calculated from Shake

Figure 8.9: Boreholes used to find the amplification factors

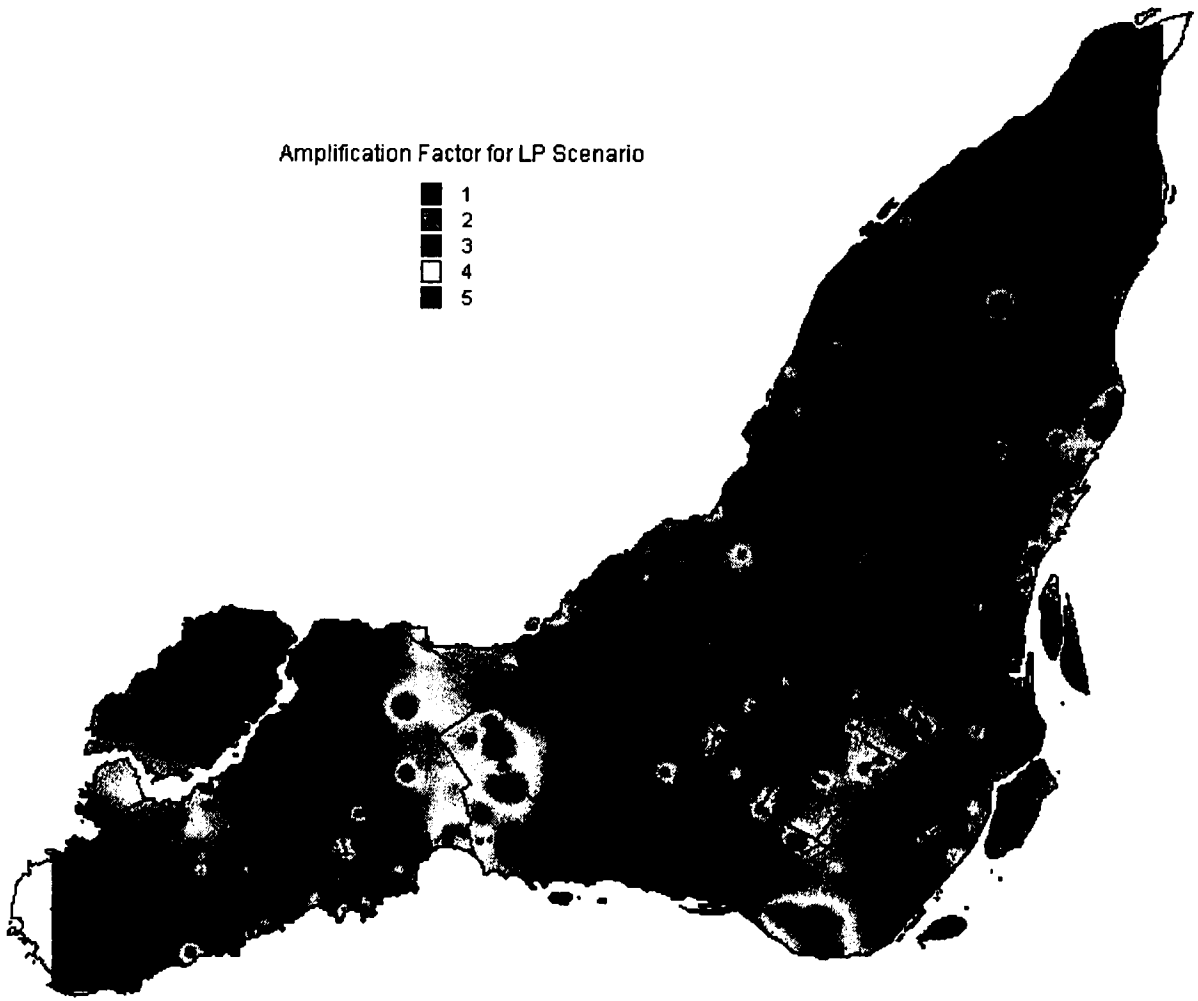

Figure 8.10: Amplification Factors for the LP Scenario

Figure 8.11: Amplification Factors for the IP Scenario

Figure 8.12: Amplification Factors for the HP Scenario

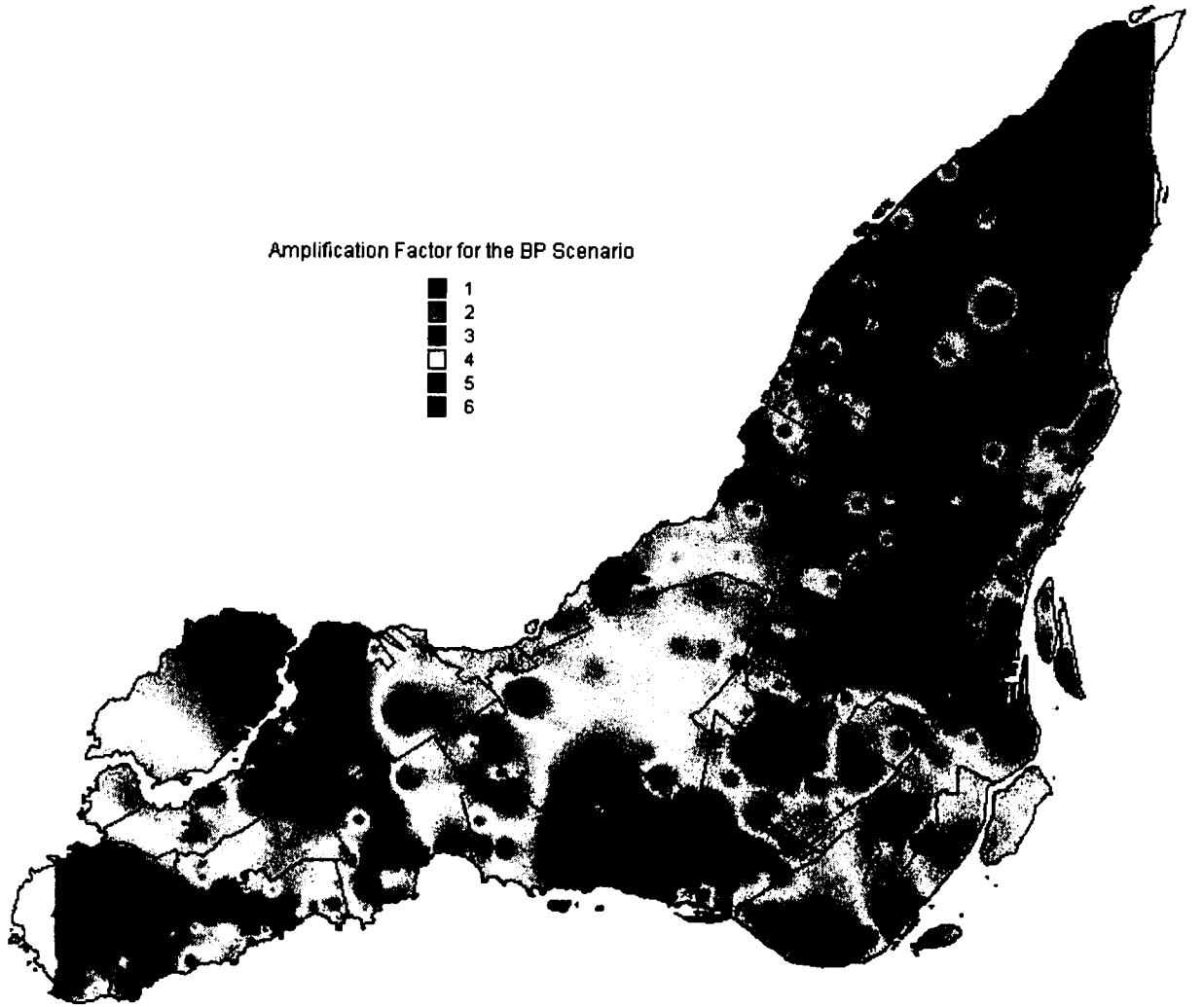

Figure 8.13: Amplification Factors for the BP scenario

to be low for all the seismic scenarios. On the other hand, there are some areas where the amplification factor is greater than 3 for two earthquake scenarios and greater than 5 for the other 2, and the predominant frequency is lower than 5 Hz. A comparison between the two cases is included in appendix A. The maps for the IP and HP scenarios are consistent with the usual expectation that the maximum amplifications occur at locations with lower predominant frequencies.

8.5 Conclusions and Recommendations for Future Work

According to the analyses and comparisons between the frequencies found by the two methods, it can be concluded that the GAN technique is an easy, fast and accurate method for estimating the predominant frequency of soil deposits. It is good practice to validate the results with other methods since experience indicates that some results are unclear when there are many different types of soils in soil columns .

The shear wave velocities used in the numerical method were adjusted by 25% for the basal till and by 15% for clay, peat and sand deposits from the values suggested by (Rosset, 2003). The changes are considered acceptable since there was practically no information about the actual shear wave velocity of the soils on the island. It is recommended that field surveys should be conducted in the future to confirm the proper values for the shear wave velocities.

The amplification factors for the four scenarios are very different for both the sensitivity analysis conducted in Chapter 6 and for the results obtained in Shake. The IP and HP scenarios gave results which were expected. But the BP and LP scenarios have high frequency content and results in some parts of the island were unexpected. Since there is lack of knowledge about the characteristics of the earthquakes expected near Montreal, the study of several scenarios is necessary.

The research should continue with the GAN tests at the location of boreholes since

there is a very high spatial variability in the soils. The frequencies obtained with Shake 91 were similar to the ones from GAN for the boreholes closer than 100 m; although, near the 100 m limit, the differences between the two methods were increasing. Therefore, it is recommended to conduct 100 GAN tests per km^2 for areas where soils and depth to the basement have a high variability.

This research includes the maximum amplification factor and the frequency at which it occurs. The worst case would be if a building has the same predominant frequency as the soil, which creates resonance. The microzonation should be done also for other frequencies, from 1 to 10 Hz, which is the usual range of the predominant frequencies of most structures. The amplification factors should be calculated for those frequencies. This will allow users to estimate the actual amplification factor when resonance is expected.

This research has demonstrated that GAN results provide quick and useful estimates of the predominant frequency of soil deposits. It could be useful though to conduct field and laboratory tests to better characterize dynamic properties of soils in Montreal.

Even so, this study has highlighted how the sensitivity of amplification factors are to the scenario selected for input ground motions. This uncertainty can only be decreased as more strong motion data on rock and soft soil sites are recorded in the Montreal area. For this reason, it would be desirable to set up a network of strong motion instruments in the Montreal area to obtain actual data in the event of any future seismic event.

References

1. Adams, J. and Atkinson, G. *"Development of seismic hazard maps for the proposed 2005 edition of the National Building Code of Canada". Canadian journal of Civil Engineering (CJCE) 30, no. 2, pp 255 -271*
2. Adams, J., and Basham, P. (1989). "*The Seismicity and Seismotectonics of Canada East of the Cordillera.*" Geoscience Canada, 16(1):3-16.
3. Andrus, R.D., Piratheepan, P. and Hsein Juang C. *"Shear Wave Velocity – Penetration Resistance Correlations for Ground Shaking and Liquefaction Hazards Assessment".* ***http://erp-web.er.usgs.gov/reports/annsum/vol44/ep/01HQGR0007.pdf***
4. Atkinson, G. and Beresnev (1998). "*Compatible ground-motion time histories for new national seismic hazard maps*". Can. J. of Civil Eng. 25, pp305-318.
5. Byers, A.R. (1949). "*The nature and Origin of the Glacial and Post-Glacial Deposits Lying between the City of Montreal and the Canadian Shield*". McGill University, Post-Doctoral Thesis, Montreal.
6. Chilès, JP and Delfiner, P. (1999*). "Geostatics Modeling Spatial Uncertainty".* Toronto: John Wiley & Sons, INC. p 35-57.
7. Clark, T.H. (1972). "*Montreal Area*". Geological Report-152, Ministère des Richesses Naturelles, Ottawa.
8. Leger, P., Mitchell, D. and Rogers, C. Course notes from "*Earthquake-Resistant design of Structures*", CIVE 612, Department of Civil Engineering and Applied Mechanics, McGill University, winter 2003.
9. De la Puente, A and Rosset, P. (2002). "*Excel-Shake interface User's Manual*". Technical Report, McGill University, Department of Civil Engineering and Applied Mechanics, 43 pp.
10. Duval. A.M., Chatelain, J.L., Guillier, B. (2004). *"Influence of Experimental Condition for «H/V» for Ambient Noise Vibration Method".* 13th World

Conference on Earthquake Engineering (WECC), Vancouver, B.C., Canada. Paper No. 306

11. ElFashny K.N.G, Chouinard, L.E., Hguyen, V.T.V. and Laflamme, J.N. (200) *"Spatial Analysis of Ice Observations in Quebec, Canada". International Workshop of Atmospheric Icing of Structures (IWAIS), Chester, England, 11 pages.*
12. Fäh, D. "Earthquake Scenarios from Earthquake Hazard to Loss Estimates". www.ndk.ethz.ch/downloads/publ/Faeh.PDF
13. Filiatrault, A. (2002). "*Elements of Earthquake Engineering and Structural Dynamics*". Second Edition, Polytechnic International Press.
14. Fillingim, M. "*Intraplate Earthquakes: Possible Mechanisms for the New Madrid and Charleston Earthquakes*". http://www.geophys.washington.edu/People/Students/matt/seismo.html
15. Finn, W.D.L. and Wightman, A. (2003) *"Ground Motion amplification factors for the proposed 2005 edition of the National Building Code of Canada"* Canadian Journal of Civil Engineering (CJCE), vol. 30, pp 272-278
16. Fulton, R.J. (1989). "*Quaternary Geology of Canada and Greenland*". Geological Survey of Canada, Ottawa.
17. Goula, X., Susagna, S., Figueras, S. and Cid, J. *"Comparison of numerical simulation and microtremor measurement for analysis of site effects in the city of Barcelona (Spain)*". http://www.icc.es/pdf/publibienni/35.pdf
18. Idriss, I.M., Sun, J.I. (1992). "*User's Manual for Shake91*". Department of Geotechnical Modeling and Department of Civil & Environmental Engineering University of California.
19. Kokusho, T. and Yoshida, Y. (1997). *"SPT N-Value and S-Wave Velocity for Gravelly Soils with Different Grain Size Distribution".* Soils and Foundations, Japanese Geotechnical Society, Vol. 37, No. 4, 105-113
20. Lacave, C., Bard, P.-Y., and Koller, M.G. "*Microzonation: Techniques and Examples"*

www.ndk.ethz.ch/downloads/publ/Koller.pdf

21. Nakamura, Y. (1989). "*A Method for Dynamic Characteristics Estimation of Subsurface Using Microtremor on the Ground Surface*". Quarterly Report of Railway Technical Research Institute, 30, N°1, pp 25-33.

22. Nakamura, Y. (2000). "*Clear Identification of Fundamental Idea of Nakamura's Technique and Its Applications*". 12 World Conference of Earthquake Engineering (12WCEE), New Zealand, paper number 2656.

23. Olea, R. (1999). "*Geostatistics For Engineers and Earth Scientists*". Massachusetts: Kluwer Academic Publishers, p68-90

24. Parvez, I., Jade, S. and Gaur V.K. (2001). "*Microzonation And Site Specific Ground Motion Modelling Of Delhi City*". Project proposal CM0102. Bangalore, India.

25. Prest V.K. and Hode-Keyser, J. (1977). "*Geology and Engineering Characteristics of Surficial Deposits, Montreal Island and Vicinity, Quebec*". Geological Survey Paper 27-75, Montreal.

26. Prest, V.K. and Hode-Keyser, J. (1962). "*Surficial Geology and Soils, Montreal Area, Quebec*" Department of Public Works, Montreal, 1962.

27. Rosset, P (2002). "*SPCRatio User's Manual: A tool to analyze ambient noise records*". Internal paper, McGill University, Department of Civil Engineering and Applied Mechanics, 20 pp.

28. Rosset, P (2003). "*Identification of site effects in the Montreal Urban Community, Canada: Pilot study and methodological developments*". Geological Survey of Canada, Open file 3724.

29. Rosset, P., del Puente, A., Chouinard, L., Mitchell, D. and Adams, J. (2002). "Site Effect Assessment at Small Scales in Urban Areas: a Tool for Preparedness and Mitigation". http://www.grif.umontreal.ca/pages/i-rec%20papers/philipros.PDF

30. Schnabel, P.B., Lysmer, J. and on Seed, H. (1972). "*SHAKE, A Computer Program For Earthquake Response Analysis Of Horizontally Layered Sites*". Report No. EERC72-12. College of Engineering, University of California.

31. Stansfield, J. (1915). "*The Pleistocene and Recent Deposits of the Island of Montreal*". Geological Survey Canada – 73, Ottawa.

32. Wackernagel, H. (2003). "*Multivariate Geostatistics*". Third Edition, New York: Springer.

A - Appendix

Large amplification factors are usually expected for soft soil deposits and small amplifications are usually expected for stiff soils. According to this research, two of the earthquake scenarios presented amplification factors between 1 and 2 for thick clays. On the other hand, amplification factors for thick basal till are larger than 5, for the same seismic scenarios.

This appendix presents the borehole data, the H/V plots for GAN, and Shake frequencies and amplification factors for two locations in the Island of Montreal: 1) Thick clay site and 2) Thick basal till site (Figure A-1 and A-2).

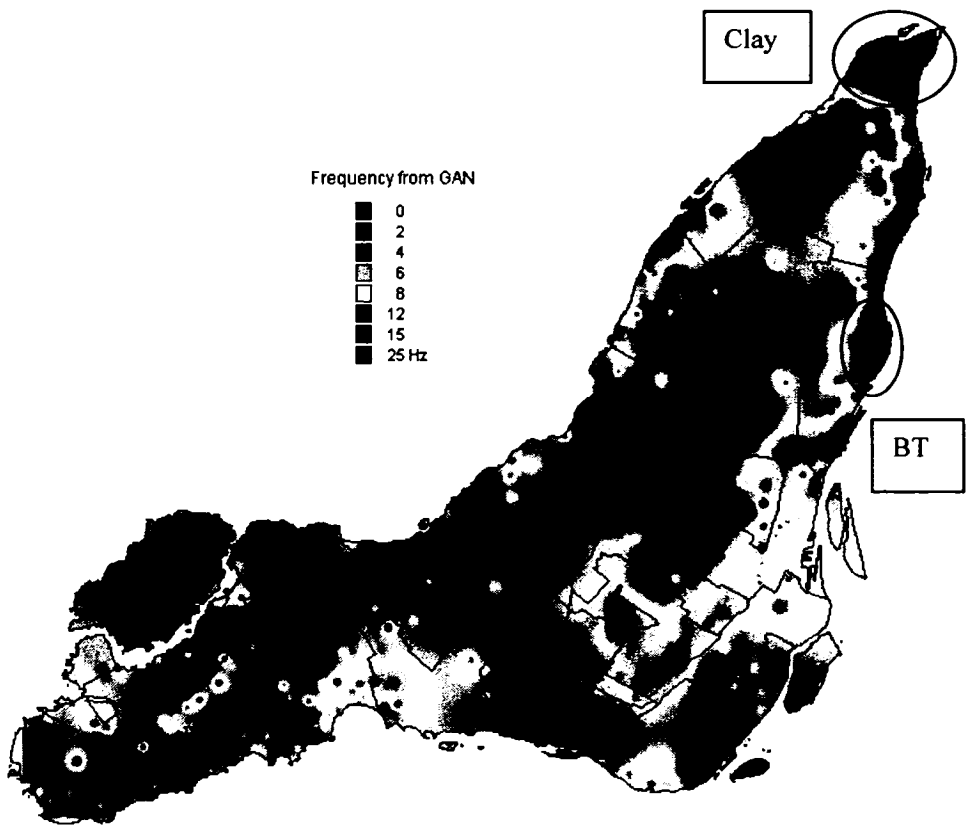

Figure A.1: Selected locations on the Predominant Frequencies map from GAN.

A.1 Clay site

A.1.1 Locations

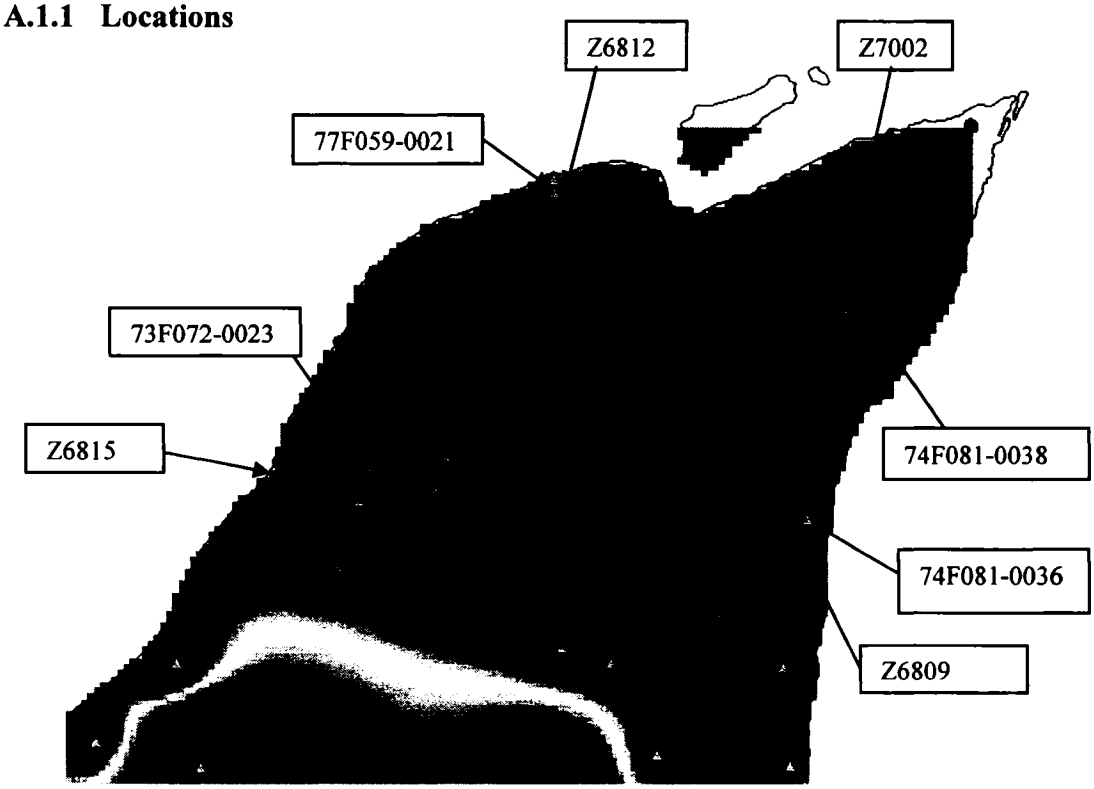

Figure A.2: Boreholes and GAN tests locations at the clay site

A.1.2 Boreholes

Borehole 74F081-0038			
From	*To*	*Thickness (m)*	*Description of Soil*
0	1.219	1.219	Sable et argile graveleux. (Remblai)
1.219	3.048	1.829	Sable silteux. (Dépôt de cours d'eau)
1.319			Fin à moyen. Couleur brun.
3.048	4.572	1.524	Argile sableuse. (Dépôt marin)
3.148			Couleur gris.
4.572	30.785	26.213	Argile. (Dépôt marin)
4.672			Plasticité moyenne. Couleur gris.
30.785	31.699	0.914	Sable silteux, un peu de gravier. (Dépôt glaciaire)
30.885			Fin. Couleur gris.

74F081-0036			
From	*To*	*Thickness (m)*	*Description of Soil*
0	2.134	2.134	Sable. (Dépôt de cours d'eau)
0.1			Fin à moyen. Couleur brun.
2.134	4.724	2.59	Sable argileux. (Dépôt de cours d'eau)
2.234			Fin à grossier. Couleur gris, brun. Présence de coquillages.
4.724	23.47	18.746	Argile. (Dépôt marin)
4.824			Plasticité moyenne. Couleur gris.
23.47	24.232	0.762	Sable et silt graveleux. (Dépôt glaciaire)
23.57			Couleur gris.

77F059-0021			
From	*To*	*Thickness (m)*	*Description of Soil*
0	1.372	1.372	Argile et sable graveleux. (Dépôt marin)
0.1			Couleur gris, brun.
1.372	4.572	3.2	Argile. (Dépôt marin)
1.472			Plasticité moyenne. Couleur gris.
4.572	7.925	3.353	Argile. (Dépôt marin)
4.672			Plasticité moyenne. Couleur gris. Présence de coquillages.
7.925	13.106	5.181	Argile. (Dépôt marin)
8.025			Plasticité moyenne. Couleur gris.
13.106	13.716	0.61	Argile. (Dépôt marin)
13.716	16.764	3.048	Argile. (Dépôt marin)
13.816			Plasticité moyenne. Couleur gris. Présence de coquillages.
16.764	18.288	1.524	Argile et gravier. (Dépôt glaciaire)
16.864			Couleur brun.
18.288	21.336	3.048	Argile et silt sableux, un peu de gravier. (Dépôt glaciaire)
18.388			Couleur brun.

73F072-0023			
From	*To*	*Thickness (m)*	*Description of Soil*
0	0.152	0.15	Terre noire. (Remblai)
0.152	0.457	0.31	Argile silteuse, traces de sable. (Remblai)
0.252			Couleur brun. Présence de matières organiques.
0.457	1.524	1.07	Argile silteuse. (Dépôt marin)
0.557			Couleur brun.
1.524	10.668	9.14	Argile, traces de silt. (Dépôt marin)
1.624			Plasticité moyenne. Couleur gris.
10.668	15.24	4.57	Argile, traces de silt. (Dépôt marin)
10.768			Aucune plasticité. Aucune plasticité. Passées argileuses. Couleur gris.
15.24	16.764	1.52	Silt argileux, un peu de sable. (Dépôt glaciaire)
15.34			Couleur gris.
16.764	19.608	2.84	Sable et gravier silteux. (Dépôt glaciaire)
16.864			Fin à grossier. Couleur gris.

A.1.3 GAN H/V Ratio

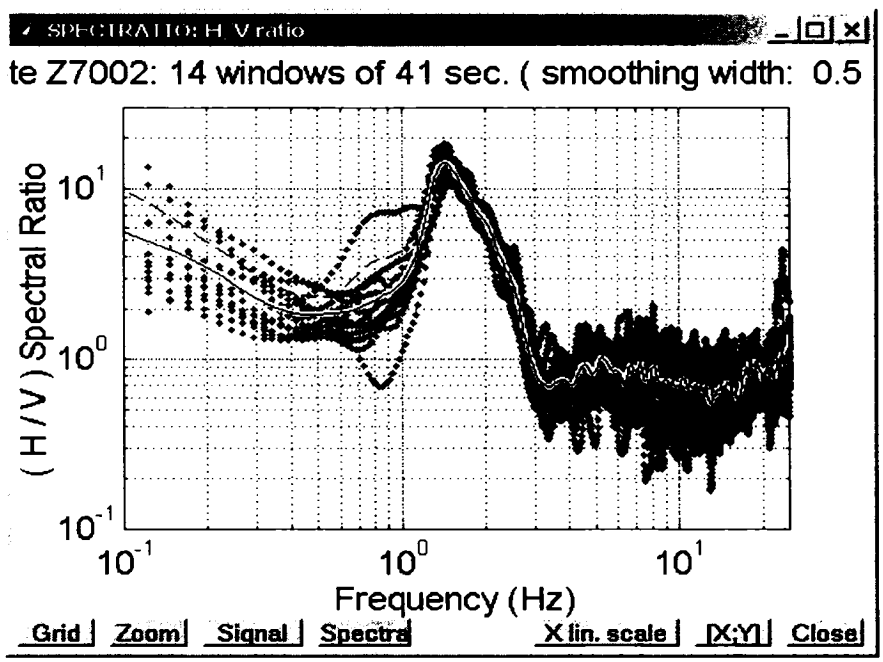

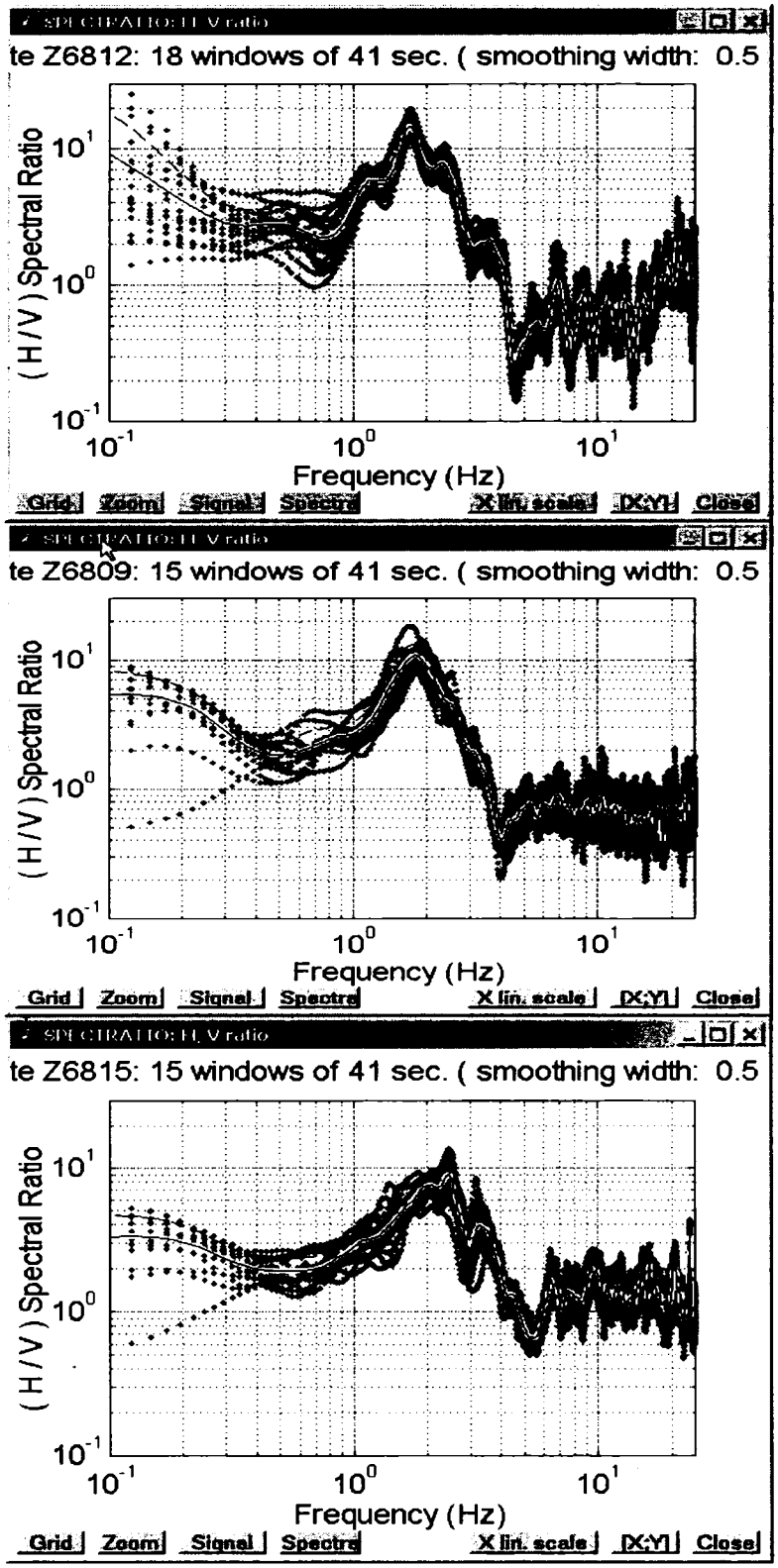
te Z6812: 18 windows of 41 sec. (smoothing width: 0.5
(H / V) Spectral Ratio
Frequency (Hz)
Grid
Zoom
Signal
Spectra
X lin. scale
[X;Y]
Close
te Z6809: 15 windows of 41 sec. (smoothing width: 0.5
(H / V) Spectral Ratio
Frequency (Hz)
Grid
Zoom
Signal
Spectra
X lin. scale
[X;Y]
Close
te Z6815: 15 windows of 41 sec. (smoothing width: 0.5
(H / V) Spectral Ratio
Frequency (Hz)
Grid
Zoom
Signal
Spectra
X lin. scale
[X;Y]
Close

A.1.4 Frequencies and Amplification Factors

- Frequencies from Shake

ode	81125S02 Quebec, Saguenay	81125S05 Tadoussac, Saguenay	81125S08 La Malbaie, Saguenay	81125S16 Chicoutimi-Nord, Saguenay	81125S17 St-Andre, Saguenay	BES-EW Loma Prieta EQ	ElcentroH El Centro, California	GBZ-NS Kocaeli, Turkey EQ	MDR-NS Duzce, Turkey EQ
73F072-0023	2	2	1.88	2.13	2.25	1.38	1.88	1.63	1.88
74F081-0038+15	1.13	1.25	1.13	1.25	1.25	0.88	0.88	0.88	1
77F059-0021	1.75	1.88	1.75	2	2	1.25	1.63	1.5	1.75
74F081-0036	1.25	1.38	1.25	1.38	1.5	0.88	1	0.88	1.13

Code	AtkM6_1 Atkinson's artific.	AtkM6_2 Atkinson's artific.	AtkM6_3 Atkinson's artific.	AtkM6_4 Atkinson's artific.	AtkM7_1 Atkinson's artific.	AtkM7_2 Atkinson's artific.	AtkM7_3 Atkinson's artific.	AtkM7_4 Atkinson's artific.	Average
73F072-0023	2	2	2.13	2.13	1.75	1.88	1.88	1.75	1.9147
74F081-0038+15	1.13	1.25	1.13	1.13	1	1	1.13	1	1.0835
77F059-0021	1.88	1.88	1.88	1.75	1.63	1.63	1.75	1.5	1.73
74F081-0036	1.25	1.38	1.25	1.25	1.13	1	1.25	1.13	1.1935

-Amplification Factors

Code	81125S02 Quebec, Saguenay	81125S05 Tadoussac, Saguenay	81125S08 La Malbaie, Saguenay	81125S16 Chicoutimi-Nord, Saguenay	81125S17 St-Andre, Saguenay	LP	BES-EW Loma Prieta EQ	ElcentroH El Centro, California	HP	GBZ-NS Kocaeli, Turkey EQ	MDR-NS Duzce, Turkey EQ	IP
73F072-0023	1.59	1.91	2.41	1.68	1.47	1.81	3.39	1.60	2.49	1.70	1.44	1.57
74F081-0038+15	1.28	1.20	1.08	0.75	0.45	0.95	1.53	1.35	1.44	1.39	1.54	1.47
77F059-0021	1.63	2.32	2.62	1.96	2.13	2.13	2.93	1.89	2.41	1.67	1.26	1.46
74F081-0036	1.50	0.80	1.16	0.76	0.50	0.94	1.57	1.25	1.41	1.26	1.19	1.22

Code	AtkM6_1 Atkinson's artific.	AtkM6_2 Atkinson's artific.	AtkM6_3 Atkinson's artific.	AtkM6_4 Atkinson's artific.	AtkM7_1 Atkinson's artific.	AtkM7_2 Atkinson's artific.	AtkM7_3 Atkinson's artific.	AtkM7_4 Atkinson's artific.	BP
73F072-0023	1.90	1.64	1.90	1.94	2.24	2.08	2.05	2.40	2.02
74F081-0038+15	1.06	1.09	1.23	1.12	1.14	1.35	0.99	1.11	1.14
77F059-0021	1.99	1.72	2.47	2.34	2.24	1.96	2.35	2.13	2.15
74F081-0036	1.30	0.97	0.90	0.79	1.07	0.99	0.97	0.99	1.00

A.2 Basal Till site

A.2.1 Locations

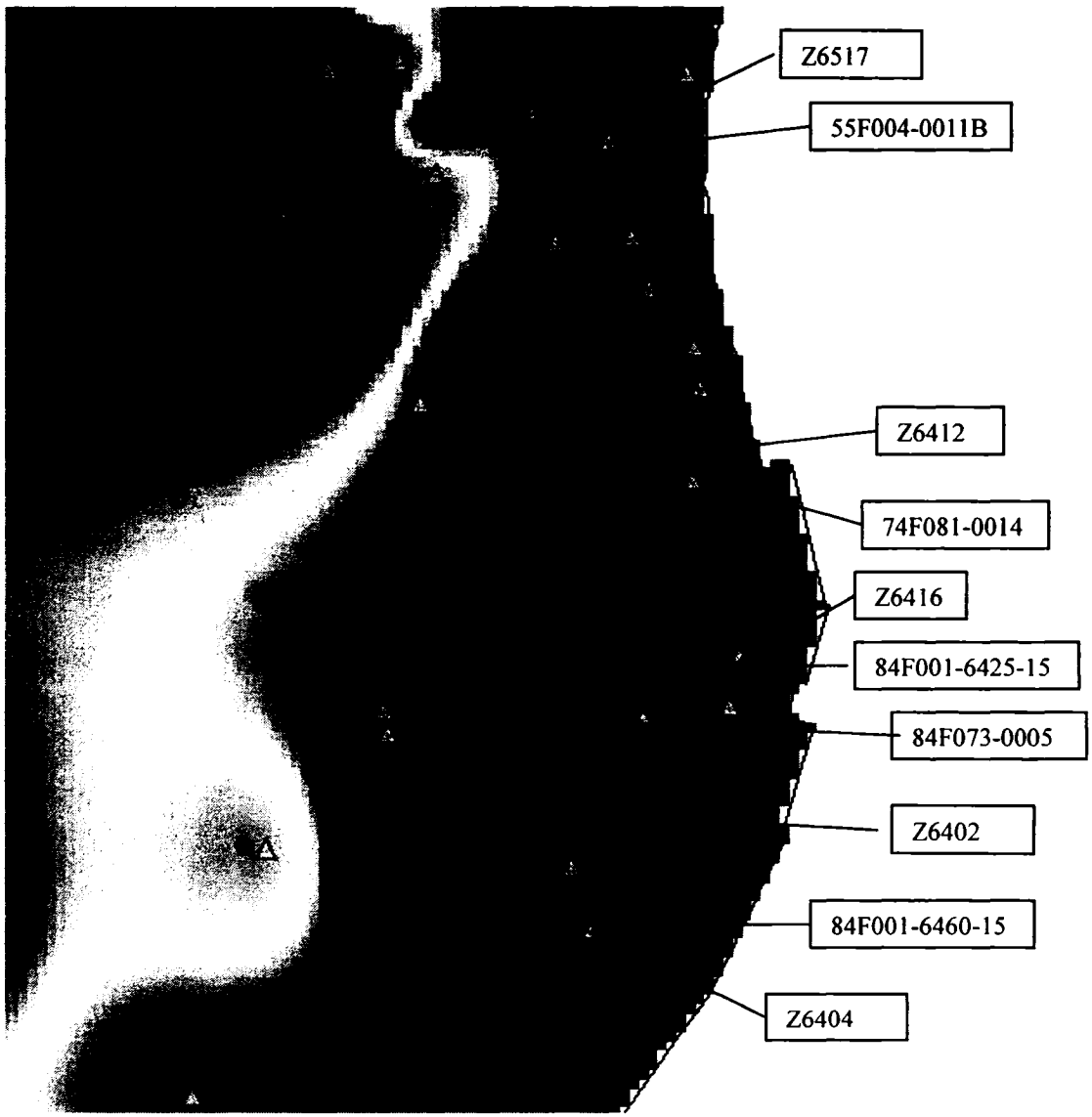

A.2.2 Boreholes

84F001-6460			
From	To	Thick. (m)	Description
0	0.9	0.9	Remblai (?) graveleuse.
0.1			Présence d'asphalte, de béton.
0.9	1.4	0.5	Argile silteuse. (Dépôt marin)
1			Consistance ferme. Couleur brun.
1.4	1.9	0.5	Argile silteuse. (Dépôt marin)
1.5			Consistance ferme. Couleur gris.
1.9	5.35	3.45	Silt et argile argileux. (Dépôt glaciaire)
2			Consistance ferme à molle. Couleur gris.
5.35	9	3.65	Silt, un peu de sable, traces de sable. (Dépôt glaciaire)
5.45			Fin. Consistance dure. Couleur gris.
9	10	1	Silt et sable. (Dépôt glaciaire)
9.1			Fin. Consistance dure. Couleur gris.
10	11.6	1.6	Silt, un peu de sable, traces de sable. (Dépôt glaciaire)
10.1			Fin. Consistance dure. Couleur gris.
11.6	21	9.4	Silt, un peu d'argile, traces de sable. (Dépôt glaciaire)
11.7			Fin. Consistance dure. Couleur gris.
21	22.25	1.25	Sable, un peu de gravier, traces de silt. (Dépôt glaciaire)
21.1			Densité très dense. Couleur gris.

84F001-6425			
From	To	Thick. (m)	Description
0	0.6	0.6	Remblai (?) graveleux.
0.1			Présence d'asphalte, de béton.
0.6	2.2	1.6	Argile silteuse, traces de sable. (Dépôt marin)
0.7			Consistance ferme. Couleur brun, gris.
2.2	3	0.8	Argile silteuse. (Dépôt marin)
2.3			Consistance ferme. Couleur gris.
3	3.7	0.7	Argile et silt. (Dépôt marin)
3.1			Consistance molle. Couleur gris. Présence de matières organiques.
3.7	22.1	18.4	Silt, un peu d'argile, traces de sable. (Dépôt glaciaire)
3.8			Fin. Consistance dure à très raide. Couleur gris.

84F073-0005			
From	To	Thick. (m)	Description
0	0.05	0.05	Remblai (matériau non défini).
0.1			Présence d'asphalte.
0.05	1.07	1.02	Gravier sableux, traces de silt. (Remblai)
1.07	1.27	0.2	Remblai (matériau non défini).
1.17			Présence de béton.
1.27	1.68	0.41	Argile silteuse. (Remblai)
1.37			Couleur gris.
1.68	2.29	0.61	Argile silteuse. (Dépôt marin)
1.78			Couleur brun, gris.
2.29	3.66	1.37	Argile silteuse, traces de sable. (Dépôt marin)
2.39			Couleur gris, brun.
3.66	5.79	2.13	Argile silteuse. (Dépôt marin)
3.76			Couleur gris, rose.
5.79	7.32	1.53	Argile silteuse, traces de sable. (Dépôt marin)
5.89			Couleur gris. Présence de coquillages.
7.32	8.84	1.52	Silt sableux, un peu d'argile, traces de gravier. (Dépôt glaciaire)
7.42			Couleur gris.
8.84	10.36	1.52	Sable silteux, un peu de gravier. (Dépôt glaciaire)
8.94			Couleur gris.

55F004-0011B			
From	To	Thick. (m)	Description
0	1.524	1.524	Sable et argile jaune, un peu de gravier.
1.524	5.486	3.962	Argile grise et rose.
5.486	7.01	1.524	Argile grise et sable gris foncé.
7.01	12.802	5.792	Sable gris et gravier; lâche à compact.
12.802	16.764	3.962	Roc friable et sable gris très foncé.

74F081-0014			
From	To	Thick. (m)	Description
0	1.524	1.524	Sable et gravier, traces de blocs. (Remblai)
1.524	6.096	4.572	Argile. (Dépôt marin)
1.624			Plasticité élevée. Couleur brun, gris.
6.096	13.411	7.315	Sable silteux. (Dépôt glaciaire)
6.196			Fin. Couleur gris.
13.411	14.478	1.067	Sable silteux, un peu de gravier. (Dépôt glaciaire)
13.511			Fin. Couleur gris.

A.2.3 GAN H/V Ratio

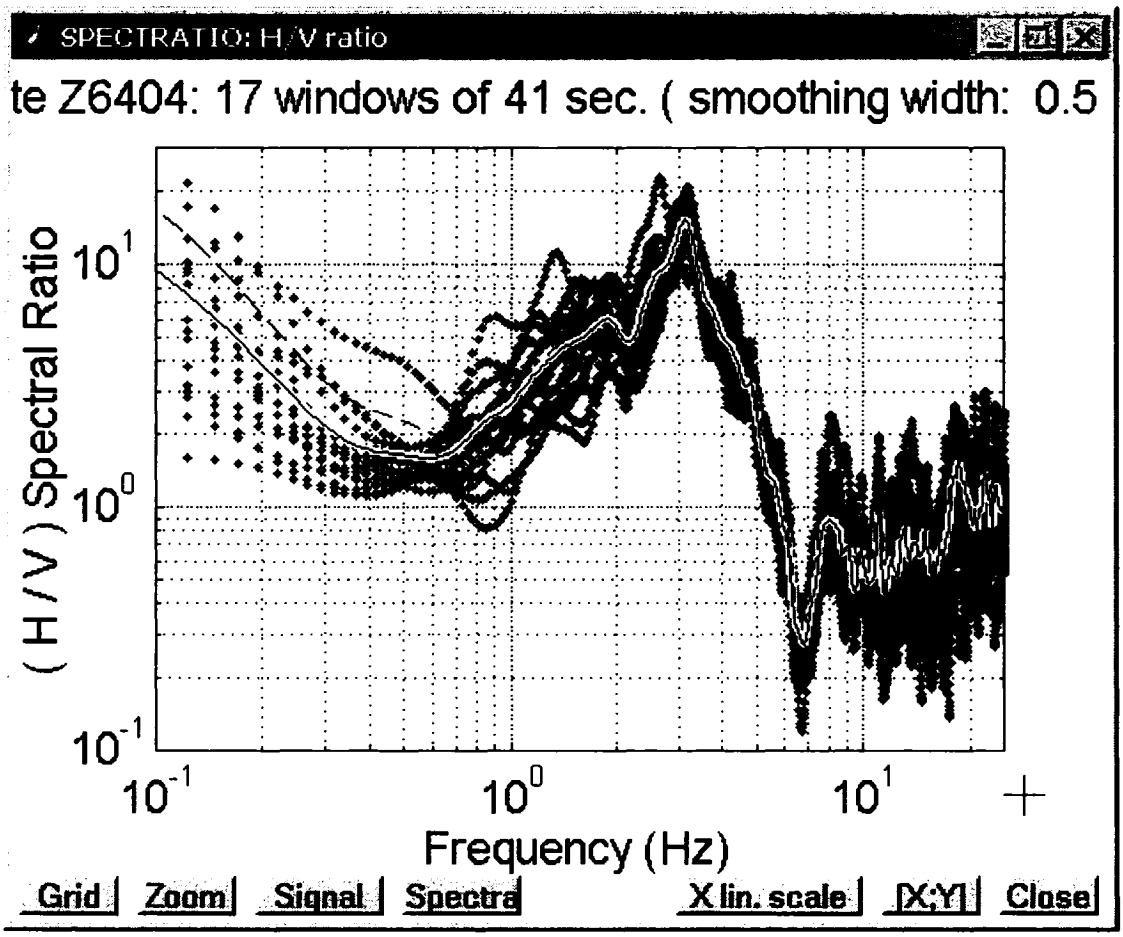

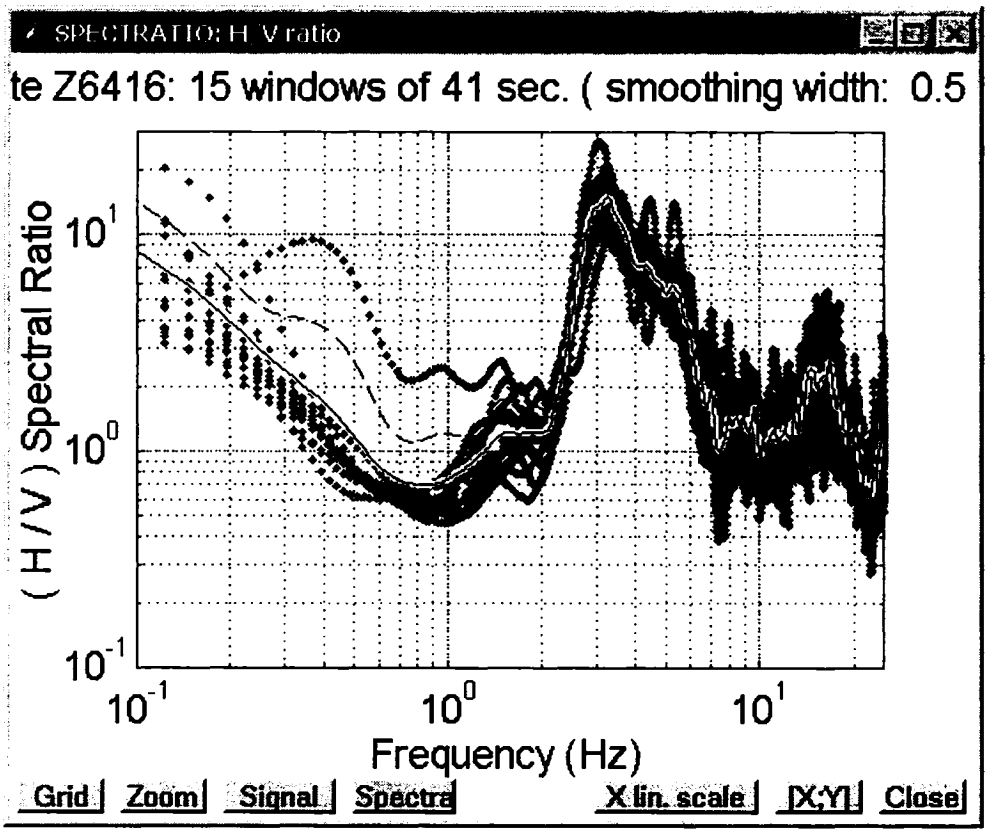
SPECTRATIO: H/V ratio
te Z6416: 15 windows of 41 sec. (smoothing width: 0.5
(H / V) Spectral Ratio
10^{1}
10^{0}
10^{-1}
10^{-1}
10^{0}
10^{1}
Frequency (Hz)
Grid
Zoom
Signal
Spectra
X lin. scale
[X;Y]
Close

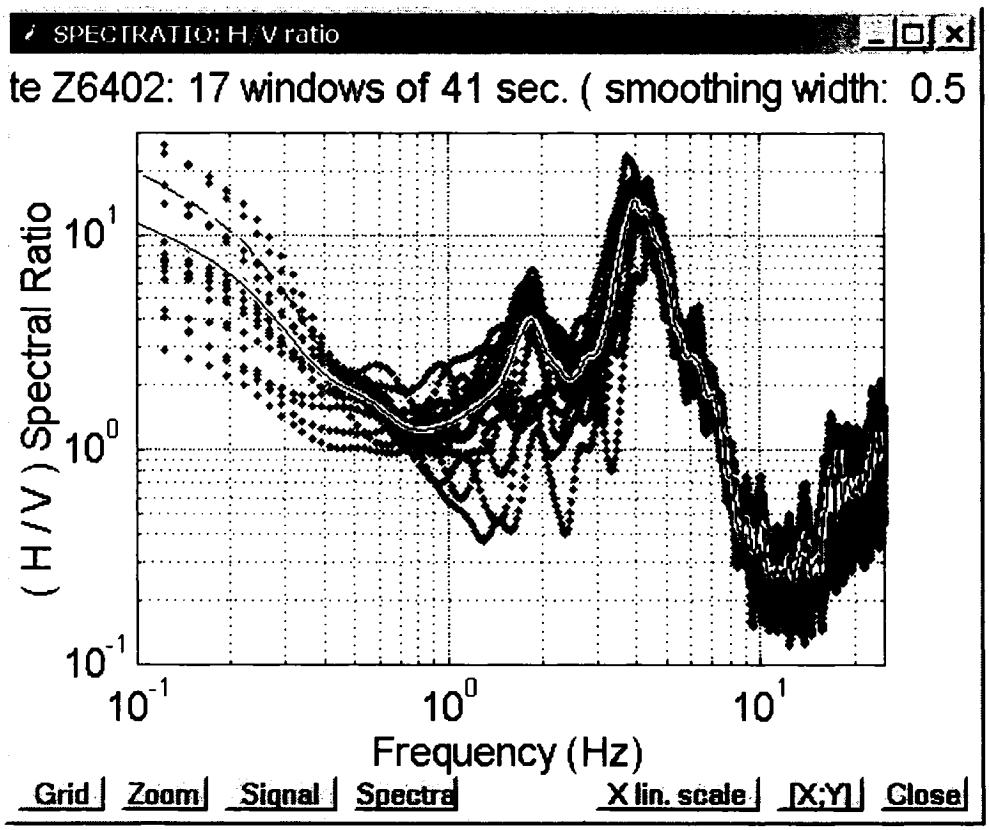
SPECTRATIO: H/V ratio
te Z6402: 17 windows of 41 sec. (smoothing width: 0.5
(H / V) Spectral Ratio
10^{1}
10^{0}
10^{-1}
10^{-1}
10^{0}
10^{1}
Frequency (Hz)
Grid
Zoom
Signal
Spectra
X lin. scale
[X;Y]
Close

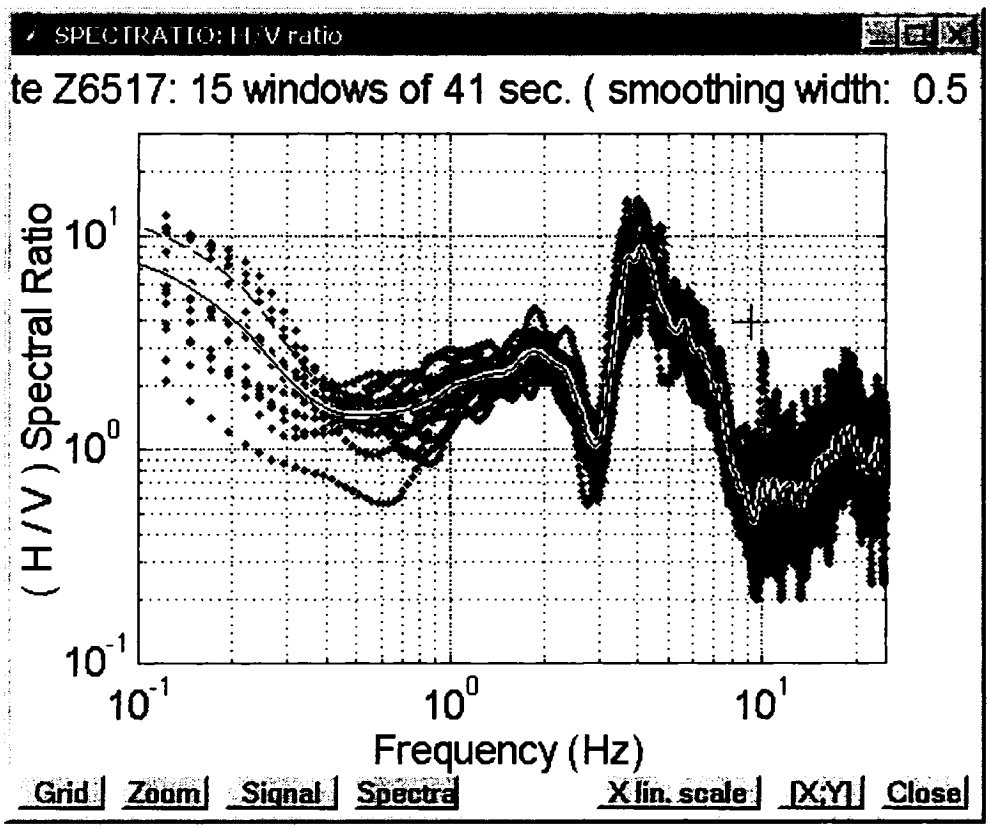
SPECTRATIO: H/V ratio
te Z6517: 15 windows of 41 sec. (smoothing width: 0.5
(H / V) Spectral Ratio
10^1
10^0
10^{-1}
10^{-1}
10^0
10^1
Frequency (Hz)
Grid
Zoom
Signal
Spectra
X lin. scale
[X;Y]
Close

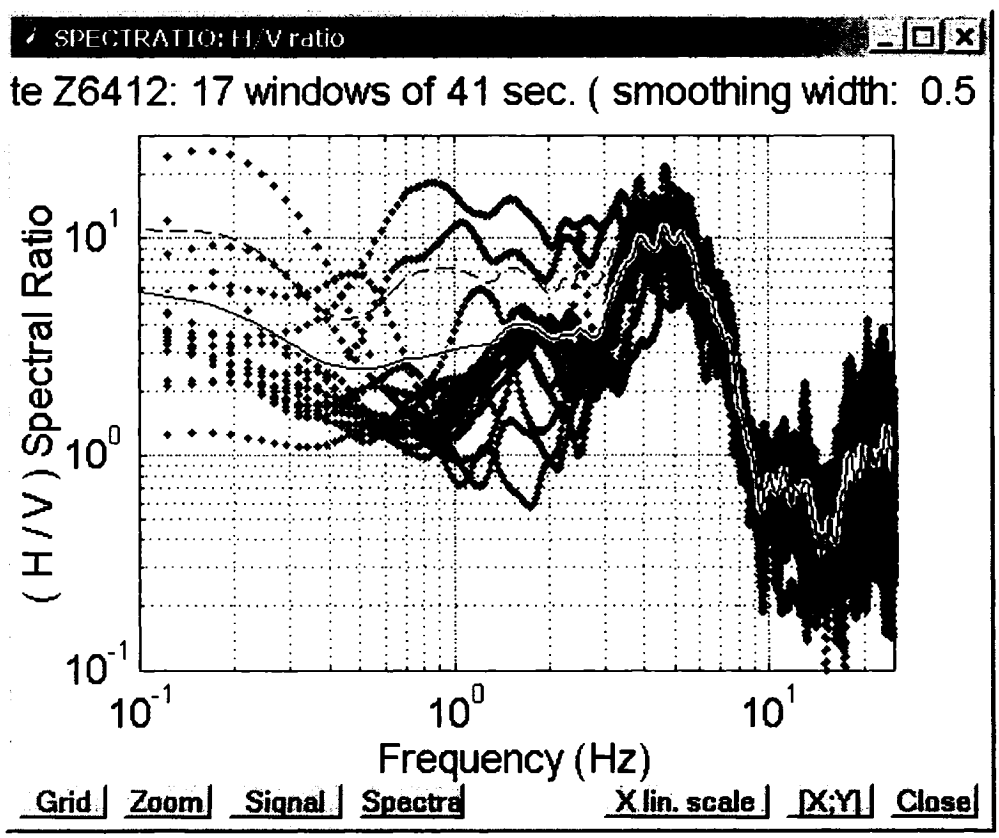
SPECTRATIO: H/V ratio
te Z6412: 17 windows of 41 sec. (smoothing width: 0.5
(H / V) Spectral Ratio
10^1
10^0
10^{-1}
10^{-1}
10^0
10^1
Frequency (Hz)
Grid
Zoom
Signal
Spectra
X lin. scale
[X;Y]
Close

A.2.4 Frequencies and Amplification Factors

- Frequencies

Code	81125S02 Quebec, Saguenay	81125S05 Tadoussac, Saguenay	81125S08 La Malbaie, Saguenay	81125S16 Chicoutimi-Nord, Saguenay	81125S17 St-Andre, Saguenay	BES-EW Loma Prieta EQ	ElcentroH El Centro, California	GBZ-NS Kocaeli, Turkey EQ	MDR-NS Duzce, Turkey EQ
84F001-6460-15	5.25	5.63	5.25	5.63	6.13	6	6	5.63	6
84F001-6425-15	4	4.5	4.13	4.5	4.75	4.5	4.63	4.25	4.25
84F073-0005	3.5	4.25	4	4.25	4.5	4.13	4.25	3.88	3.75
55F004-0011B	3.5	4	3.88	4.13	4.25	3.88	4.13	3.88	3.25
74F081-0014	4.38	4.75	4.25	4.88	5.13	4.63	5	4.5	4.5

Code	AtkM6_1 Atkinson's artific.	AtkM6_2 Atkinson's artific.	AtkM6_3 Atkinson's artific.	AtkM6_4 Atkinson's artific.	AtkM7_1 Atkinson's artific.	AtkM7_2 Atkinson's artific.	AtkM7_3 Atkinson's artific.	AtkM7_4 Atkinson's artific.	Average
84F001-6460-15	5.63	5.75	5.75	5.63	5.25	5.13	5.25	5.25	5.597647
84F001-6425-15	4.38	4.25	4.5	4.38	4	4	4.25	4.13	4.317647
84F073-0005	4	4	4.25	4	3.63	3.75	3.75	3.88	3.986471
55F004-0011B	3.63	3.75	3.75	3.75	3.63	3.63	3.5	3.63	3.774706
74F081-0014	4.5	4.5	4.75	4.38	4	4	4.5	4.25	4.523529

- Amplification Factor

Code	81125S02 Quebec, Saguenay	81125S05 Tadoussac, Saguenay	81125S08 La Malbaie, Saguenay	81125S16 Chicoutimi-Nord, Saguenay	81125S17 St-Andre, Saguenay	LP	BES-EW Loma Prieta EQ	ElcentroH El Centro, California	HP	GBZ-NS Kocaeli, Turkey EQ	MDR-NS Duzce, Turkey EQ	IP
84F001-6460-15	6.51	5.40	6.79	4.62	2.53	5.17	2.11	3.35	2.73	3.44	1.68	2.56
84F001-6425-15	6.40	4.53	5.61	4.22	2.23	4.60	2.30	2.54	2.42	3.61	3.09	3.35
84F073-0005	3.28	2.14	2.53	2.36	1.52	2.36	1.52	1.35	1.43	1.81	2.08	1.94
55F004-0011B	3.61	4.06	2.92	3.01	3.01	3.32	1.86	1.95	1.90	2.02	3.55	2.79
74F081-0014	3.06	4.71	3.24	2.92	2.58	3.30	1.86	2.16	2.01	2.10	2.05	2.07

Code	AtkM6_1 Atkinson's artific.	AtkM6_2 Atkinson's artific.	AtkM6_3 Atkinson's artific.	AtkM6_4 Atkinson's artific.	AtkM7_1 Atkinson's artific.	AtkM7_2 Atkinson's artific.	AtkM7_3 Atkinson's artific.	AtkM7_4 Atkinson's artific.	BP
84F001-6460-15	4.86875	4.63875	4.051875	5.39	6.151875	6.2375	5.83625	5.370625	5.318203
84F001-6425-15	4.42125	5.03875	3.6525	4.5175	6.099375	5.5225	4.525625	4.750625	4.816016
84F073-0005	2.714375	2.453125	2.4575	2.665625	2.4025	2.446875	2.58125	2.443125	2.520547
55F004-0011B	3.683125	3.46625	4.1175	3.631875	3.455625	3.4925	3.16125	3.380625	3.548594
74F081-0014	3.821875	3.71	3.274375	4.21375	3.92125	3.430625	2.75625	3.565625	3.586719